

WATER PERMEABILITY OF SILICA

FUME/CEMENT MORTARS

By

ASHRAF ELAZOUNI

**Bachelor of Science
Zagazig University
Zagazig, Egypt
1984**

**Masters of Science
Zagazig University
Zagazig, Egypt
1989**

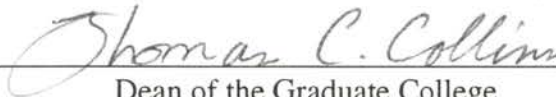
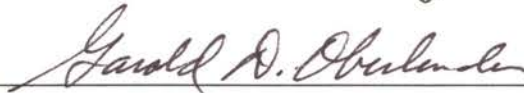
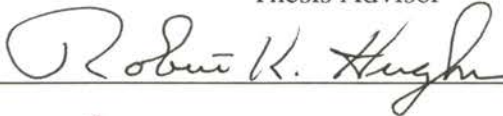
**Submitted to the Faculty of the
Graduate College of the
Oklahoma State University
in partial fulfillment of
the requirements for
the Degree of
DOCTOR OF PHILOSOPHY
July, 1993**

WATER PERMEABILITY OF SILICA
FUME/CEMENT MORTARS

Thesis Approved:



Thesis Advisor



Dean of the Graduate College

ACKNOWLEDGMENTS

I sincerely appreciate the assistance of those who assisted during the course of this study. I would like to thank and express my appreciation to Prof. M. E. Ayers, my major advisor, for his instruction, advice, time and continuous encouragement during my study program. Appreciation is extended to Prof. R. K. Hughes, Prof. G. D. Oberlender, and Prof. C. A. Rich for serving on my committee.

I would like to offer special thanks to my friends for their cooperation and assistance.

I am deeply grateful, and wish to express my appreciation to my brother and sister whose support and encouragement made my education possible.

TABLE OF CONTENTS

Chapter	Page
I. INTRODUCTION	1
Basis of Study	1
Statement of Problem	4
Objectives of Study	6
Scope of Work	6
II. LITERATURE REVIEW	7
Background	7
Test Methods and Apparatus	7
Problems with Permeability Measurements	16
Effect of Silica Fume on Microstructure	17
Permeability and Microstructural Properties	24
III. RESEARCH METHODOLOGY	30
Test Apparatus	30
Permeability Cells	31
Design Details	31
Assembly of Permeability Test Apparatus.	33
Test Program	33
Test Procedure for Permeability Measurement	37
Darcy's Law for Uniaxial Water Flow.	38
Determination of Relative Permeability	
Using the ASTM C 642-90 Procedure	39
IV. EXPERIMENTAL RESULTS AND DISCUSSION.	42
Experimental Results	42
Effect of Water/Cement Ratio.	43
Effect of Curing	50
Effect of Silica Fume Content	55

Chapter	Page
Correlation of Permeability Coefficient on Volume of Permeable Voids	60
V. SUMMARY AND CONCLUSIONS	63
Recommendations for Future Research	65
REFERENCES	66
APPENDICES	71
APPENDIX A - TABLES FOR TESTED SPECIMENS	72
Gradation of Silica Sand	73
Rates of Flow for the Tested Specimens	74
Dimensions of the Specimens and the Pressure used in Test	77
Permeability Coefficients and Coefficients of Variation	80
The Percentage Volume of Permeable Voids	83
APPENDIX B - FIGURES	86
Schematics for Permeability Apparati	87
Regression Relationships	101
APPENDIX C - MEASURED PERMEABILITY DATA	116

LIST OF TABLES

Table	Page
1. A Summary of the Water Permiability Apparatus Developed in Literature	18
2. The Average Coefficients of Permeability and Volume of Permeable Voids	44
3. Regression Equations, (R^2) Values, and P-values for the Regression of Permeability Coefficients and Percent Volume of Permeable Voids on W/C Ratio	49
4. Regression Equations, (R^2) Values, and P-values for the Regression of Permeability Coefficients and Percent Volume of Permeable Voids on Curing Periods	54
5. Regression Equations, (R^2) Values, and P-values for the Regression of Permeability Coefficients and Percent Volume of Permeable Voids on Silica Fume Content.	59
6. Regression Equations, (R^2) Values, and P-values for the Regression of Permeability Coefficients on Percent Volume of Permeable Voids	62
7. Gradation of the Silica Sand	73
8. Water/Cement Ratio, Silica Fume Content, Curing Periods and Rate of Flow for the Test Specimens	74
9. The Diameter, Height, and Test Pressure for the Test Specimens	77
10. The Coefficients of Permeability of Test Specimens with the Coefficients of Variation Within Each Group	80
11. Percentage Volume of Permeable Voids Obtained from ASTM C 642-90	83

LIST OF FIGURES

Figure		Page
1.	Construction of Permeability Cell Developed by Ayers and Elazouni	32
2.	Schematic of the Permeability Apparatus Developed by Ayers and Elazouni	34
3.	The Relationship between the Water/Cement Ratio and Permeability Coefficients	45
4.	The Relationship between the Water/Cement Ratio and Percentage Volume of Permeable Voids	46
5.	The Relationship between the Permeability Coefficient and the Curing Period	51
6.	The Relationship between the Percent Volume of Permeable Voids and the Curing Period	52
7.	The Relationship between the Permeability Coefficient and the Silica Fume Content	56
8.	The Relationship between the Percent Volume of Permeable Voids and the Silica Fume Content	57
9.	Schematic of the Permeability Apparatus Developed by McMillan and Lyse.	88
10.	Schematic of the Permeability Apparatus Developed by Ruetters et. al	89
11.	Schematic of the Permeability Apparatus Developed by US Army Corps of Engineers	90

Figure		Page
12.	Section View of the Permeability Apparatus Developed by Meulen and Dijk	91
13.	The Water Permeability Apparatus Developed by Figgs	92
14.	Section View of the Permeability Pressure Cell Developed by Hope and Malhotra	93
15.	Schematic of the Permeability Apparatus Developed by Hope and Malhotra	94
16.	Section View of the Permeability Cell Developed by Janssen	95
17.	Schematic of the Permeability Apparatus Developed by Janssen	96
18.	Schematic of the "Old" Apparatus Developed by Ludirdja, Berger and Young	97
19.	Schematic of the "New" Apparatus Developed by Ludirdja, Berger and Young	98
20.	A Cross Section View of Hassler Core Holder Used by Sullivan	99
21.	Schematic of the Apparatus Developed by Reinhardt and Gaber	100
22.	The Correlation of the Permeability Coefficient on the Water/Cement Ratio at all Silica Fume Contents	102
23.	The Correlation of the Permeability Coefficient on the Water/Cement Ratio at 0% Silica Fume Content	102
24.	The Correlation of the Permeability Coefficients on the Water/Cement Ratio at 3.75% Silica Fume Content	103

Figure		Page
25.	The Correlation of the Permeability Coefficient on the Water/Cement Ratio at 7.5% Silica Fume Content	103
26.	The Correlation of the Percent Volume of Permeable Voids on the Water/Cement Ratio at all Silica Fume Contents	104
27.	The Correlation of the Percent Volume of Permeable Voids on the Water/Cement Ratio at 0% Silica Fume Content	104
28.	The Correlation of the Percent Volume of Permeable Voids on the Water/Cement Ratio at 3.75% Silica Fume Content	105
29.	The Correlation of the Percent Volume of Permeable Voids on the Water/Cement Ratio at 7.5% Silica Fume Content	105
30.	The Correlation of the Permeability Coefficient on the Curing Period at all Silica Fume Content	106
31.	The Correlation of the Permeability Coefficient on the Curing Period at 0% Silica Fume Content	106
32.	The Correlation of the Permeability Coefficient on the Curing Period at 3.75% Silica Fume Content.	107
33.	The Correlation of the Permeability Coefficient on the Curing Period at 7.5% Silica Fume Content	107
34.	The Correlation of the Percent Volume of Permeable Voids on the Curing Period at all Silica Fume Contents	108
35.	The Correlation of the Percent Volume of Permeable Voids on the Curing Period at 0% Silica Fume Content	108

Figure		Page
36.	The Correlation of the Percent Volume of Permeable Voids on the Curing Period at 3.75% Silica Fume Content	109
37.	The Correlation of the Percent Volume of Permeable Voids on the Curing Period at 7.5% Silica Fume Content	109
38.	The Correlation of the Permeability Coefficient on the Silica Fume Content at all w/c Ratios	110
39.	The Correlation of the Permeability Coefficient on the Silica Fume Content at 0.5 w/c Ratio	110
40.	The Correlation of the Permeability Coefficient on the Silica Fume Content at 0.6 w/c Ratio	111
41.	The Correlation of the Permeability Coefficient on the Silica Fume Content at 0.7 w/c Ratio	111
42.	The Correlation of the Percent Volume of Permeable Voids on the Silica Fume Content at all w/c Ratios	112
43.	The Correlation of the Percent Volume of Permeable Voids on the Silica Fume Content at 0.5 w/c Ratio	112
44.	The Correlation of the Percent Volume of Permeable Voids on the Silica Fume Content at 0.6 w/c Ratio	113
45.	The Correlation of the Percent Volume of Permeable Voids on the Silica Fume Content at 0.7 w/c Ratio	113
46.	The Correlation of the Permeability Coefficient on the Percent Volume of Permeable Voids at all Silica Fume Contents	114

Figure		Page
47.	The Correlation of the Permeability Coefficient on the Percent Volume of Permeable Voids at 0% Silica Fume Contents	114
48.	The Correlation of the Permeability Coefficient on the Percent Volume of Permeable Voids at 3.75% Silica Fume Contents	115
49.	The Correlation of the Permeability Coefficient on the Percent Volume of Permeable Voids at 7.5% Silica Fume Contents	115

CHAPTER I

INTRODUCTION

Concrete is an extensively used construction material in many fluid-exposed structures. The performance and longevity of these structures depend to a great extent on being impervious to water and other fluids. Unless concrete exhibits enough resistance to fluid penetration, it would not be able to fulfill its desired function and would deteriorate excessively. Thus, the permeability of concrete is a significant factor in determining the durability of concrete. A lack of durability in concrete structures has become a serious problem in many parts of the world. Therefore, the permeability of concrete has received increasing interest from designers and researchers over the past several years.

Numerous studies have been performed to evaluate the permeability of concrete, mortars, and pastes. These studies have included development of new devices for measuring the rate of fluid flow and determining permeability coefficients, studying the microstructure of cement-based materials, correlating the microstructural characteristics with permeability coefficients, and evaluating the effect of additives on the permeability coefficients.

Basis of Study

The permeability of concrete can be defined as the ease with which water (or other fluids) can move through concrete. Being an essentially porous material, the flow of water through concrete is similar to flow through any porous medium and relies on the existence

of pores within the structure. Both the hydrated cement paste and the aggregate in hydrated concrete contain pores. In addition, the concrete matrix as a whole contains voids caused by incomplete compaction or by bleeding. The voids in hydrated concrete can range from less than one percent to greater than ten percent of the volume of the concrete. Since aggregate particles are enveloped by the cement paste in fully hydrated concrete, it is the permeability of the paste that has the greatest effect on the permeability of concrete.

The amount and type of pores in cement paste can be determined by studying the structure of cement paste. At any stage of hydration, the hardened paste consists of calcium silicate hydrates referred to collectively as gel, calcium hydroxide, some minor compounds, unhydrated cement, and the residue of the water-filled spaces in the fresh paste. Those voids are referred to as capillary pores. However, within the gel itself there exist interstitial voids called gel pores. The former constitutes between 0 and 40 percent of the paste volume, and the latter about 28 percent, depending on the water/cement ratio and the degree of hydration.

The diffusion characteristics and permeability of concrete are not a simple function of its porosity, but depend also on the size, distribution, and continuity of the pores. In cement paste, water can flow more easily through the capillary pores than through the much smaller gel pores. Thus, the permeability of cement paste is primarily controlled by its capillary porosity.

In recent years, many industrial by-products have been used as additives in concrete to reduce its permeability and improve its strength and durability. These materials have proved to be very effective in reducing permeability via the substantial change they cause in the paste structure. Several of the most widely used mineral additives include fly ash and silica fume. It is necessary to obtain information about the effects of these materials on the short term permeability of concrete.

The primary objective of using permeability reducing additives is to reduce the rate

at which aggressive agents can penetrate and react with concrete. These aggressive agents may be gases (CO_2 , SO_3), or liquids (acid rain, acidic water, sea water, sulphate rich water). Therefore, the permeability of concrete is a critical factor in limiting many types of adverse reactions including:

- a) Sulfate Attack - Sulfate attack occurs due to the movement of water containing sulfate ions into the concrete. The sulfates react with calcium hydroxide and calcium aluminate hydrate in the cement matrix. The products of the reaction, gypsum and calcium sulfoaluminate, have considerably greater volume than the compounds they replace. This leads to the expansion and ultimate cracking of the affected concrete. The damage usually begins at the edges and corners, followed by progressive cracking and spalling towards the interior, thereby reducing the concrete to a friable state.
- b) Frost Attack - The likelihood of frost attack depends on the relative ease with which concrete is permeable to water and the degree of saturation. As the temperature of saturated hardened concrete is reduced to below freezing, the water held in the capillary pores of the cement paste freezes and expands. If subsequent thawing is followed by refreezing, cumulative expansion occurs. When the dilating pressure in the concrete exceeds its tensile strength, damage occurs. The extent of the damage varies from surface scaling to complete disintegration. Lenses of ice are typically formed at the exposed surfaces of the concrete and progress through its depth.
- c) Alkali-Aggregate Reaction - This reaction occurs due to the movement of water-transported alkali ions into the concrete aggregates and results in the formation of expansive gels. The most common reaction is between the active silica constituents of the aggregates and the alkaline hydroxides derived from the alkalis (Na_2O and K_2O) in the cement. As a result, an expansive alkali-silicate gel is formed near the surface of the aggregates. The gel is confined by the surrounding cement matrix

resulting in an increase in internal stresses within the concrete. Eventually, this expansion leads to cracking and disruption of the cement matrix.

- d) Acid Attack - Acid attack occurs due to the exposure of concrete to acidic gases including SO_2 and CO_2 . These gases react adversely with concrete and form weak acids in the presence of water and subsequently dissolve the cement matrix. This can result in a drastic reduction in the strength of concrete over time.
- e) Corrosion of steel - Corrosion of steel results from the ingress of water and air in reinforced concrete. In the case of deicing salts, dissolved chloride ions corrode the steel, resulting in an increase in its volume. The increased volume results in internal stress build-up and subsequent cracking and spalling of the concrete cover.

Statement of Problem

Concrete specifications do not currently provide enough information to specify acceptable limits of permeability. The lack of a standard procedure for determining water permeability is a contributing factor in the lack of appropriate permeability specifications [7]. Although numerous test procedures exist, there are a number of problems associated with each. Difficulties include specialized sample requirements, measurement of minute quantities of flow, leakage around samples, entrainment of air in PCC voids, high variability of test results, high equipment costs, and difficulty in performing the tests [19].

Recently, as a means of predicting the permeability coefficients of cement-based materials, advances have been made relating permeability coefficients with microstructural characteristics that can be easily and rapidly measured. Microstructural parameters include the pore size distribution and the volume of pores larger than a specific radius. The mercury intrusion porosimetry technique has been used extensively to obtain data in regards to microstructural properties. However, it was recently reported that the pore size distribution of cement pastes is not adequately described by mercury intrusion

porosimetry [16]. A similar conclusion was noted by Feldman [12] for blended cements and was attributed to the damage that occurs to the microstructure under high pressures. Hooton [16] stated that predicting permeability coefficients, based on data obtained by the mercury intrusion technique, is not accurate. Therefore, the need for a reliable and rapid method to characterize the microstructure and/or measure permeability coefficients still exists.

Several experimental test procedures are available to assess the permeability characteristics of cement-based materials. These tests include the volume of permeable voids (ASTM C 642) and the rapid chloride permeability test (AASHTO T 277). Although these tests do not measure permeability as conventionally defined, they can be used to predict relative permeability [46]. Comparisons of measured permeability coefficients with the corresponding results of these two tests afford a greater confidence in their use as a rapid and indirect means of predicting permeability coefficients. A reasonable correlation of the results of these tests with the permeability coefficients of plain cement and cement/silica fume concrete was recently reported in the Literature [46]. However, there are no similar correlation studies for mortars.

As outlined above, a common experience regarding cement-based permeability tests is that numerous problems are involved in conducting the tests. A review of the Literature suggests that permeability should be directly related to pore structure [18]. The proposed research addresses this topic by defining the quantitative relationship between the volume of permeable voids determined by ASTM C 642 and permeability coefficients for type I portland cement and cement/silica fume mortars. A significant aspect of the research is that it determines the effects on permeability of using silica fume as a mineral additive. The Literature contains very limited data on the extent of the reduction in mortar and concrete permeability achieved by partially replacing cement with silica fume.

Objectives of Study

The major objectives of the proposed research are as follows:

1. Establishment of a quantitative relationship between permeability coefficients and the volume of permeable voids for plain cement and cement/silica fume mortars at a significance level of 0.1.
2. Determination of the effects of the silica fume/cement ratio on the permeability of mortars at various water to cementitious-material ratios.

Scope of Work

1. Permeability measurements are conducted on specimens with water/cementitious-materials ratios of 0.5, 0.6, and 0.7. Silica fume/cementitious-materials ratios of 0, 3.75, and 7.5 % by weight are evaluated. Curing periods of 3 and 7 days at a constant temperature of 80.6 to 82.4 degrees Fahrenheit (27 to 28 degrees centigrade) are used. All specimens are prepared with a constant sand-cement ratio of 3:1 by weight.
2. Cube specimens, identical to the permeability specimens, are cast to determine the volume of permeable voids according to ASTM C 642-90.
3. A correlation between the permeability values obtained from the permeability test and the volume of permeable voids obtained from ASTM C 642-90 is established.

CHAPTER II

LITERATURE REVIEW

Background

Research related to concrete permeability is focused on three areas and includes the development of new devices for measuring the rate of flow and determining permeability coefficients, evaluating the effects on permeability of using industrial by-products as mineral additives, and relating the microstructural characteristics of cement-based materials to the rate of fluid transport. This chapter includes a review of research done within each of these three major areas.

Test Methods and Apparatus

In 1929, McMillan and Lyse [25] performed a series of water permeability tests on 6-inches (150-mm) diameter samples of concrete and mortar with thicknesses of 1-inch (25.4-mm) and 2-inches (50.8-mm). They reported no difference between cast and cored samples of the same size. A schematic diagram of the test apparatus is shown in Figure 9 (Appendix B). The primary design consideration was that the apparatus could be easily duplicated and that the specimens could be rapidly inserted and removed. They used a variety of hydrostatic pressures between 20 psi (0.1379 MPa) and 80 psi (0.5516 MPa) with the maximum being 140 psi (0.9653 MPa). Initial tests on samples moist-cured for 28 days showed no measurable flow. The second series of samples was then moist-cured

for 3 to 7 days and air-cured for a period extending to 177 days.

The permeability was determined after 48 hours of testing in units of $\text{cm}^3/\text{hr}/\text{ft}^2$ with a range of 0 to $1600 \text{ cm}^3/\text{hr}/\text{ft}^2$. The results showed a decrease in flow with time and with reduced water/cement ratios. Continued hydration during testing and clogging of pores with fine particles were reported to be the main causes of decreasing flow with time. It was reported that a 50 to 70 percent difference in values was common for duplicate tests. The effects of gradation or proportion of aggregates with a constant water content were not evaluated.

The authors noted that the application of water pressure produces tensile stresses on the bottom side of the specimen. A 20 psi (0.1379 MPa) hydrostatic pressure on the one-inch (25.4-mm) thick mortar samples produced the same bending stress as an 80 psi (0.5516 MPa) pressure on the 2.0-inch (50.8-mm) thick concrete samples. No further analysis was presented as to how these stresses (tensile and compressive) may affect the pore structure and resulting flow characteristics.

The results obtained for concrete and mortar specimens were consistent in all regards, giving an indication that the apparatus was reliable. The authors concluded that the greatest factor influencing concrete permeability was the length of moist-curing and corresponding sample age at the time of testing. The second controlling factor was determined to be the water/cement ratio of the mix.

In 1931, Norton and Pletta [31], tested 34 cylindrical concrete samples 9.5-inches (241.3-mm) in diameter and 6.0-inches (150-mm) thick. The specimens were placed horizontally in a confining chamber with a stucco bedment used as a leak proof seal along the interface. The pressure head used for the majority of tests was 40 psi (0.2758 MPa). Only the inflow was measured and expressed in $\text{gal}/\text{ft}^2\text{-hr}$. They concluded that measuring the inflow was superior to measuring outflow since the latter is too small to record. In fact, the outflow face of the specimen was open to the atmosphere. The authors noted that in most cases, this surface remained dry during testing (40-50 hrs) although in some

tests, they reported the surface to be moist. Numerous comparisons of inflow rates were made, most of which exhibited a high degree of scatter. They did, however, report an apparent trend when comparing inflow with the cement void ratio e_c , defined as:

$$e_c = \frac{c}{1 - p}$$

where; e_c = cement void ratio

c = volume of cement / volume of concrete

p = density

In 1935, Ruettgers, et. al. [39] investigated the permeability of mass concrete. Using hydrostatic pressures up to 400 psi (2.758 MPa), a number of 6-inches (150-mm) x 12 inches (300-mm) cylindrical concrete specimens were tested. Several additional sizes were also evaluated including 6-inches (150-mm) x 6-inches (150-mm) and 18-inches (450-mm) x 18 inch (450-mm). The maximum coarse aggregate size was 4.5-inches (114.3-mm). The experimental apparatus is shown in Figure 10 (Appendix B).

Both inflow and outflow were recorded with outflow being collected in a jar. Corrections for evaporation from the jar and the surface of the specimens were made since both were open to the atmosphere which was maintained at 80% relative humidity. Samples were tested for 200 to 500 hours. The results indicate that the inflow rapidly decreases within the first 100 hours, and both inflow and outflow decrease linearly after approximately 200 hours.

The permeability coefficients were determined using Darcy's law for constant head, steady state flow. The authors used a different method for determining the quantity of flow "Q" which is as follows: at a time corresponding to one half the time required for observation of visible outflow plus 250 hours, a tangent was drawn on the cumulative inflow versus time graph. The slope (units of $\text{ft}^3/\text{sec.}$) was used as Q. The authors did not present any rational argument for using 250 hours plus half the time of visible outflow as a time criterion.

The main purpose of this work was to study the permeability of the mass concrete mix designs that were to be used in Boulder dam. The test mixtures reflected the final mix design composition with the exception of the maximum coarse aggregate size which was changed from 4.5-inches (114.3-mm) to 9-inches (228.6-mm) as used in the actual dam. Results were extrapolated for this aggregate size. By comparing the permeability coefficients of mixes with a w/c ratio of 0.5 and maximum aggregate sizes of 1.5-inches (38.1-mm) and 4.5-inches (114.3-mm), the authors reported that the maximum aggregate size is not a determining factor in permeability.

In 1938, Wiley and Coulson [44] presented what was called a simple test for water permeability of concrete. A concrete cup measuring 6 3/8-inches (161.9-mm) high x 3 3/8-inches (85.7-mm) diameter was filled with water to a predetermined height. A gage was placed inside the sample and the amount of water required to fill the cavity back to its original level was recorded daily. Samples were covered during the test to minimize evaporation. The claim was made that this procedure was not only simple but also eliminated the need for obtaining a leak tight seal between the specimen and the supply of the pressurized water. The permeability coefficients were determined by Darcy's law.

In a discussion of the Wiley and Coulson study, Wing [45] claimed that the test procedure was actually measuring water movement due to capillary action. This was the primary reason that results were 2 to 3 orders of magnitude higher than the results reported in the Boulder Dam investigation. It had been suggested that water may move faster due to capillary forces than under higher water pressures. It is not clear, however, that these two sets of data have a common basis for comparison. Wiley and Coulson made no mention of moisture being present on the exterior surface of the cup at any time during the testing period. Clearly, this implies a non-saturated condition as opposed to the approximate equal inflow and outflow rates reported by Wing, et.al. In addition, Darcy's law that was used to calculate the permeability coefficients presumes that the specimen is fully saturated.

In 1951, Cook [6] investigated the permeability of lean mass concrete. This investigation was mainly concerned with work that was being done at that time by the Corps of Engineers. Cylindrical samples 14.5-inches (368.3-mm) in diameter and 15-inches (381-mm) long were cast vertically in a steel mold which was sealed and placed horizontally to produce bleeding channels perpendicular to the flow of water during the test. The specimens were cured for 2 days at 50 degrees Fahrenheit (10 degrees centigrade), 5 days at 70 degrees Fahrenheit (21.1 degrees centigrade), and 3 months at 80 degrees Fahrenheit (26.7 degrees centigrade) after which they were stripped and sand blasted. The cylindrical surface of each sample was coated with a mixture of paraffin-resin and sealed in the testing chamber with hot asphalt. A hydrostatic pressure of 200 psi (1.379 MPa) was used to force tap water through the top of the specimen. The inflow was periodically checked for air content. When it exceeded 0.2 percent, the entire system was drained and refilled to minimize the effect of entrained air on the flow rate. A schematic of the apparatus is shown in Figure 11 (Appendix B).

It is clear that a more rapid and universally adaptable method of measuring concrete permeability was required. In 1961, Tyler and Erlin [43] proposed a method in which the rate and the total volume of pressurized water forced into a 6-inches (150-mm) diameter and 12-inches (300-mm) high concrete specimen were measured. Pressures ranging from 40 psi (0.2758 MPa) to 5000 psi (34.5 MPa) were used. The low pressure apparatus was essentially the same as used for high pressure determinations. All fittings were made leak proof including the top of the pressure vessel by means of molded rubber O-rings. The major drawback of this apparatus was a lack of reproducibility. In addition, the values of the calculated permeability coefficients were generally below those that had been obtained by other methods of permeability testing. It was suggested by Tyler and Erlin [43] that this method can be used for the determination of the relative permeability of different concrete mixtures.

Test procedures and equipment development favored the use of small specimen sizes

as compared to previous methods. Innovations were also evident in new methods of sealing the apparatus/sample interfaces.

In 1969, Meulen and Dijk [29], developed a permeability apparatus in which the specimen is placed in such a manner that water or air, under pressure, can be applied to one face of the sample and the amount of fluid that permeates through the specimen measured. The apparatus consists of a permeameter pot with a brass ring bolted to its base. The ring was designed with two circular solid neoprene sealing rings, one to seal the ring to the base of the permeameter, and the other to provide a seal between the ring and an epoxy resin casting surrounding the specimen. The epoxy resin ring was cast around the specimen and allowed to harden before the specimen was inserted in the brass ring on the base of the permeameter. The method was found to be an easy and reliable means of sealing permeability specimens into permeameter pots. An added benefit was that the samples could be used repeatedly without further preparation. A diagram of the apparatus, with a specimen in position, is shown in Figure 12 (Appendix B).

In 1973, Figgs [9] developed an apparatus for estimating the water permeability of in-situ concrete. In this method, pressurized water is injected in a hole drilled in the concrete. Water displaces all air within the apparatus and concrete cavity, and its meniscus is brought to a convenient position in a capillary tube. The time for the meniscus to travel 2.0-inches (50-mm) is taken as a measure of the water permeability of concrete. During laboratory evaluations, it was determined that the modified "Figg test" suffered several drawbacks. The most important was the lack of control of the moisture content of the concrete and uncertainty regarding the actual volume of concrete affected (i.e. the extent to which the water flows through the concrete under the conditions of the test). In addition, other problems appeared including the presence of air bubbles in the system and the lack of proper sealing. A schematic for the apparatus used for water permeability measurements is shown in Figure 13 (Appendix B).

In 1983, Hope and Malhotra [17], developed a test apparatus based on the same

principles as previous designs. The apparatus consisted of a series of pressure cells connected to a common hydraulic line which facilitated pressurization of the water of up to 500 psi (3.45 MPa). Each cell contained a cylindrical concrete sample 6-inches (150-mm) in diameter and 6-inches (150-mm) in height, through which water passed in the axial direction. The equipment design and preparation of the specimens ensured one-dimensional flow. The volume of water passing through the concrete sample was measured and recorded. This test method and apparatus were considered to present a valid means of determining the permeability coefficients for concrete mixes with a wide range of water-cement ratios and air contents.

Details of the pressure cells and the connection of the cells to a common pressure vessel are shown in Figures 14 and 15 (Appendix B), respectively. In this method, the hydraulic gradient can be easily varied, fluids other than water can be used, and the device can be modified to simulate actual field conditions to which the concrete was subjected. The authors recommended that this test method and apparatus be adopted by the Canadian Standards Association as a Canadian Standard Test Method.

In 1988, Bisailon and Malhotra [2], modified the apparatus developed by Hope and Mathotra [17]. Modifications were made in both sample preparation procedures and the hydraulic system. In the original test procedure, the sides of the concrete samples were sealed with a fibreglass resin compound to ensure uniaxial flow. However, this procedure was cumbersome and the resin occasionally developed cracks. Therefore, the resin was replaced by an epoxy mortar which eliminated cracking in the concrete jackets. The original vessel consisted of two closed hollow cylinders fitted with collars which were bolted together. The top section was connected directly to a nitrogen tank while the bottom section was connected via water filled lines to the pressure cells. When the gas pressure in the top of the vessel was increased by means of a valve on the nitrogen tank, a diaphragm was pushed downwards pressurizing the water in the lower half of the vessel. This increased the water pressure in the lines and, in turn, the pressure in each cell. The

intent of the diaphragm was to prevent the dissolution of nitrogen by water under pressure.

It was found that the diaphragm did not always fulfill its intended function, and nitrogen leaks occurred, forming bubbles in the water. Thus the measurement of water in the capillary tube was affected. The nitrogen pressure system was replaced by a constant pressure oil system which could provide pressures of up to 500 psi (3.45 MPa) in increments of 3 psi (0.02 MPa). The modifications made to the pressure system resulted in making the tests relatively simple to set up. However, these modifications did not contribute to any significant decrease in the variability of the permeability test results.

Janssen [19], developed an apparatus for laboratory permeability measurements of concrete samples obtained from existing highway pavements. Concrete cores 3-inches (75-mm) in diameter and 3 1/8-inches (80-mm) long were used. Samples were sealed in a brass sample ring 3 1/2-inches (90-mm) in diameter and 3 1/8-inches (80-mm) long using Dow-Corning concrete sealer which was allowed to cure overnight. Leakage between the cell top and base and the brass sample ring was eliminated by rubber O-rings and a thin film of silicone high vacuum grease. The water reservoir was made of an acrylic tube 4-inches (100-mm) in diameter and 1/4-inch (6-mm) wall thickness. A regulated air pressure source was used to pressurize the system to approximately 40 psi (0.2758 MPa). A cross section and schematic of the apparatus are shown in Figures 16 and 17 (Appendix B) respectively. This test method gave accurate and reliable results for a wide range of permeabilities and could be used with laboratory or field samples.

Ludirdja, Berger and Young [23], after attempting various modifications to existing equipment, undertook an entirely new approach. They used gravity induced flow to determine permeability. Test specimens were obtained from saw cutting either laboratory test cylinders or field cores. This approach has proved to be reliable and efficient. A schematic view of an "old" and a "new" version of the apparatus is shown in Figures 18 and 19 (Appendix B) respectively. Advantages of the new apparatus include eliminating

unnecessary drying that may cause cracking, providing the ability to change the pipette size at any time during an experiment, and eliminating absorption effects during the test.

Sullivan [41] described a permeability testing system which can accommodate up to seven samples simultaneously. The apparatus features a computer-controlled data acquisition system, thereby eliminating a source of operator error. The system consists of seven core holders of the Hassler type which can accommodate cylindrical samples ranging from 1.5-inches (38-mm) to 4-inches (100-mm) in diameter, and from 4-inches (100-mm) to 11-inches (275-mm) in length. A schematic diagram for a core holder is shown in Figure 20 (Appendix B). The confining and driving pressures can be independently varied up to 4000 psi (27.58 MPa). Stainless steel tubing was used so that the test medium could be either liquid (including brine) or gas. The automated control system utilizes a Hewlett Packard 200 series computer and a model 3497 data acquisition/control unit. This permeability testing system worked satisfactorily.

Reinhardt and Gaber [37] developed a new method for testing mortar permeability. Specimens were cast as circular plates 6-inches (150-mm) in diameter and 0.787-inches (20-mm) thick. The samples were embedded in a steel support ring with epoxy resin. A schematic of the apparatus is shown in Figure 21 (Appendix B). The water pressure acts on the lower side of the specimens while a perforated steel plate on the upper side prevents the specimen from breaking. The outflow is collected and weighed to within 0.1 gram. This appeared to be sensitive enough for most of the specimens. However, for very dense mortars with total flow as low as 1 gram per day, the results were within an error range of 20%. All specimens were water-saturated prior to testing. A water pressure of 145 psi (1 MPa) was applied during the first day, 290 psi (2 MPa) during the next day, and 580 psi (4 MPa) during the third day.

A substantial amount of data and numerous test procedures are cited in the Literature, however there is no recognized standard test method. Most permeability tests require the application of high pressure necessitating expensive equipment. The tests must

be conducted by skilled technicians further adding to the expense. In addition, there are numerous practical problems which make PCC permeability measurements difficult.

Problems with Permeability Measurements

The fact that a variety of PCC permeability measurement methods exist indicates that there are numerous problems encountered when measuring concrete permeability as indicated below. Research is ongoing on to develop test methods that minimize these problems.

Specialized Sample Requirements. Tests that require specially made samples are currently not applicable to field cores. Therefore they may not be realistic for special finishing and sealing applications.

Quantity of Flow. Typical permeabilities for medium and high strength portland cement concrete are approximately 10^{-10} cm/sec or less. For low hydraulic gradients and reasonable sample sizes, the quantity of flow through the sample is small. This was recognized by McMillan and Lyse [25], who resorted to reducing the moist curing period of their PCC samples to increase the permeability. This would not be applicable for field samples. Several solutions include longer time periods for measuring flow, high hydraulic gradients as used by the U.S. Army Corps of Engineers [6], or a combination of these.

Leakage At the Sample/Apparatus Interface. When high pressures are used to overcome the low flow problem, sealing a sample becomes quite difficult. Some researchers have resorted to tapered samples which are very difficult to produce from field samples, and may still leak if not properly made.

Effect of Air in PCC Voids. Air in a small pore effectively blocks water flow through that pore. Not only must a sample be saturated for reliable permeability measurements to be made, it must also remain saturated during the test. When high hydraulic gradients are used to increase the quantity of flow, the drop in pressure across the sample can cause air dissolved in the water to come out of solution, thereby decreasing permeability over time.

Expense of Equipment and Difficulty of Test. Due to the high cost of the equipment and the difficulty in performing permeability tests, the test is often omitted unless it is absolutely necessary. The result is a slow-down in the development of new approaches and test methods.

The inclusion of permeability criteria in specifications for certain concrete applications is likely to be mandated in the future. Some specifications may require values of permeability so low that they can not be measured by current techniques, the aim being to obtain permeabilities low enough to prevent ionic migration into concrete. In such cases more appropriate test methods are needed.

Table 1 presents a summary of the permeability apparatus outlined in this chapter. An abbreviated list of the advantages and disadvantages of each is included.

Effect of Silica Fume on Microstructure

The effects of adding silica fume to cement mortars include alteration of the composition and microstructure of the paste matrix and changes in the paste/aggregate interfacial bond.

Hooton [16] investigated the potential improvements to the permeability and pore structure of sulphate resistant portland cement pastes with various replacement levels of

TABLE 1

A SUMMARY OF THE WATER PERMEABILITY APPARATUS
DEVELOPED IN LITERATURE.

APPARATUS DEVELOPER	YEAR	ADVANTAGES	DISADVANTAGES	REFERENCE #
McMillan and Lyse	1929	<ul style="list-style-type: none"> • Easily duplicated. • Rapid insertion and removal. • Consistent results. • Reliable. 	<ul style="list-style-type: none"> • Development of tensile stresses at specimen's bottom. 	25
Norton and Pletta	1931	<ul style="list-style-type: none"> • Reliable. 	<ul style="list-style-type: none"> • Specimen outflow face is open to atmosphere. 	31
Ruettgers, et. al.	1935	<ul style="list-style-type: none"> • Flow measurements at steady state conditions. • Studied the effect of aggregate size on permeability. 	<ul style="list-style-type: none"> • No explanation given for the used criteria of steady state. 	39
Wiley and Coulson	1938	<ul style="list-style-type: none"> • Simple and inexpensive test. • No water evaporation. • Eliminates leakage. 	<ul style="list-style-type: none"> • Results are not consistent with other studies. • Tests were performed in a non-saturated condition. 	44
Cook	1951	<ul style="list-style-type: none"> • Minimizes the effect of air-entrainment. 	*	6
Tyler and Erlin	1961	<ul style="list-style-type: none"> • Used high pressure. • The used fittings eliminate leakage. 	<ul style="list-style-type: none"> • Lack of reproducibility. • Permeability coefficients were below those obtained by others. 	43
Meulen and Dijk	1969	<ul style="list-style-type: none"> • Easy and reliable means of sealing specimens. • Samples of specimens could be used repeatedly without further preparation. 	*	29

TABLE 1 (cont)

APPARATUS DEVELOPER	YEAR	ADVANTAGES	DISADVANTAGES	REFERENCE #
Figgs	1973	<ul style="list-style-type: none"> • Estimates the permeability of in-situ concrete. 	<ul style="list-style-type: none"> • Lack of control of the moisture content of the concrete. • Uncertainty regarding the actual volume of concrete affected. • The presence of air bubbles in the system. • Lack of proper sealing. 	9
Hope and Malhotra	1983	<ul style="list-style-type: none"> • Tests more than one specimen simultaneously. • Ensures one-dimensional flow. • Fluids other than water can be used. • The hydraulic gradient can be easily varied. • The device can be modified to simulate actual field conditions. 	<ul style="list-style-type: none"> • Cumbersome procedure for sealing specimens. 	17
Bisailon and Malhotra	1988	<ul style="list-style-type: none"> • Better procedure for specimen sealing than the Hope and Malhotra device. • Prevents the dissolution of gas by water under pressure. • Simple to set up. 	<ul style="list-style-type: none"> • Formation of bubbles in water still occurs. • High variability in test results. 	2
Janssen	1988	<ul style="list-style-type: none"> • Can be used with laboratory or field specimens. • Eliminates leakage. • Accurate and reliable results. 	*	19

TABLE 1 (cont)

APPARATUS DEVELOPER	YEAR	ADVANTAGES	DISADVANTAGES	REFERENCE #
Ludirdja, Berger and Young	1989	<ul style="list-style-type: none"> • Can be used with laboratory or field specimens. • Reliable and efficient. • Eliminates unnecessary drying. • Provides the ability to change the pipette size during an experiment. • Eliminates absorption. 	*	23
Sullivan	1988	<ul style="list-style-type: none"> • Accommodate up to seven specimens simultaneously. • Utilizes computer-controlled data acquisition system. • Tests specimens of different sizes. • The pressure can be independently varied. • Can use either liquids or water. 	*	41
Reinhardt and Gaber	1990	<ul style="list-style-type: none"> • Eliminates tensile stresses caused by high pressures. • Low variability. • Easy check for leakage. 	*	37

* No reported data.

fly ash, slag, and silica fume at water/cementitious material ratios of 0.25, and 0.36. The results were presented in terms of water permeability and pore size distribution after 7, 28, 91, and 182 days of moist curing. It was observed that silica fume was the most effective mineral additive in reducing the permeability at early ages. In addition, silica fume was the most effective in reducing the amount of calcium hydroxide present in the hydrated matrix. The author observed that 20 percent replacement by volume of silica fume completely eliminated calcium hydroxide after 91 days moist curing.

Cohen and Klitsikas [5] reviewed selected papers to document details of the pozzolanic reaction and the subsequent mechanisms by which silica fume affects strength development. They stated that three mechanisms are associated with this process: pore-size refinement and matrix densification, reduction in the content of calcium hydroxide, and cement-aggregate interfacial refinement. They concluded that the high water demand and the premature hardening observed in silica fume-portland cement pastes are caused by the formation of a silica-rich, calcium-poor "gel" which forms coatings on the surfaces of the silica fume and causes agglomeration of the particles. With time, this "gel" starts dissolving thereby allowing the silica fume particles to react with calcium hydroxide to form calcium-silicate hydrates.

Rosenberg and Gaidis [38] proved experimentally that the inclusion of silica fume in concrete does not densify the concrete in the usual sense or reduce its porosity. However, they emphasized that the presence of silica fume enhances the paste-aggregate bond which is the weakest part of concrete. They attributed this enhancement to the reduction in the amount of bleed water produced. The authors cited chemical and physical evidence to support their conclusions.

A study of the effect of condensed silica fume on the microstructure of the interfacial zone in portland cement mortars was conducted by Bentur and Cohen [1]. They concluded that the microstructure of the interfacial zone, extending to about 1.96×10^{-3} -inches (50 micrometers) from the sand grain surface is significantly different from that of

the bulk paste matrix away from the sand grain. This area is characterized by a thick calcium hydroxide layer engulfing the sand grain and by some channel-type gaps. They suggested that the formation of this zone could be due to the presence of some water-filled gaps that form around the sand grains as a result of bleeding and inefficient filling with cement particles that takes place in the vicinity of the sand grain surface. A number of very porous hydration products have been observed in the interfacial zone. They concluded that, when 15% condensed silica fume by weight of cement is added to the mortar, the microstructure of the interfacial zone is significantly changed. Its structure is homogeneous and dense without the presence of a thick calcium hydroxide layer or water-filled gaps. These changes could be the result of the suppression of bleeding in the fresh mortar and the ability of the condensed silica fume particles to fill the space in the vicinity of the sand grain surface much more efficiently than the larger cement particles.

Buil and Delage [3] evaluated a silica fume-calcium hydroxide-water mixture in an effort to characterize the pore structure in portland cement mortars modified by silica fume. The mixture contained 80 percent silica fume particles, 20 percent calcium hydroxide crystals, 0.41 water to solids ratio, and a superplasticizer content of 4 percent by weight of silica fume. The existence of large voids corresponding to the initial calcium hydroxide crystal sites which were not filled by precipitation after the 28 days hardening period was evidenced. These observations provide a reasonable explanation for the appearance of coarse pores in the range of 1-2 micrometers that were observed earlier in hydrated silica fume mortars by one of the authors. The results of this study were in accordance with what has been observed before with silica fume mortars [8,13] and with the interpretation provided by one of those authors [13].

Feldman [11] investigated the effect of adding silica fume on the microstructure of mortars at different sand/cement ratios. He prepared cement mortars containing 0 and 10 percent silica fume at a water/(cement+silica fume) ratio of 0.6 and sand/cement ratios of 0, 0.5, 1.0, 1.5, 1.8, 2.0, 2.25, and 3.0. Pore-size distributions were studied by mercury

intrusion and reintrusion. The pore volume was calculated as a percent of the paste volume and not the total volume of the mortar to exclude the effect of inclusion of different proportions of the nonporous sand. Pore size distributions were based on four ranges of pore sizes corresponding to (97-0.875, 0.875-0.175, 0.175-0.0175, and 0.0175-0.0029) $\times 10^3$ nm. The study concluded that pores of the coarsest two ranges are formed at the sand/paste interface in mortars. The pore volume increases with sand/cement ratio in mixes with and without silica fume. The effect of adding silica fume is such that it increases the largest coarse pore component, but since a portion of these pores is relatively inaccessible, the addition of silica fume will eventually reduce permeability. It was also determined that the use of mercury intrusion partly breaks the pore structure by entering the large pores at high pressures.

Ping et.al [33] studied the structural features of the transition zone between granular aggregate and portland cement paste. Two types of aggregates were used, quartz and limestone. They used a parameter referred to as "interfacial excess conductance" to characterize the transition zones structurally. This parameter is based on electrical conductivity methods. The experimental results indicate that the transition zones between quartz particles, as well as larger limestone particles, and portland cement paste are always less dense than the bulk paste, regardless of the aggregate size, and that the thickness of these transition zones decreases with the decrease of aggregate size. Conversely, a transition zone denser than bulk paste occurs when smaller limestone particles are used. They attributed this phenomenon to the possibility of a chemical interaction between the limestone particles and the portland cement paste.

Marusin [27] used Scanning Electron Microscopy (SEM) to study the microstructure and pore characteristics of concretes containing condensed silica fume (CSF) and superplasticizer. The mixes evaluated contained 360 kg/m³ type I portland cement, an air-entraining agent, water cement ratios of 0.35 to 0.38, and 2.5, 5, and 10 percent condensed silica fume by weight of cement. The SEM examination was made

using 4-inch (100-mm) concrete cube samples that were vibrated and cured in sealed plastic bags containing a wet sponge for 21 days. Marusin performed compressive strength tests and absorption tests on these samples. He found that with an increasing amount of condensed silica fume in concrete, the microstructure became very dense in texture. He believed that it is the dense microstructure that contributed to the high compressive strength values which increased with increasing amounts of CSF. Based on his experience, he recommended that the optimum CSF content to use is approximately 10 percent by weight of cement.

Kayyali [22] observed changes in the porosity of concrete as compared with the individual porosities of the cement paste and aggregates. This study involved the measurement of porosities for concrete and the corresponding portland cement paste using 9 types of ground aggregate, two different cement/aggregate proportions, and two curing periods. The porosities of the nine aggregate types used in the study were determined by the author in a separate study. It was observed that the porosity of concrete is higher than that of the aggregate used in the mix but lower than the porosity of plain paste with the same w/c ratio and curing conditions as that of the cement paste matrix. The author interpreted this observation as an indication of the presence of an interfacial layer at the surfaces of the aggregate. This interfacial zone has a very low porosity. This zone makes a great amount of aggregate pores unintrudable, thus the typical features of plain paste become more dominant over typical features of the aggregate.

Permeability and Microstructural Properties

There is a growing awareness of the importance of permeability with regard to the long-term durability of concrete structures. A renewed interest in this subject has led to the development of numerous permeability and related test procedures. Each of these test procedures has a number of problems related to performing the test or interpreting the

data. Therefore, researchers have expanded the realm of work to include substitute methods that can be used to estimate permeability in lieu of conducting the more complex flow testing. The need for incorporating permeability limits in concrete specifications has resulted in numerous "new" procedures.

A significant amount of research has been conducted to establish relationships between permeability coefficients and the properties of the pore structure that can be easily measured. Examples of these properties include pore size distribution and the volume of pores larger than specific radii.

Powers and Brownyard [34] developed an equation based on concepts adopted by Carman [4] for flow in granular materials. The equation estimates the permeability coefficient in terms of the density of the fluid, a gravitational constant, the viscosity of water, and other paste-related factors. These paste-related factors include a tortuosity-shape factor, volume of the specimen, a surface area factor, the weight of evaporable water, and an evaporable water factor. Attempts at verifying this equation indicated fundamental discrepancies and the Carman approach was set aside.

In 1958, Powers et. al. [35] presented a theory of permeability of cement paste utilizing the Steiner concept of viscous drag on concentrated suspensions. The development accounted for variable water viscosity due to the colloidal microstructure of the paste and particle concentration effects proposed by Hawksley. The equation developed gives the permeability coefficient in terms of parameters including pore diameter, porosity, and several other constants. The permeability coefficients computed by this equation were compared with the corresponding measured permeability coefficients at various temperatures. A very good agreement was indicated between the observed and calculated values.

Garboczi [14] reviewed popular theories that relate pore structure to permeability coefficients. The author outlined the features that make a reasonable Pore Structure-Transport theory (PST). First, the theory must be based on experimental parameters of

the pore structure that are reproducible, simply interpreted, and are directly relevant to transport properties. Second, the PST must be able to formulate these measured parameters into a prediction using mathematical principles that are relevant for the random geometry of the pore space. Finally, the PST must be applicable to a single sample, and not be dependent on analyzing a series of samples related in some way. After a discussion of many PST theories, the author concluded that the Katz-Thompson [20,21,42] is the only PST which fits all three criteria. This PST is based on an electrical conductivity measurement or a diffusivity measurement and a pore diameter measurement determined from a mercury intrusion, both well-defined pore space parameters with direct relevance to transport. In addition, these parameters are combined into an equation using the mathematics of percolation theory which was originally formulated to deal with the random geometry of pore spaces. The author demonstrated the applicability of the Katz-Thompson permeability equation to determine the coefficient of permeability of 0.4 w/c paste with good agreement with experiment results.

Garboczi reviewed several parameters that had been formulated into permeability prediction models in the Literature. Katz and Thompson defined the critical pore diameter, d_c , as the minimum diameter of pores that are geometrically continuous throughout all regions of the hydrated cement paste. The importance of d_c on permeability is obvious since only the pores with diameters greater than d_c contribute significantly to water flow through a sample. The critical pore diameter is identical to the threshold diameter described by Winslow and Diamond [47], and is similar to the maximum continuous pore radius ($0.5 d_c$) described by Nyame and Illston [32].

Reinhardt and Gaber [37] performed an experimental and theoretical study with the aim of quantifying pore size distribution curves and correlating them with water and oxygen permeability. Twenty mortars have been investigated which contained portland cement, blast-furnace slag cement, and silica fume as binders. The water/cement ratios varied between 0.4 and 0.75 and two curing conditions were used. By the use of mercury

intrusion porosimetry, the pore size distribution was determined. Water and oxygen permeability have been measured under steady-state conditions. The authors calculated a parameter called "equivalent pore size" which quantifies the pore size distribution by a single number. This number is not a constant but depends on the physical transport mechanism. The authors stated that equivalent pore size and porosity are sufficient to predict the physical properties with acceptable accuracy.

Hughes [18] developed a simple model, based upon Poiseuille's formula, to relate the coefficients of permeability for hardened cement pastes to their pore size distribution. Tests were made on Ordinary Portland Cement (OPC), OPC containing Pulverized Fly Ash (PFA), and Sulphate Resisting Portland Cement (SRPC) cured for 1, 4, and 12 weeks in a calcium hydroxide solution. Pore size distribution was determined by using a two-stage mercury intrusion technique. The model was shown to yield a reasonable correlation with the experimental determination of permeability for the OPC pastes and on SRPC paste cured for 4 weeks. The correlation was not adequately strong for the OPC pastes that contained PFA. The author commented that this could be a consequence of structural damage during mercury intrusion in such pastes.

Hooton [16], in an evaluation of the parameters used in the literature to characterize pore structure, reported several relationships that were established between permeability and the volume of pores larger than specific radii including 0.079 [26], 0.075 [15], 0.059 [10], and 0.030 [28] micrometers. However, based on Hooton's experimental data, none of these parameters could be uniquely related to permeability. Hooton attributed the lack of a definite relationship to the use of the mercury intrusion porosimetry technique which results in damage to the pore structure and therefore does not adequately describe the pore size distribution. In addition, the mercury intrusion porosimetry measurements are performed on dried specimens while the permeabilities were measured on water saturated samples. Hooton concluded his review by stating that "no reliable method of accurately predicting permeability from other, more easily attainable properties is presently offered".

In an attempt to find a rapid test procedure that can be used reliably to estimate permeability, Whiting [47] investigated the rapid chloride permeability test (AASHTO T 277) and the test for determining the volume of permeable voids (ASTM C 642). Whiting found, by regression analysis, that the results of the test of the volume of permeable voids (ASTM C 642) correlate reasonably well with the results obtained from the permeability tests conducted on concrete samples. However, the existence of such a correlation still needs to be verified for mortars.

During the past two decades, significant emphasis has been placed on the use of pozzolanic admixtures, such as fly ash, silica fume, slag, and natural pozzolans in concrete. At the present time, there are few concretes that are made without the addition of pozzolanic admixtures. The primary beneficial effects of pozzolans in concrete are improved strength and durability. The most commonly used pozzolanic admixtures are fly ash and silica fume. However, the use of silica fume on a commercial basis is still somewhat limited.

The introduction of silica fume in concrete has challenged the standard mix design procedures and construction practices established for plain cement concrete. The behavior of cement-based materials containing silica fume is an area of active investigation. Several conferences have been organized to present research on the effects of silica fume on reducing concrete permeability [24,48]. However, very little information exists in the Literature regarding the effects of silica fume on reducing water permeability for mortars.

As discussed above, the Literature suggests that the permeability should be related to pore structure properties [18], particularly those which can be easily measured [47]. The purpose of the proposed research is to address this topic by defining a quantitative relationship between the volume of permeable voids determined by ASTM C 642 and permeability coefficients for type I portland cement and cement/silica fume mortars.

A significant aspect of the research is that it determines the effects on permeability of using silica fume as a mineral additive. The Literature contains very limited data on the

extent of the reduction in mortar and concrete achieved by partially replacing cement with silica fume.

CHAPTER III

RESEARCH METHODOLOGY

This chapter outlines the research methodology employed in this study. In addition, the features of the permeability apparatus are detailed. The experimental work includes two test procedures which were performed concurrently. The first is the permeability test procedure and the second is the test procedure for determining the volume of permeable voids.

Test Apparatus

The permeability test apparatus consists of three permeability cells and associated piping and valving. Each cell consists of the same sub-assemblies and is constructed of stainless steel and inert plastics. These materials eliminate the corrosion problems that were encountered in earlier studies. The apparatus is capable of sustained pressures of 1500 psi (10.3 MPa).

Three samples may be tested simultaneously. The design of the apparatus and the sample configuration ensures one-dimensional flow. Specific details of the subassemblies are included in the following sections.

Permeability Cells

Design Details

The permeability cells and the hydraulic system are constructed of stainless steel and inert plastics. The system was built such that up to three samples are subjected to equal, constant, and externally controlled hydrostatic pressure. Details and dimensions of a typical permeability cell are shown in Figure 1. The permeability cell consists of three main parts:

1. A 5-inch (127-mm) diameter and 1 3/8-inch (35-mm) thick cell base, machined in the center so that the sample cylinder is a snug slip fit. An O-ring is used to ensure a watertight seal. A fluid feed is provided in the base so that water is delivered uniformly over the sample face at a predetermined pressure.
2. A sample cylinder 2 1/4-inches (57-mm) outside diameter, 2-inches (50-mm) long, with fine threads machined at an inside diameter of 1 1/4-inches (32-mm). Threaded annular rings 1 1/4-inches (32-mm) in diameter were used to secure the sample in the sample cylinder. Neoprene O-rings are forced against the sample and the cylinder wall thereby eliminating sample/cylinder leakage.
3. The cell top is of the same dimensions as the cell base with only a slight modification. A 1/4-inch (6-mm) tapped hole is provided to allow attachment of a nylon tube fitting reamed to accept a micro-pipette. The micro-pipette is used to measure the amount of flow through the sample in a specified time interval. The three cell components are assembled using three 1/4-inch (6-mm) high tensile bolts. The bolts ensure a tight seal between the cell base, sample cylinder, and cell top by compressing the annular O-rings.

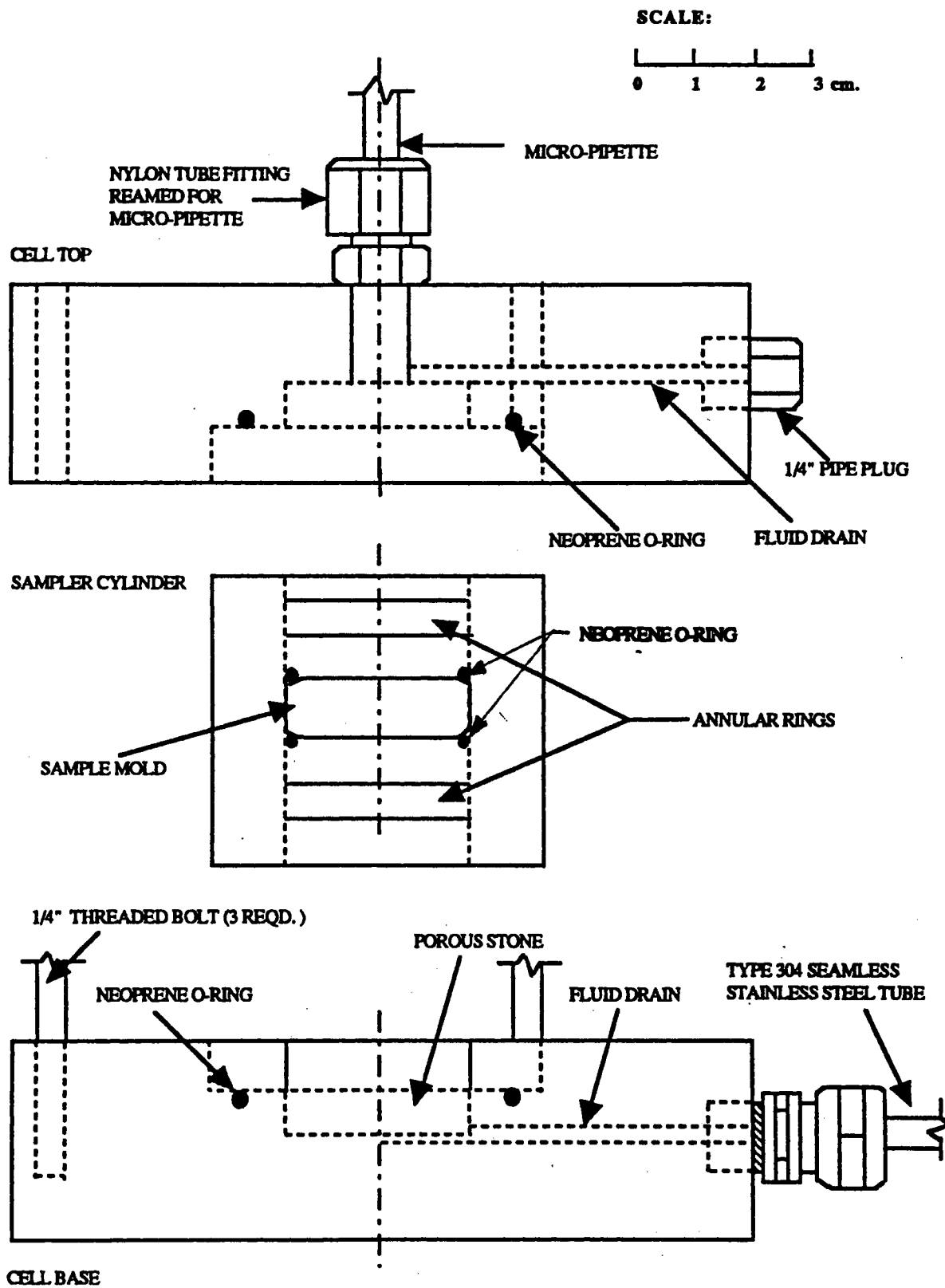


Figure 1. Construction of Permeability Cell Developed by Ayers and Elazouni

Assembly of Permeability Test Apparatus

The permeability cells and fluid delivery system are permanently attached to a reinforced frame. A schematic of the apparatus is shown in Figure 2.

All cells are connected to the fluid delivery system by means of 1/4-inch (6-mm) diameter, type 304, seamless stainless steel high pressure tubing. Each cell is connected to a 1/4 inch (6-mm) stainless steel high pressure ball valve which controls the flow of fluid into the cell. The fluid is stored in a stainless steel cylinder which is maintained half full to account for elevation head. The top of the cylinder is connected to a nitrogen cylinder through a check valve and pressure regulator. The nitrogen pressure in the fluid cylinder is indicated by a gage connected to the top of the cylinder. A one-inch (25.4-mm) thick layer of highly viscous mineral oil is poured on the top of the water in the cylinder to prevent nitrogen entrainment. Since all fittings, tubing, valves, cylinder and permeability cells are made of stainless steel, the apparatus allows the use of corrosive fluids. The entire apparatus is capable of sustaining pressures of 1500 psi (10.3 MPa).

Test Program

Type I portland cement and cement/silica fume mortars were evaluated in the study. The test program includes measuring the permeability of 1.0-inch (25.4-mm) diameter x 0.32-inch thick (8-mm) mortar discs and determining the volume of permeable voids of 2.0-inches (50.8-mm) mortar cubes.

The mortar specimens, evaluated in the test program, have a common sand/cementitious ratio of 3:1 by weight and water/cementitious-material ratios of 0.5, 0.6, and 0.7. Type I portland cement and commercially available silica fume were used to prepare all specimens. Mortar specimens with cement replacement of 0, 3.75, and 7.5 percent by equal weight of silica fume were evaluated after curing periods of 3 and 7 days.

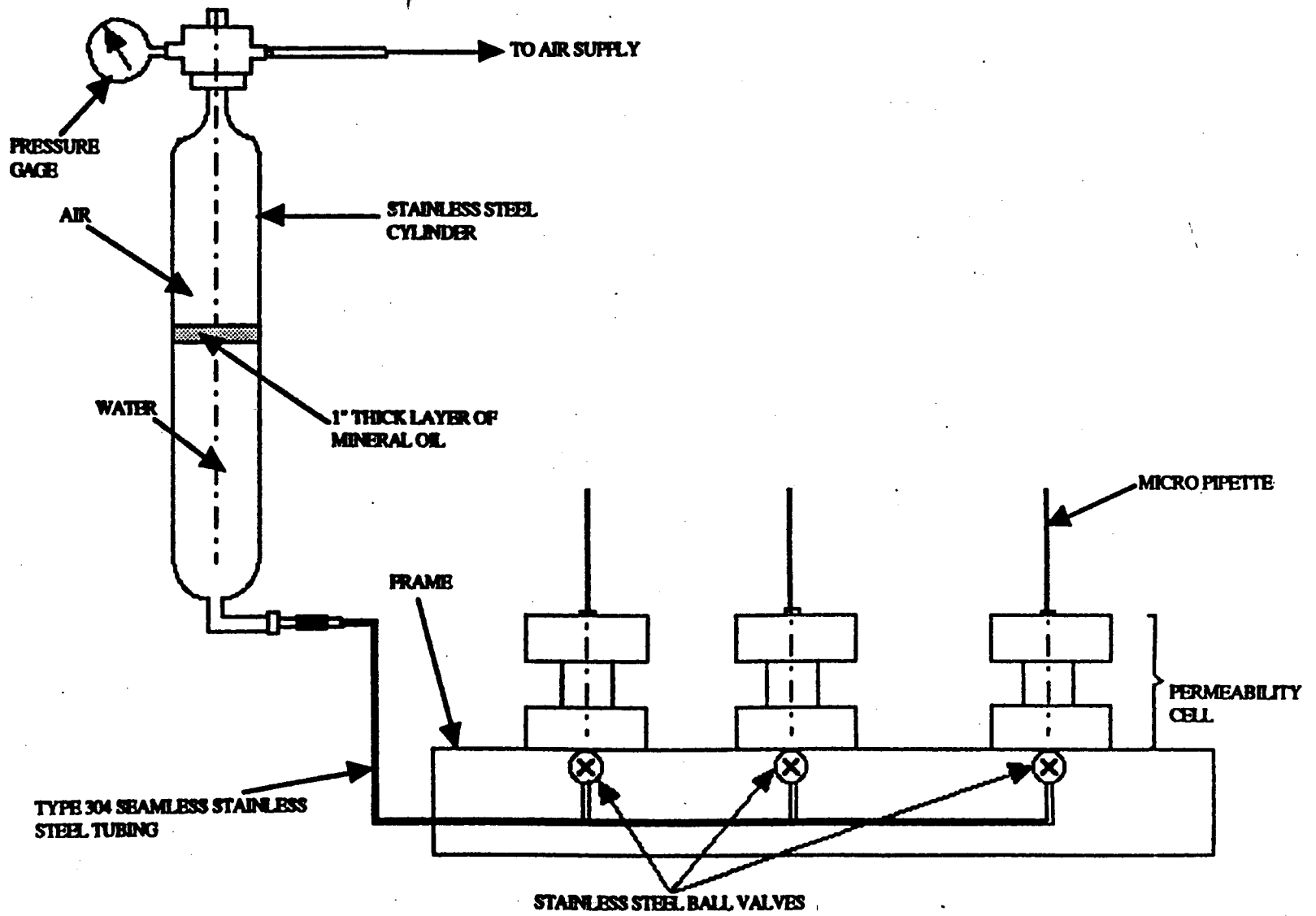


Figure 2. Schematic of the Apparatus Developed by Ayers and Elazouni

A uniformly graded silica sand was selected to maintain uniform aggregate-paste interface characteristics throughout the specimens. The gradation of the silica sand is shown in Table 7 (Appendix A). The gradation selected ensures that the sand is uniformly distributed throughout the specimen and to facilitate specimen preparation.

Generally, the extreme fineness of silica fume particles significantly increases the water demand in the mortar mixes. However, through preliminary experimentation, the water/cementitious-materials ratios and the silica fume/cement ratios were selected to allow uniform sample preparation without the use of superplasticizers. Therefore, the use of superplasticizers was eliminated in order to limit the number of variables in the study.

The experimental program included 18 sets of specimens, each set consisting of three replicate 1.0-inch (25.4-mm) diameter x 0.32-inch thick (8-mm) disc specimens for permeability measurements and three replicate 2.0-inches (50.8-mm) cube specimens for determining the volume of permeable voids. The six specimens were prepared from the same mortar batch and cured under the same conditions. The 18 sample sets were divided into three equal groups prepared at water/cementitious-materials ratios of 0.5, 0.6, and 0.7. The six sets included in each group represented specimens with three levels of silica fume replacement corresponding to 0, 3.75, and 7.5 percent by weight and cured at two curing periods (3 and 7 days).

Preparing mortar for one set of specimens (3 discs and 3 cubes) requires 750-grams of silica sand, 250-grams of cementitious materials, and the required weight of distilled water. Dry mixing of all ingredients was done prior to adding water to ensure homogeneity. Hand mixing was continued until the mix was uniformly blended.

The permeability specimens were cast in internally-threaded plexiglass molds to ensure a leakproof mortar/mold interface. The molds were fabricated by machining a plexiglass tube. The outside diameter of the mold is 1.39-inches (35-mm), the inside diameter is 1.0-inch (25-mm) and the height is 0.32-inch (8-mm). The top and bottom faces of the mold were chamfered for placement of the neoprene O-rings used to seal the

samples in the permeability cells.

The permeability specimens were prepared by affixing molds to a temporary base plate with melted paraffin at the mold/base-plate interface. A silicone release agent was sprayed on the plate to facilitate removal of the discs after curing. The mortar was placed in two layers and each layer was rodded 16 times over the area of the specimen. A collar with an internal diameter equal to that of molds was used to compact the top layer so as to avoid disturbance of the material with the compacting rod. The excess mortar was struck off even with the top edge of the mold.

The cube specimens were cast in a three-compartment 2.0-inch (50.8-mm) mold. The joints between the mold sections were brushed with paraffin to eliminate leakage and maintain the target water/cementitious-materials ratio. A silicone release agent was used to facilitate removal of the cubes after curing and to eliminate sample contamination. Mortar placement was done in two layers; each layer was vibrated for 5 seconds on a vibrating table to eliminate excess voids due to placement. The excess mortar was struck off flush with the top edge of the mold.

After casting, the specimens were placed in a moist room maintained at 80 percent relative humidity and approximately 77 degrees Fahrenheit (25 degrees centigrade) for 24 hours. The specimens were then removed from the moist room and immersed in a water bath maintained at a temperature of 80.6 to 82.4 degrees Fahrenheit (27 to 28 degrees centigrade) until testing.

Following the specified curing period, the three cubes and three discs were removed from the water bath. The three discs were placed in the permeability apparatus shown in Figure 2. The pressure head on the specimens was kept constant and was a function of the specimen permeability. The specimens were tested until a steady state flow condition was reached. The rate of flow through the specimens was measured periodically by means of the micro pipettes attached to the top of each permeability cell. The permeability coefficients were calculated based on the rate of flow in the steady-state condition. The

test for determining the volume of permeable voids was performed simultaneously on the three cube specimens according to ASTM C 642.

Test Procedure for Permeability Measurements

The permeability tests assess the flow of pressurized, air-detrained water through the mortar specimens. The amount of water passing through the mortar specimens was measured by means of micro pipettes.

Leakage at the specimen/cylinder interface was a major concern during the preliminary experimentation stage because of the use of high water pressures of 270 psi (1.86 MPa). However, leakage problems were alleviated by coating the fine threads of the permeability cylinder with Dow Corning High Vacuum grease. The cylinder was fitted in the cell base with the lower annular ring and neoprene O-ring at approximately one third of the cylinder height as measured from the cell base. Water was injected to the level of the O-ring by means of a serological syringe in an effort to eliminate trapped air under the specimen. The specimen was positioned above the lower annular ring and neoprene O-ring. A second neoprene O-ring was secured in the top chamfered edge of the specimen. The upper threaded annular ring was then tightly fastened, forcing the specimen against the O-rings at both ends, ensuring a leak-proof seal.

After tightening the top annular ring, water was injected in the space above the specimen up to the top of the cylinder. The water was added to reduce the time required to initiate water flow through the micro-pipette. As a final step, the cell top was fitted to the cylinder, the base and top bolted together for a leakproof fit, and the micro-pipette connected to the cell top.

Leakage at the mortar/mold interface was encountered at high water pressures. Using molds with thicker walls and threading the internal wall of the mold alleviated the problem by providing an effective mechanical bond between the hardened mortar and the

mold. Since the minimum curing period was 3 days, high pressures were used without the possibility of specimen erosion.

The flow through the specimens was measured by observing the water rise in the micro-pipettes as a function of time until it reached steady state flow. Steady state flow was reached when the difference between two successive readings was less than 20 percent. Permeability coefficients were calculated using Darcy's law for uniaxial steady state flow.

Darcy's Law for Uniaxial Water Flow

Darcy's law for uniaxial water flow through a saturated medium states that:

$$Q = k i A$$

where,

Q = Volume of water flow per unit time (cm^3/sec)

A = Cross-sectional area of the sample (cm^2)

k = Coefficient of permeability (cm/sec)

i = Hydraulic gradient ($\text{cm head}/\text{cm}$)

The hydraulic gradient is defined as the pressure differential across the specimen divided by the height of the specimen.

The pressure at the bottom of the specimen was assumed equal to the pressure in psi indicated by the gage affixed to the fluid cylinder. The pressure at the top of the specimen was always assumed to be zero in terms of gage pressure. The elevation head was minimal and therefore neglected in the calculations.

Assuming the pressure differential across the specimen is (P) psi, the specimen diameter was 1.0-inch (25-mm) and the specimen height was 0.32-inch (8-mm), the values of P , A , i , and k were calculated as follows:

$$P = \frac{p \times 6.895}{101.3} \times 10.34 \times 100 = 70.379p \text{ cm}$$

$$A = \frac{3.14 \times (1.0 \times 2.54)^2}{4} = 5.06 \text{ cm}^2$$

$$i = \frac{70.379p - 0.0}{0.31 \times 2.54} = 89.38p \text{ cm/cm}$$

$$k = \frac{q}{3600 \times 89.32p \times 5.07} = \frac{q}{p} \times 6.13 \times 10^{-7} \text{ cm/sec}$$

The validity of Darcy's law to determine the coefficient of permeability depends on the following assumptions:

1. The degree of saturation at the start of the test is uniform throughout the specimen.
2. The penetration of water is uniform.
3. Back pressure from air compressed within the mortar specimens is negligible.
4. Compressibility of the specimens is neglected.
5. Humidity within specimens at the time of testing is 100 percent (no tension in water)
6. Flow through the specimens is laminar. Because portland cement concrete and mortar permeability values are not often required to a high degree of precision and the hydraulic gradients are low, the laminar/turbulent error is ignored.

Determination of Relative Permeability

Using the ASTM C 642-90 Procedure

The relative permeability of the mortar specimens was determined in order to

compare and correlate the test results with those obtained from the permeability apparatus.

ASTM test specification C 642-90 entitled "Specific Gravity, Absorption and Voids in Hardened Concrete" was used to determine the relative permeability of the specimens in terms of percent volume of permeable voids. The procedure is outlined below:

1. The specimens were weighed in a saturated surface dry (SSD) condition and then oven dried for a minimum of 24 hours at a temperature of 300-310 degrees Fahrenheit (100-110 degrees centigrade). After removal from the oven, the specimens were allowed to cool in a desiccator and were weighed. The drying and weighing procedures were repeated until the difference between two successive dry weights was less than 0.5 percent. The final dry weight was designated as (A).
2. The specimens were removed from the desiccator and immersed in water for approximately 48 hours or until two successive weights were within 0.5 percent. The SSD weight of the specimens was designated as (B).
3. Following step 2, the specimens were boiled in water for approximately 5 hours, and then allowed to cool in the water for a minimum of 14 hours. The SSD weight was obtained and designated as (C).
4. Following immersion and boiling, the specimens were suspended and weighed in water. This weight was designated as (D).
5. The percentage volume of permeable voids was determined from the relationship:

$$V_p = \frac{C - A}{C - D} \times 100$$

Where;

V_p = Volume of permeable voids (percent)

A = Weight of the oven dried specimen in air (grams).

C = Weight of the SSD sample in air after immersion and boiling (grams).

D = Weight of sample in water after immersion and boiling in (grams).

CHAPTER IV

EXPERIMENTAL RESULTS AND DISCUSSION

Experimental Results

The rate of water flow through the permeability specimens and the corresponding time measured from the moment the water is first observed in the micro pipettes are presented for the 18 sample sets in Appendix C. Generally, the rate of water flow through specimens decreases with time. The time-flow relationships obtained as a function of time are consistent with those in the literature. The prominent characteristics of time-flow relationships are that the flow rate decreases very rapidly initially and then decreases slowly until it approaches a relatively constant or steady state flow. It is mandatory for the application of Darcy's law and the comparison between different specimens to measure the flow rate in the steady-state condition. Table 8 (Appendix A) presents the flow rates for the specimens tested in the permeability apparatus. The sample dimensions and corresponding water pressures used in the tests are summarized in Table 9 (Appendix A).

Table 10 (Appendix A) presents the permeability coefficients for all the specimens tested. Although the three replicates within each set were prepared, cured, and tested under nearly identical conditions, it was observed that the permeability coefficients vary appreciably. A measure of the variability in permeability coefficients is the coefficient of variation which is defined as the ratio between the standard deviation and the average of the test results for one set. As shown in Table 10 (Appendix A), the coefficients of variation ranged from 1.3 to 106.4 percent. This level of variation is comparable to those

reported in the Literature.

Table 2 presents the average permeability coefficients for all sets. The average permeability coefficient ranged from as low as 3.56×10^{-11} cm/sec to as high as 522×10^{-11} cm/sec. This wide range of the average permeability coefficient is attributed to the variability in material composition, the curing period, sample preparation, and the precision of the test method.

The ASTM 642 C procedure was followed to determine the volume of permeable voids. Table 11 (Appendix A) presents the percentage volume of permeable voids for the tested specimens and the coefficient of variation between the replicates involved in each set. Generally, the variation within the three replicates is very low. The average percentage volume of permeable voids for each set of replicates are presented in Table 2. The average percentage volume of permeable voids ranged from 15.08 to 24.49 percent and depended on the silica fume content, the curing period, and primarily the water/cement ratio.

Effect of Water/Cement Ratio

Figures 3 and 4 show the relationship between the water/cement ratio and the permeability coefficients and water/cement ratio and the percentage volume of permeable voids respectively. The relationships are shown for three and seven day curing periods and at three levels of cement replacement corresponding to 0, 3.75, and 7.5 percent by equal weight of silica fume.

Figure 3 illustrates that, as the water/cement ratio increases, the permeability coefficient increases appreciably. Generally, the permeability coefficient at high water/cement ratios (above 0.6) increases at a faster rate. This phenomenon is consistent with that presented by Powers et. al. [36] which is a non-linear relationship showing increasing slope with increased water/cement ratio. The only exception to this

TABLE 2
THE AVERAGE COEFFICIENTS OF PERMEABILITY AND
VOLUME OF PERMEABLE VOIDS

W/C RATIO	SILICA FUME CONTENT(%)	CURING (DAYS)	AVERAGE PERMEABILITY COEFFICIENT "K" cm/s x 10 ⁻¹¹	AVERAGE % VOLUME OF PERMEABLE VOIDS
0.5	0	3	18.80	15.59
	0	7	15.40	15.08
	3.75	3	15.50	16.17
	3.75	7	10.86	15.96
	7.50	3	5.16	16.35
	7.50	7	3.56	16.98
0.6	0	3	409.00	19.55
	0	7	95.60	19.71
	3.75	3	55.00	20.10
	3.75	7	19.70	20.33
	7.50	3	47.30	20.54
	7.50	7	4.47	20.89
0.7	0	3	522.00	22.00
	0	7	477.00	21.10
	3.75	3	130.50	23.55
	3.75	7	116.40	22.43
	7.50	3	124.50	24.49
	7.50	7	27.10	22.80

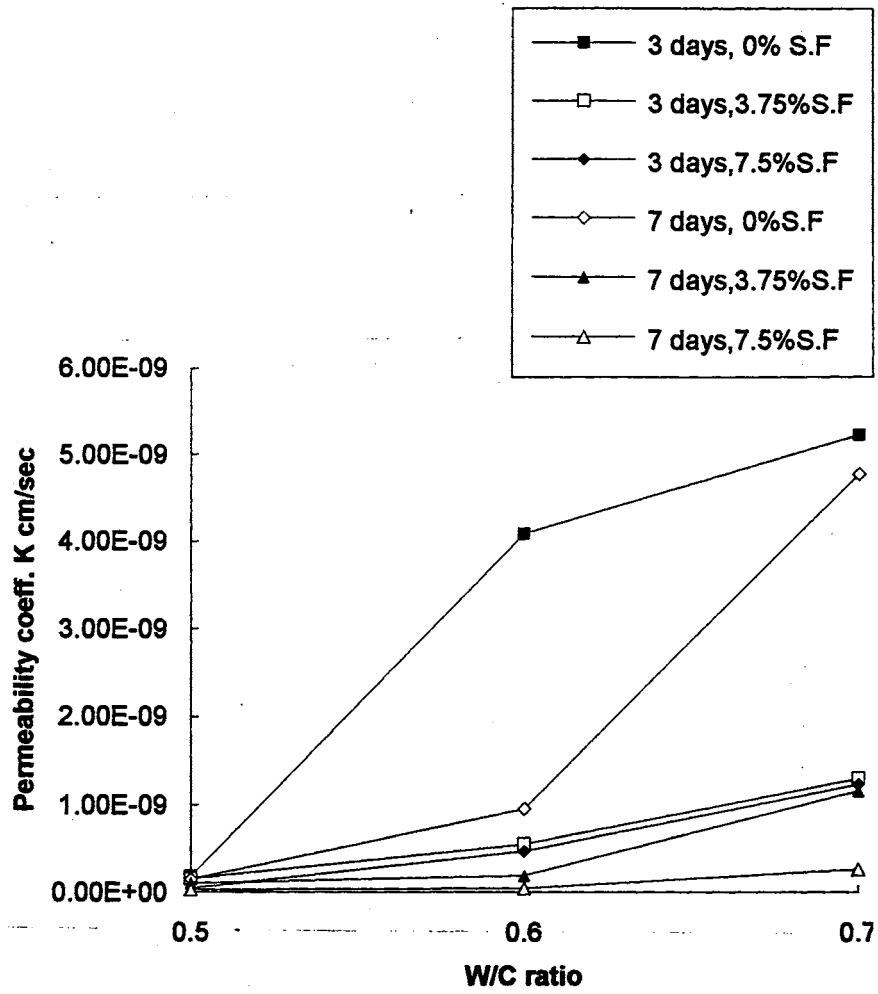


Figure 3. The Relationship Between the Water/Cement Ratio and Permeability Coefficients

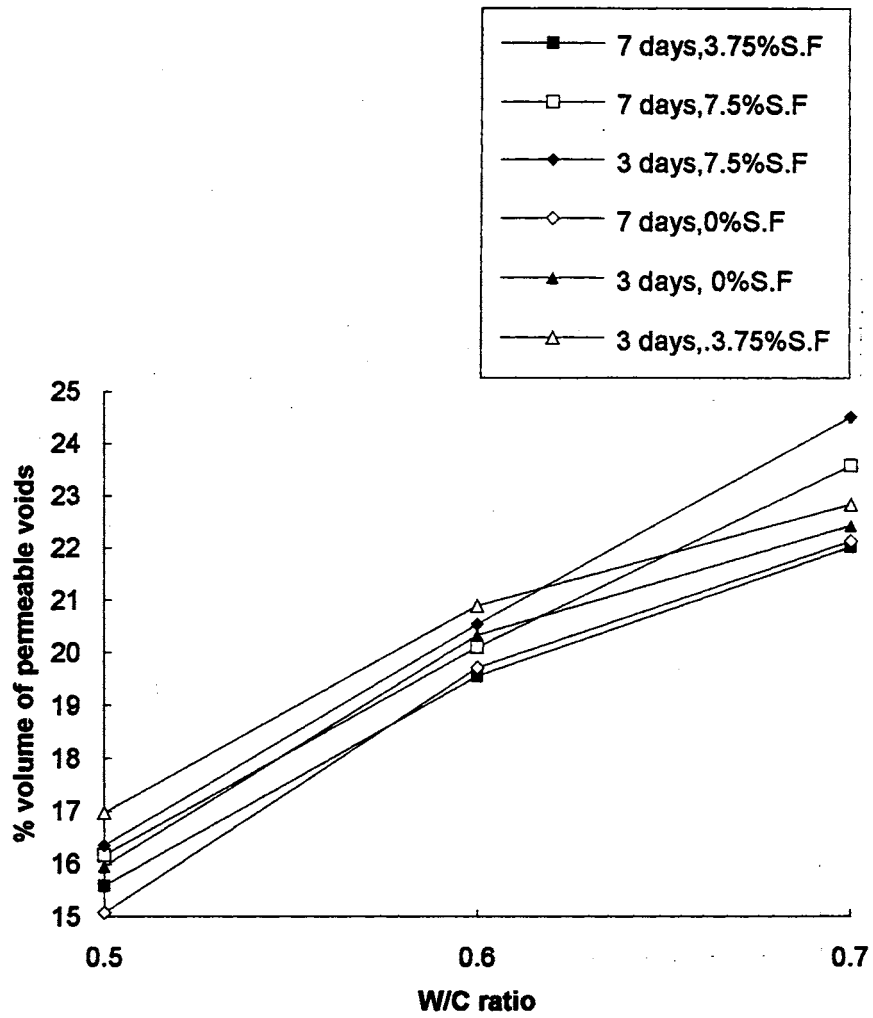


Figure 4. The Relationship Between the Water/Cement Ratio and Percentage Volume of Permeable Voids

trend in Figure 3 is for the zero percent silica fume mortar cured for 3 days. These samples show a slower rate of increase in the permeability coefficients at water/cement ratios above 0.6 compared to the rate below 0.6. There is no obvious reason for this discrepancy and experimental error is likely. Figure 3 also illustrates that increasing silica fume content substantially reduces the mortar permeability.

The percentage volume of permeable voids increases with increases in the water/cement ratio as shown in Figure 4. The rate of increase in the volume of permeable voids at water/cement ratios greater than 0.6 is lower than that at water/cement ratios lower than 0.6. It is observed that increasing the silica fume content increases the volume of permeable voids.

The effect of water/cement ratio on the volume of permeable voids and permeability coefficient was explained by Neville [30]. When water is added to cement, the hydration process is initiated. At any stage of hydration, the hardened paste consists of hydrates of various compounds (referred to collectively as a gel), calcium hydroxide crystals, several minor components, unhydrated cement, and the residue of water-filled spaces in the fresh paste. These voids are referred to as the capillary pores and are responsible for the majority of water permeability. The capillary pores form from zero to forty percent of the total paste volume. At the same degree of hydration, the higher the water/cement ratio, the larger the volume of capillary pores and continuous flow channels and, the larger the permeability coefficient. As hydration proceeds, the pore volume reduces and becomes discontinuous. When the water/cement ratio exceeds 0.7, capillary pore discontinuity can not be achieved, and therefore the paste will exhibit relatively high permeabilities.

The permeability coefficients for various water/cement ratios are illustrated in Figures 22,23,24, and 25 (Appendix B) for all silica fume contents, 0, 3.75, and 7.5 percent respectively. The regression equations of the permeability coefficients and water/cement ratios are shown in the figures and in Table 8. Also, included in Table 3 are the coefficient of determination (R^2) and the P-value for each data set. The regression

equations for the percentage volume of permeable voids and water/cement ratio are illustrated in Figures 26, 27, 28, and 29 (Appendix B) for all silica fume contents, 0, 3.75, and 7.5 percent respectively. The regression equations, coefficients of determination (R^2), and the P-values are shown in Table 3.

The P-value is the lowest level of significance that can be used and still reject the hypothesis that the correlation coefficient is equal to zero. If the P-value is high (more than 0.1), the data do not introduce significant evidence to reject the hypothesis that the correlation coefficient of the population is equal to zero. If the P-value is low (less than 0.1), the collected data are significant enough to reject the hypothesis that the correlation coefficient of the population is equal to zero.

The coefficient of determination for the permeability coefficient and water/cement ratios for all tests are shown in Figure 22 (Appendix B) and is equal to 0.30. The corresponding P-value for this R^2 value is 0.0180 which is considered to be very low. The data are significant enough to reject the hypothesis that the correlation coefficient of the population is equal to zero. This relationship is investigated for 0, 3.75, and 7.5 percent silica fume contents, as shown in Figures 23, 24, and 25 (Appendix B) respectively. The coefficients of determination are equal to 0.82, 0.86, and 0.46 respectively. The corresponding P-values for these relationships are 0.0126, 0.0079, and 0.1368. The P-values for the 0 and 3.75 percent silica fume contents provide significant evidence to reject the hypothesis that the population correlation coefficient is zero. These P-values suggest that the permeability coefficients for mortars containing 0 and 3.75% silica fume can be predicted reliably by the water/cement ratio, within the range of the water/cement ratios evaluated. However, the reliability of the prediction does not extend to the higher silica fume percentages.

The coefficient of determination for the percentage volume of permeable voids and water/cement ratio, as shown in Figure 26 (Appendix B) is very high (0.93). Ninety three percent of the variation of the percentage volume of permeable voids can be explained by

TABLE 3

REGRESSION EQUATIONS, (R^2) VALUES, AND P-VALUES FOR THE REGRESSION OF PERMEABILITY COEFFICIENTS AND PERCENT VOLUME OF PERMEABLE VOIDS ON W/C RATIOS

DEPENDENT VARIABLE IN REGRESSION (Y)	W/ C RATIO (X)			
	ALL S.F CONTENTS	0% S.F CONTENT	3.75% S.F CONTENT	7.5% S.F CONTENT
	PERMEABILITY COEFF.	$Y = -5.4e^{-9} + 1.1e^{-8}X$ $R^2 = 0.30$ $P\text{-value} = 0.0126$	$Y = -1.2e^{-8} + 2.4e^{-8}X$ $R^2 = 0.82$ $P\text{-value} = 0.0079$	$Y = -2.7e^{-9} + 5.5e^{-9}X$ $R^2 = 0.86$ $P\text{-value} = 0.1368$
VOLUME OF PERMEABLE VOIDS	$Y = -0.9 + 34.3X$ $R^2 = 0.93$ $P\text{-value} = 0.0003$	$Y = -1.1 + 33.6X$ $R^2 = 0.97$ $P\text{-value} = 0.0003$	$Y = -0.9 + 34.6X$ $R^2 = 0.97$ $P\text{-value} = 0.0007$	$Y = -0.6 + 34.9X$ $R^2 = 0.96$ $P\text{-value} = 0.0001$

the regression of these results and the water/cement ratio. The P-value for this relationship is very low (0.0001) which indicates that the obtained data give very significant evidence to reject the hypothesis that the population correlation coefficient is zero. The regression analyses were carried out for silica fume contents corresponding to 0, 3.75, and 7.5 percent and are shown in Figures 27, 28, and 29 (Appendix B) respectively. The coefficients of determination for these relationships are very high and equal to 0.97, 0.97, and 0.96 respectively. The corresponding P-values for these relationships are considered to be very low (0.0003, 0.0003, and 0.0007). These strong relationships show that the percentage volume of permeable voids can be predicted reliably by the water/cement ratio, within the range of water/cement ratios evaluated.

Effect of Curing

The effect of the curing period on the percentage volume of permeable voids and the permeability coefficient is shown in Figures 5 and 6. These figures reflect water/cement ratios of 0.5, 0.6, and 0.7 and cement replacement levels corresponding to 0, 3.75, and 7.5 percent by equal weight of silica fume.

Figure 5 shows that the permeability coefficients of the mortars evaluated are reduced appreciably by increasing the length of curing. Figure 6 shows that the percentage volume of permeable voids is generally reduced by increasing the length of curing. However, the reduction was negligible in most cases. There were several mixes which showed an unexpected increase in the percentage volume of permeable voids with increased curing periods. This anomaly is not associated with a specific water/cement ratio or silica fume content.

The effect of curing on the permeability coefficient and percentage volume of permeable voids can be explained in terms of the microstructure of the paste. As curing proceeds, the hydration products increase in volume. As a result, the volume of capillary

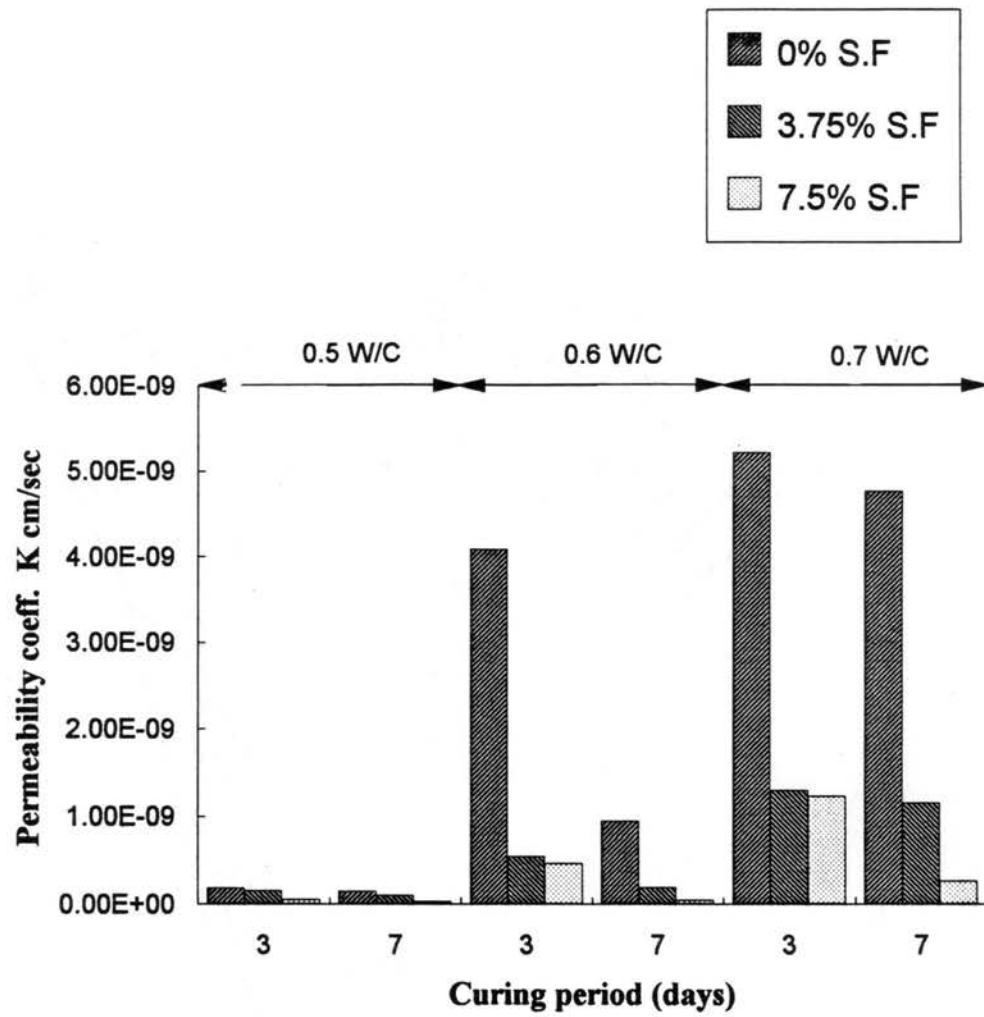


Figure 5. The Relationship between the Permeability Coefficient and the Curing Period

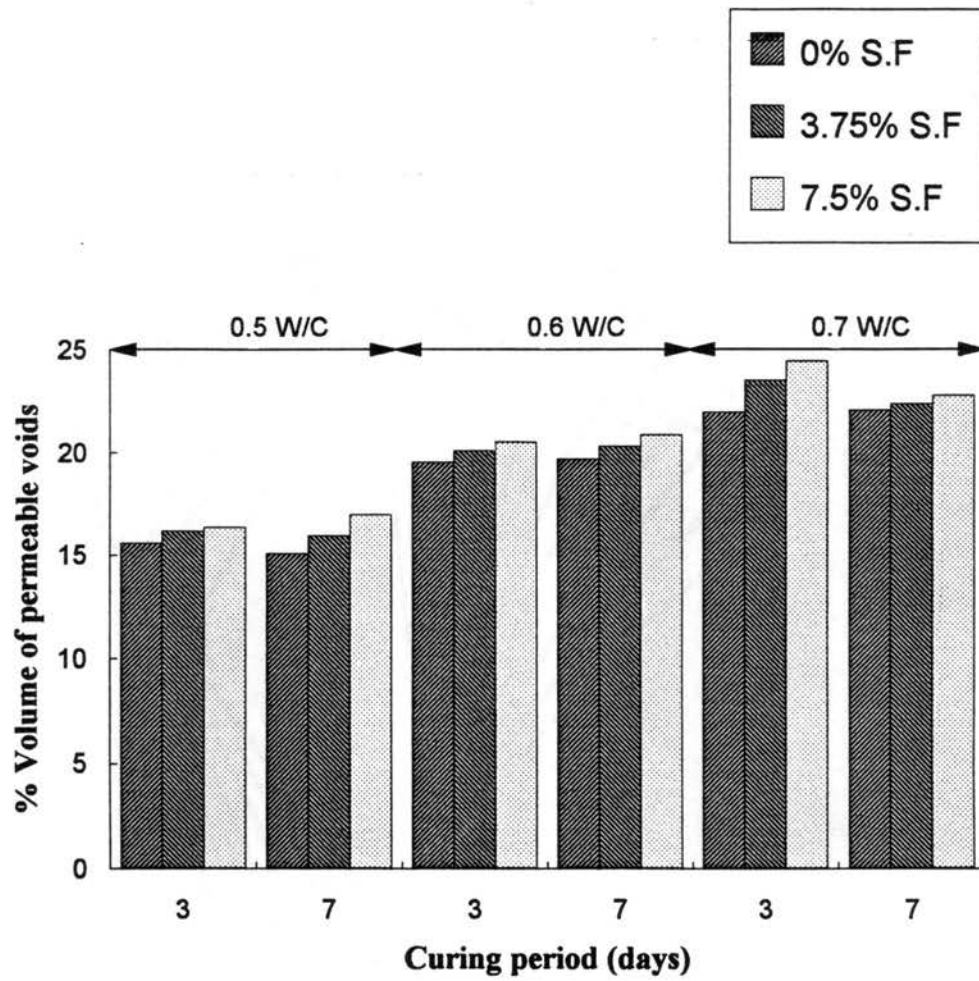


Figure 6. The Relationship between the Percent Volume of Permeable Voids and the Curing Period

pores decreases and becomes discontinuous. The discontinuous pore structure results in decreased permeability.

Part of conducting the ASTM 642 C test is to boil the mortar specimen in water for 5 hours. However, considering the early ages at which the specimens were evaluated, the boiling process has an accelerating effect on the mortar hydration process. This accelerated hydration affected the measured volume of permeable voids by an undetermined amount.

The plots relating permeability coefficients to curing periods are presented in Figures 30, 31, 32, and 33 (Appendix B) for all the silica fume contents, 0, 3.75, and 7.5 percent respectively. The percentage volume of permeable voids and water/cement ratios are illustrated in Figures 34, 35, 36, and 37 (Appendix B) for all silica fume contents, 0, 3.75, and 7.5 percent respectively. The regression equations, the coefficients of determination (R^2), and the P-values for these relationships are presented in Table 4.

The coefficient of determination for the permeability coefficient versus curing period is shown in Table 4 and is equal to 0.04. As the curing duration increases, the permeability coefficient decreases. The P-value for this relationship is 0.4538 which is considered to be very high. Therefore, the data are not significant enough to reject the hypothesis that the correlation coefficient of the population is equal to zero. This relationship is investigated for 0, 3.75, and 7.5 percent silica fume contents with no change in the conclusion.

The coefficient of determination for percentage volume of permeable voids versus curing period is considered to be very low and is equal to 0.0016. The P-value for this relationship is very high (0.87) and this indicates that the data provide no significant evidence to reject the hypothesis that the population correlation coefficient is zero. The regression analysis was carried out for silica fume contents of 0, 3.75, and 7.5 percent as shown in Figures 35, 36, and 37 (Appendix B). These relationships support a similar conclusion.

TABLE 4
REGRESSION EQUATIONS, (R^2) VALUES, AND P-VALUES FOR THE
REGRESSION OF PERMEABILITY COEFFICIENTS AND PERCENT
VOLUME OF PERMEABLE VOIDS ON CURING PERIODS

DEPENDENT VARIABLE IN REGRESSION (Y)	CURING PERIOD (X)			
	ALL S.F CONTENTS	0% S.F CONTENT	3.75% S.F CONTENT	7.5% S.F CONTENT
PERMEABILITY COEFF.	$Y = 1.9e^{-9} - 1.6e^{-10}X$ $R^2 = 0.04$ $P\text{-value} = 0.4538$	$Y = 4.1e^{-9} - 3.0e^{-10}X$ $R^2 = 0.08$ $P\text{-value} = 0.5941$	$Y = 8.1e^{-10} - 4.5e^{-11}X$ $R^2 = 0.03$ $P\text{-value} = 0.7252$	$Y = 9.4e^{-10} - 1.2e^{-10}X$ $R^2 = 0.30$ $P\text{-value} = 0.2566$
VOLUME OF PERMEABLE VOIDS	$Y = 19.9 - 5.8e^{-2}X$ $R^2 = 0.00$ $P\text{-value} = 0.8748$	$Y = 19.1 - 2.1e^{-2}X$ $R^2 = 0.00$ $P\text{-value} = 0.9775$	$Y = 20.2 - 9.4e^{-2}X$ $R^2 = 0.00$ $P\text{-value} = 0.9014$	$Y = 20.6 - 5.9e^{-2}X$ $R^2 = 0.00$ $P\text{-value} = 0.9390$

Effect of Silica Fume Content

The relationship between the silica fume content, as a percentage of the total cementitious materials, and the permeability coefficients is shown in Figure 7. The data indicate that, as the silica fume content increases, the permeability coefficient decreases. The rate of decrease is more pronounced when adding 3.75 percent silica fume versus 7.5 percent silica fume. Moreover, the rate of decrease in permeability coefficients below 3.75 percent silica fume decreases as the water/cement ratio increases and the curing period increases. Increasing the silica fume content from 3.75 percent to 7.5 percent does not contribute significantly to the reduction in the permeability coefficients. It was reported in the Literature that 5 percent silica fume content improves the paste properties significantly [5].

Figure 8 shows the relationship between the silica fume content, as a percentage of the total cementitious material, and the percentage volume of permeable voids. This relationship indicates that as the silica fume content increases, the percentage volume of permeable voids increases for all water/cement ratios and curing periods evaluated. The rate of increase is relatively constant for all the silica fume replacement levels used in the study.

It was believed that the incorporation of silica fume reduces the voids within the paste matrix by physically filling in voids. However, it was recently reported that the silica fume affects the pore-size distribution of mortars by reacting with the calcium hydroxide formed around sand grains as well as with the calcium hydroxide dispersed throughout the hydrated cement. It was reported that this reaction results in empty voids in place of the original calcium hydroxide crystals. Therefore, the pore-size distribution of mortars containing silica fume differs from that of equivalent mortars without silica fume by having a larger coarse pore component. However, another effect of adding silica fume is that it

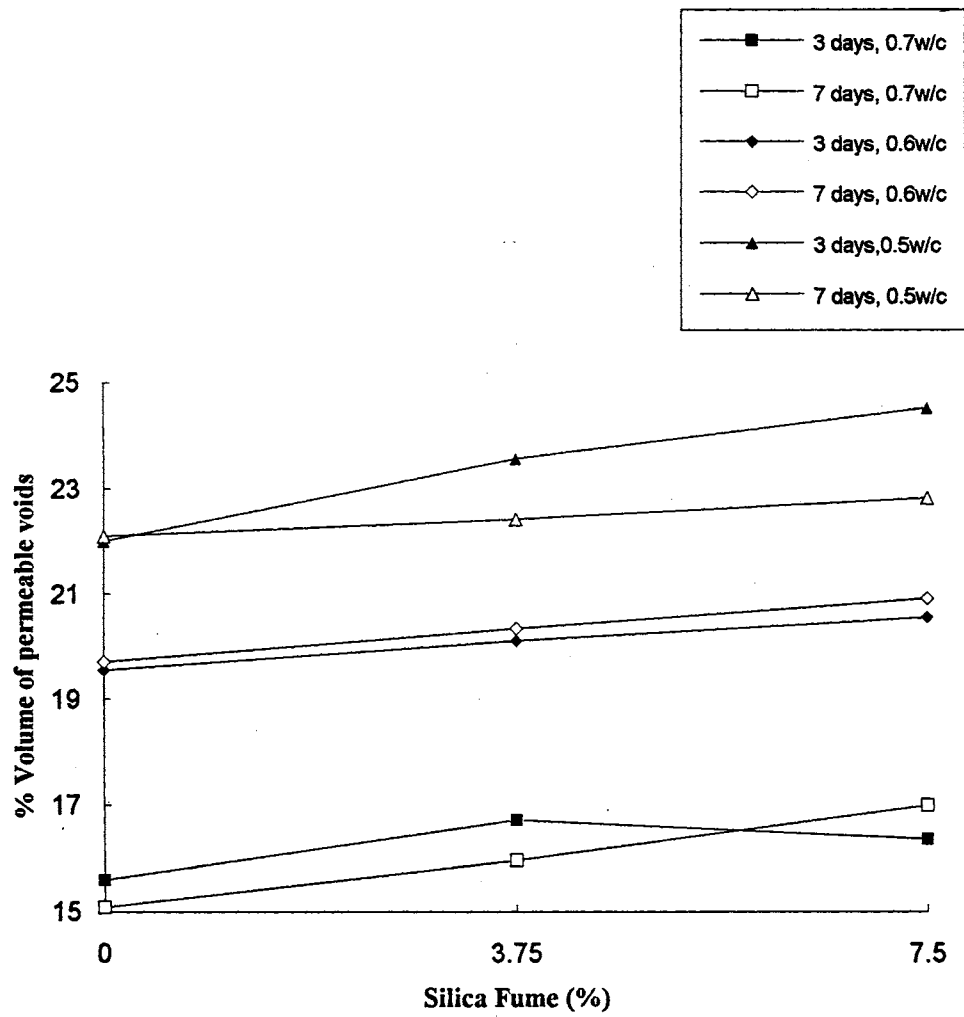


Figure 7. The Relationship between the Permeability Coefficient and the Silica Fume Content

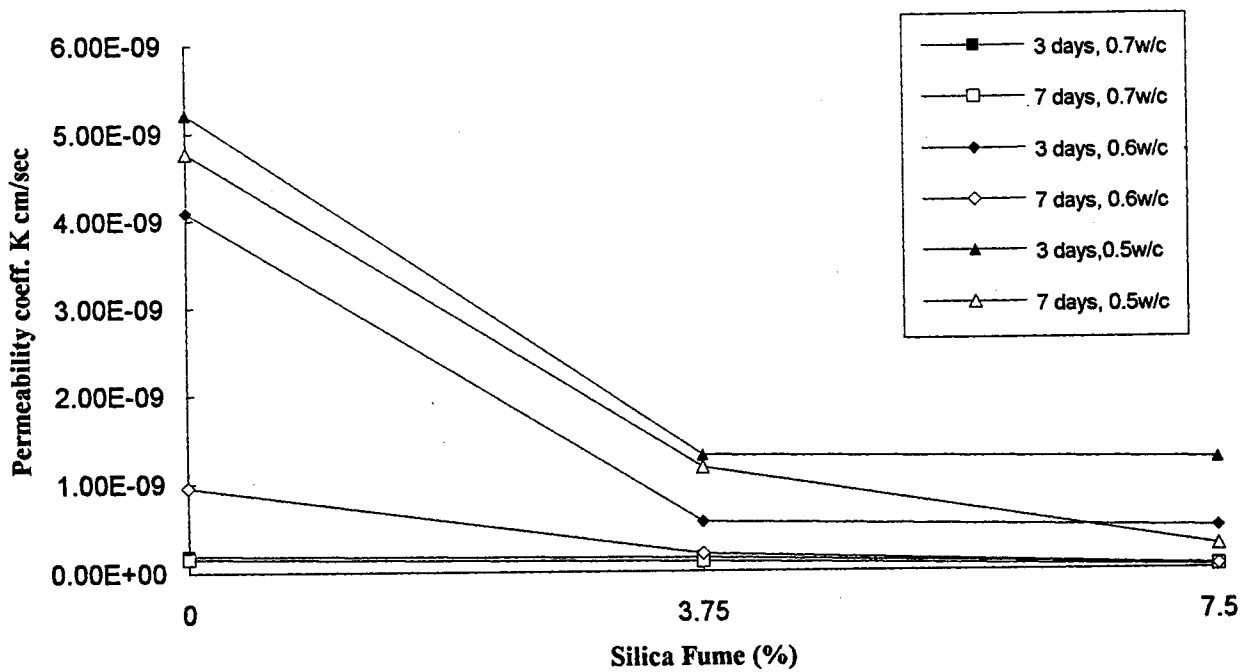


Figure 8. The Relationship between the Percent Volume of Permeable Voids and the Silica Fume Content

refines the primary pore structure and changes the large continuous pores to narrow and discontinuous voids which in turn reduces the mortar porosity significantly. Although the addition of silica fume in mortars increases the percentage volume of permeable voids, it decreases the permeability coefficients.

The permeability coefficients versus water/cement ratio are illustrated in Figures 38, 39, 40, and 41 (Appendix B) for all water/cement ratios, 0.5, 0.6, and 0.7 respectively. An inverse relationship between the silica fume content and the permeability coefficients exists. The regression equations, coefficients of determination (R^2), and P-values for these relationships are shown in Table 5. The coefficient of determination for the permeability coefficient versus silica fume content is equal to 0.3. The P-value for this relationship is equal to 0.0180, which is considered very low. The data are significant enough to reject the hypothesis that the correlation coefficient of the population is equal to zero. This relationship is investigated for 0.5, 0.6, and 0.7 water/cement ratios. The coefficients of determination are equal to 0.86, 0.44, and 0.81 respectively and the corresponding P-values for these relationships are 0.0074, 0.1490, and 0.0142. These values give significant evidence to reject the hypothesis that the population correlation coefficient is zero for mortars prepared at 0.5, and 0.7 water/cement ratios. The corresponding R^2 values indicate a strong relationship between the permeability coefficient and silica fume content. Consequently, the silica fume content can be used reliably to predict the permeability coefficient for mortars prepared at 0.5, and 0.7 water/cement ratios. The large P-value for mortars evaluated at 0.6 water/cement ratio do not provide significant evidence to reject the hypothesis that the population correlation coefficient is zero.

The relationships between percentage volume of permeable voids and silica fume content are presented in Figures 42, 43, 44, and 45 (Appendix B) for all water/cement ratios, 0.5, 0.6, and 0.7 respectively. These figures show that as the silica fume content increases, the volume of permeable voids increases. The P-values for these relationships

TABLE 5

REGRESSION EQUATIONS, (R^2), AND P-VALUES FOR THE REGRESSION OF PERMEABILITY COEFFICIENTS AND PERCENT VOLUME OF PERMEABLE VOIDS ON SILICA FUME CONTENT

DEPENDENT VARIABLE IN REGRESSION (Y)	SILICA FUME CONTENT (X)			
	ALL W/C RATIOS	0.5 W/C RATIO	0.6 W/C RATIO	0.7 W/C RATIO
PERMEABILITY COEFF.	$Y = 2.3e^{-9} - 2.9e^{-10}X$ $R^2 = 0.30$ $P\text{-value} = 0.0182$	$Y = 1.8e^{-10} - 1.7e^{-11}X$ $R^2 = 0.86$ $P\text{-value} = 0.0074$	$Y = 2.2e^{-9} - 3.0e^{-10}X$ $R^2 = 0.44$ $P\text{-value} = 0.1490$	$Y = 4.4e^{-9} - 5.7e^{-10}X$ $R^2 = 0.81$ $P\text{-value} = 0.0142$
VOLUME OF PERMEABLE VOIDS	$Y = 19.0 + 0.2X$ $R^2 = 0.04$ $P\text{-value} = 0.4551$	$Y = 15.4 + 0.2X$ $R^2 = 0.83$ $P\text{-value} = 0.0112$	$Y = 19.6 + 0.1X$ $R^2 = 0.92$ $P\text{-value} = 0.0025$	$Y = 22.1 + 0.2X$ $R^2 = 0.55$ $P\text{-value} = 0.0934$

are shown in Table 5. The relationship in Figure 42 shows an R^2 value of 0.04 for all water/cement ratios. The P-value for this relationship is 0.4551 which indicates that, the data do not provide enough significance to reject the hypothesis that the population correlation coefficient is zero. A regression analysis was carried out for mortars prepared at 0.5, 0.6, and 0.7 water/cement ratios. The coefficients of determination are 0.83, 0.92, and 0.55 respectively which indicate strong linear relationships. The corresponding P-values are 0.0112, 0.0025, and 0.0934. The small P-values indicate that the data provide significant evidence to reject the hypothesis that the population correlation coefficient is equal to zero. Therefore, these relationships can be used reliably to predict the percentage volume of permeable voids from the silica fume content.

Correlation of Permeability Coefficients and Volume of Permeable Voids

The results of the permeability coefficients and the percentage volume of permeable voids are shown in Figures 46, 47, 48, and 49 (Appendix B) for all the specimens and specimens prepared at 0, 3.75, and 7.5% silica fume contents. These relationships indicate that as the percentage volume of permeable voids increases the permeability coefficient increases. The regression equations, coefficients of determinations (R^2), and P-values for the four relationships are shown in Table 6. The coefficient of determination for the permeability coefficient versus the percentage volume of permeable voids for all the mortars evaluated is shown in Figure 46 and is equal to 0.18. The P-value for this relationship is equal to 0.0809. The regression analysis for all the tested specimens provides enough significance to reject the hypothesis that the correlation coefficient of the whole population is equal to zero. This relationship is investigated for mortars containing 0.0, 3.75, and 7.5 percent silica fume contents. The coefficients of determination are equal to 0.76, 0.75, and 0.53 respectively. The corresponding P-values for these

relationships are 0.0230, 0.0261, and 0.1015. These values provide significant evidence to reject the hypothesis that the population correlation coefficient is equal to zero. The corresponding R^2 values indicate strong relationships between the permeability coefficients and the percentage volume of permeable voids. Consequently, the percentage volume of permeable voids can be used reliably to predict the permeability coefficients.

TABLE 6
REGRESSION EQUATIONS, (R^2) VALUES, AND P-VALUES FOR THE
REGRESSION OF PERMEABILITY COEFFICIENTS ON
PERCENTAGE VOLUME OF PERMEABLE VOIDS

	% VOLUME OF PERMEABLE VOIDS (X)			
	ALL S.F CONTENTS	0% S.F CONTENT	3.75% S.F CONTENT	7.5% S.F CONTENT
PERMEABILITY COEFF. (Y)	$Y = -1.2e^{-1} + 1.1e^{-1}X$ $R^2 = 0.18$ $P\text{-value} = 0.0809$	$Y = -3.4e^{-2} + 2.9e^{-2}X$ $R^2 = 0.76$ $P\text{-value} = 0.0230$	$Y = -7.8e^{-2} + 6.5e^{-2}X$ $R^2 = 0.75$ $P\text{-value} = 0.0261$	$Y = -6.0e^{-2} + 4.9e^{-2}X$ $R^2 = 0.53$ $P\text{-value} = 0.1015$

CHAPTER V

SUMMARY AND CONCLUSIONS

The primary objective of this study was to establish quantitative relationships between permeability coefficients and the volume of permeable voids for plain cement and cement/silica fume mortars. A secondary objective was to determine the effects of the silica fume/cement ratio on the permeability of mortars. The scope of the work included measuring the permeability of 1.0-inch (25.4-mm) diameter x 0.32-inch (8-mm) mortar discs and determining the volume of permeable voids of 2.0-inch (50.8-mm) mortar cubes. The mortar specimens evaluated in the test program used a sand/cement ratio of 3:1 by weight and water/cementitious-material ratios of 0.5, 0.6, and 0.7. Type I portland cement and commercially available silica fume were used to prepare all specimens. Mortar specimens with cement replacement of 0, 3.75, and 7.5 percent by equal weight of silica fume were evaluated after curing periods of 3 and 7 days. Based on a thorough analysis of the test results, the following conclusions were reached:

1. The modifications in the specimen mold and the specimen placement enabled testing at high pressures without significant leakage.
2. The time-flow relationships obtained in the study were typical of those found in the Literature.
3. Increasing the water/cementitious-materials ratio increases the permeability coefficients and the volume of permeable voids at all curing periods and silica fume replacements.
4. There is a significant correlation between the permeability coefficients and the

water/cementitious-material ratio for mortars containing 0, and 3.75 percent silica fume content. The R^2 values for these two regression equations are equal to 0.82 and 0.86 respectively.

5. There is a highly significant correlation between the percentage volume of permeable voids and the water/cementitious-materials ratio for mortars containing 0, 3.75, and 7.5 percent silica fume content. The R^2 values for the three regression equations are equal to 0.97, 0.97, and 0.96 respectively.
6. The results did not indicate a significant correlation between either the permeability coefficient or the volume of permeable voids and the curing period for all the mixes evaluated.
7. The accelerated curing induced by boiling the specimens was much more significant than any of the variables evaluated, therefore the correlation may not be as accurate as described by the statistical indicators.
8. Increasing the silica fume content decreases the permeability coefficient for all the mixes evaluated. This effect is more pronounced by increasing silica fume from 0 to 3.75 than by increasing from 3.75 to 7.5 percent.
9. The effect of adding silica fume is that it increases the volume of permeable voids for all the mixes evaluated.
10. Adding silica fume to mortars refines the pore structure and changes the large continuous pores to narrow and discontinuous voids such that the permeability decreases.
11. There is a significant correlation between the permeability coefficient and the silica fume content at water/cementitious-material ratios of 0.5 and 0.7. The R^2 values for these two regression equations are equal to 0.86 and 0.81 respectively.
12. There is a strong correlation between the volume of permeable voids and silica fume content for mortars evaluated at water/cementitious-material ratios of 0.5, 0.6, and 0.7. The R^2 values for these regression equations are equal to 0.83, 0.92,

and 0.55 respectively.

13. There are significant correlations between the permeability coefficients and the volume of permeable voids for mortars prepared at 0, 3.75, and 7.5 percent silica fume contents. The R^2 values for these three regression equations are equal to 0.76, 0.75, and 0.53 respectively

Recommendations for Future Research

1. Similar Mortars should be evaluated at longer curing periods to provide permeability data at advanced degrees of hydration.
2. Sample preparation techniques should be evaluated to minimize variations in the permeability measurements.
3. Various types of data acquisition systems should be evaluated to improve the accuracy of the time/flow data.

REFERENCES

- [1] Bentur, A., and Cohen, M.D., "Effect of Condensed silica Fume on the Microstructure of the Interfacial Zone in Portland Cement Mortars," Journal of the American Ceramic Society, Vol. 70, No. 10, Oct. 1987, pp. 738-743.
- [2] Bisailon, A., and Malhotra, V.M., "Permeability of Concrete Using Uniaxial Water-Flow Method," American Concrete Institute, SP 108-10, 1988, pp. 175-193.
- [3] Buil, M., and Delage, P., "Some Further Evidence on a Specific Effect of Silica Fume on the Pore Structure of Portland Cement Mortars," Cement and Concrete Research, Vol. 17, No. 1, Jan. 1987, pp. 65-69.
- [4] Carman, P.C., "Permeability of Saturated Sands, Soils, and Clays," Journal of Agricultural Society, Vol. 29, 1939, pp. 262.
- [5] Cohen, M.D., and Klitsikas, M., "Mechanisms of Hydration and Strength Developments in Portland Cement Composites Containing Silica Fume Particles," Indian Concrete Journal, Vol. 60, No. 11, Nov. 1986, pp. 296-300.
- [6] Cook, H.K., "Permeability Tests on Lean Mass Concrete." ASTM Proceedings, Vol. 51, 1951, pp.1156-1165.
- [7] Collins, J.F., Derucher, K.N., and Korfiatis, G.P., "Permeability of Concrete Mixtures Part I: Literature Review," Civil Engineering for Practicing and Design Engineers, Vol. 5, 1986, pp. 579-638.
- [8] Delage, P., and Aitcin, P., "Influence of Condensed Silica Fume on the Pore-Size Distribution of Concretes," Industrial and Engineering Chemistry Product Research and Development, Vol. 22, No. 2, 1983, pp. 286-290.
- [9] Figgs, J.W., "Methods of Measuring the Air and Water Permeability of Concrete," Magazine of Concrete Research, Vol. 25, No. 85, Dec. 1973, pp. 213-219.

- [10] Feldman, R.F., "Pore Structure Formation Drying Hydration of Fly-Ash and Slag Cement Blends," in Effects of Fly-Ash Incorporation in Cement and Concrete, S. Diamond, Ed., Materials Research Society, Pittsburgh, PA, 1981, pp. 124-133.
- [11] Feldman, R.F., "The Effect of Sand/Cement Ratio and Silica Fume on the Microstructure on Mortars," Cement and Concrete Research, Vol. 16, No. 1, 1986, pp. 31-39.
- [12] Feldman, R.F., "Significance of Porosity Measurements on Blended Cement Performance," American Concrete Institute, SP-79, Vol. 1, 1983, pp. 415-433.
- [13] Feldman, R.F., "Influence of Condensed Silica Fume and Sand/Cement Ratio on Pore Structure and Frost Resistance of Portland Cement mortars," Fly Ash, Silica Fume, Slag and Natural Pozzolans in Concrete, American Concrete Institute, SP-91, 1986, pp. 973-989.
- [14] Garboczi, E.J., "Permeability, Diffusivity, and Microstructural Parameters: A Critical Review," Cement and Concrete Research, Vol. 20, No. 4, July 1990, pp. 591-601.
- [15] Goto, S., and Roy, D.M., "The Effect of W/C Ratio and Curing Temperature on the permeability of Hardened Cement Paste," Cement and Concrete Research, Vol. 11, 1981, pp. 575-579.
- [16] Hooton, R.D., "Permeability and Pore Structure of Cement Pastes Containing Fly Ash, Slag, and Silica Fume," Blended Cements, ASTM STP 897, G. Frohnsdorff, Editor, American Society for Testing and Materials, Philadelphia, 1986, pp. 128-143.
- [17] Hope, B.B., and Malhotra, V.M., "The Measurement of Concrete Permeability," Canadian Journal of Civil Engineering, Vol. 11, No. 2, June 1984, pp. 287-293.
- [18] Hughes, D.C., "Pore Structure and Permeability of Hardened Cement Paste," Magazine of Concrete research, Vol. 37, No. 133, Dec. 1985, pp. 227-233.
- [19] Janssen, D.J., "Laboratory Permeability Measurement," American Concrete Institute, SP 108-11, 1988, pp. 145-158.
- [20] Katz, A.J., and Thompson, A.H., "Prediction of Rock Electrical Conductivity from Mercury Injection Measurements," Journal of Geophysical Research, Vol. 92, No. B1, Jan. 1987, pp. 599-607.
- [21] Katz, A.J., and Thompson, A.H., "Quantitative Prediction of Permeability in Porous Rock," Physical Review B, Vol. 34, No. 11, Dec. 1986, p. 8179-8181.

- [22] Kayyali, O.A., "Porosity of Concrete in Relation to the Nature of the Paste-Aggregate Interface," Materials and Structures, Vol. 20, 1987, pp. 19-26.
- [23] Ludirdja, D.; Berger, R.L.; and Young, J.F.; "Simple Method for Measuring Water Permeability of Concrete," ACI Materials Journal, Vol. 86, No. 5, Sept.-Oct. 1989, pp. 433-439.
- [24] Malhotra, V.M., Editor, "Fly Ash, Silica Fume, Slag & Other Mineral By-Products in Concrete, SP-79," American Concrete Institute, Detroit, 1983, 1196 pp.
- [25] McMillan, F.R., and Lyse, I., "Some Permeability Studies of Concrete," Proceedings, Journal of American Concrete Institute, Vol. 26, 1929, pp. 101-141.
- [26] Manmohan, D., and Mehta, P.K., "Pore Size Distribution and Permeability of Hardened Cement Paste," Proceedings, 7th International Congress on the Chemistry of Cement, Paris 1980, Vol. 3, pp. VII-1 to VII-5.
- [27] Marusin, S.L., "Microstructure and Pore Characteristics of Concrete Containing Condensed Silica Fume with a Superplasticizer," Proceedings, 8th International Conference on Cement Microscopy, Florida, 1986, pp. 327-335.
- [28] Mehta, P.K., "Sulfate Resistance of Blended Portland Cements Containing Pozzolans and Granulated Blast Furnace Slag," Proceeding, Fifth International Symposium on Concrete Technology, 1981, pp. 35-50.
- [29] Meulen, Van der, G.J.R, Dijk, van, J., "A Permeability Testing Apparatus for Concrete," Magazine of Concrete Research, Vol. 21, No. 67, June 1969, pp. 121-123.
- [30] Neville, A.M. Properties of Concrete. 3rd Ed. Marshfield, Massachusetts: Pitman Publishing Inc., 1981.
- [31] Norton, P.T., Jr, Pletta, D.H., "The Permeability of Gravel Concrete," Proceedings, Journal of American Concrete Institute, Vol. 27, 1931, pp. 1093-1132.
- [32] Nyame, B.K., and Illston, J.M., "Capillary Pore Structure and Permeability of Hardened Cement Pastes," Proceedings, 7th International Congress on the Chemistry of Cement, Paris, 1980, Vol. 3, pp. VI-181 to VI-185.
- [33] Ping, X.; Beaudoin, J.J; and Brousseau, R., "Effect of Aggregate Size on Transition Zone Properties at the Portland Cement Paste Interface," Cement and Concrete Research, Vol. 21, No. 6, 1991, pp. 999-1005.

- [34] Powers, T.C., and Brownyard, T.L., "Studies of the Physical Properties of Hardened Portland Cement Paste," Portland Cement Association Research Department, Bulletin 22, 1948.
- [35] Powers, T.C., Mann, H.M., and Copeland, L.E., "Flow of Water in Hardened Portland Cement Paste," Highway Research Board, Special Report No. 40, 1958, pp. 308-323.
- [36] Powers, T.C., Copeland, L.E., Hayes, J.C., and Mann, H.M. "Permeability of Portland Cement Paste," Journal of American Concrete Institute, Vol. 51, 1954, pp. 285-298.
- [37] Reinhardt, H.W., and Gaber, K., "From Pore Size Distribution to an Equivalent Pore Size of Cement Mortar," Materials and Structures, Vol. 23, 1990, pp. 3-15.
- [38] Rosenberg, A.M., and Gaidis, J.M., "A New Mineral Admixture for High-Strength Concrete," Concrete International. Design & Construction, Vol. 11, No. 4, Apr. 1989, pp. 31-36.
- [39] Ruettgers, A., Vidal, E.N., and Wing, S.P., "An Investigation of Permeability of Mass Concrete with Particular Reference to Boulder Dam," Proceedings, Journal of American Concrete Institute, Vol. 31, March-April 1935, pp. 382-416.
- [40] "Standard Test Method for Specific Gravity, Absorption and Voids in Hardened Concrete." ASTM Designation C 642-90, American Society of Testing and Materials, Philadelphia, PA, 1991, pp. 317-319.
- [41] Sullivan, B.R., "Permeability Testing System for Grout, Concrete and Rock," American Concrete Institute, SP 108-9, 1988, pp. 159-174.
- [42] Thompson, A.H., Katz, A.J., and Krohnn, C.E., "The Microgeometry and Transport Properties of Sedimentary Rock," Advances in Physics, Vol. 36, No. 5, 1987, pp. 625-694.
- [43] Tyler, I.N., and Erlin, B., "A Proposed Simple Test Method for Determining the Permeability of Concrete," Journal of Research and Development Laboratories, PCA, Vol. 3, No. 3, Sept. 1961, pp. 2-7.
- [44] Wiley, G., and Coulson, D.C., "A Simple Test for Water Permeability of Concrete," Proceedings, Journal of American Concrete Institute, Vol. 34, 1937, pp. 65-75.

- [45] Wing, S.P., "Discussion of a Paper by G. Wiley and D.C. Coulson: A Simple Test for Water Permeability of Concrete," Proceedings, American Concrete Institute, 1938, 18-76-1 to 76-4.
- [46] Winslow, D.N., and Diamond, S., "A Mercury Porosimetry Study of the Evolution of Porosity in Portland Cement," Journal of Material, JMLSA, Vol. 5, No. 3, Sept. 1970, pp. 564-585.
- [47] Whiting, D., "Permeability of Selected Concrete," American Concrete Institute, SP 108-11, 1988, pp. 195-222.
- [48] Whiting, D., and Ealitt, A., Editors, "Permeability of Concrete, SP-108, "American Concrete Institute, Detroit, 1988, 225 pp.

APPENDICES

APPENDIX A

TABLES FOR TESTED SPECIMENS

TABLE 7
GRADATION OF THE SILICA SAND

Sieve #	Percentage Passing
16	100.0
20	99.7
30	76.0
40	14.3
50	2.2
80	0.3
100	0.1
200	0.0

TABLE 8

WATER/CEMENT RATIO, SILICA FUME CONTENT, CURING PERIODS,
AND RATE OF FLOW FOR THE TEST SPECIMENS.

W/C RATIO	SILICA FUME PERCENTAGE	CURING (DAYS)	REPLICATE #	FLOW "Q" (cm ³ /s)
0.5	0	3	1	0.0366
		3	2	*
		3	3	0.0800
0.5	3.75	3	1	**
		3	2	**
		3	3	0.065
0.5	7.5	3	1	0.0099
		3	2	0.0255
		3	3	*
0.5	0	7	1	0.0800
		7	2	**
		7	3	**
0.5	3.75	7	1	*
		7	2	0.0865
		7	3	0.0128
0.5	7.5	7	1	**
		7	2	0.0144
		7	3	0.0180

TABLE 8 (cont.)

W/C RATIO	SILICA FUME PERCENTAGE	CURING (DAYS)	REPLICATE #	FLOW "Q" (cm ³ /s)
0.6	0	3	1	0.410
		3	2	1.040
		3	3	0.570
0.6	3.75	3	1	0.084
		3	2	0.243
		3	3	0.073
0.6	7.5	3	1	*
		3	2	0.160
		3	3	0.110
0.6	0	7	1	0.170
		7	2	0.210
		7	3	0.200
0.6	3.75	7	1	0.063
		7	2	0.099
		7	3	0.068
0.6	7.5	7	1	**
		7	2	0.017
		7	3	**
0.7	0	3	1	1.200
		3	2	0.200
		3	3	0.400

TABLE 8 (cont.)

W/C RATIO	SILICA FUME PERCENTAGE	CURING (DAYS)	REPLICATE #	FLOW "Q" (cm ³ /s)
0.7	3.75	3	1	0.25
		3	2	0.24
		3	3	0.11
0.7	7.5	3	1	0.26
		3	2	0.33
		3	3	***
0.7	0	7	1	0.25
		7	2	1.65
		7	3	0.68
0.7	3.75	7	1	0.85
		7	2	*
		7	3	0.12
0.7	7.5	7	1	0.13
		7	2	0.15
		7	3	0.04

* Leakage problem.

** No flow was observed during the test period.

*** Broken specimen.

TABLE 9
 THE DIAMETER, HEIGHT, AND THE TEST PRESSURE
 FOR THE TEST SPECIMENS.

W/C RATIO	S.F %	CURING (DAYS)	REP.#	DIAMETER (INCH)	HEIGHT (INCH)	PRESSURE (PSI)
0.5	0	3	1	1.000	0.310	190
			2	1.020	0.305	
			3	1.000	0.310	
0.5	3.75	3	1	0.995	0.315	260
			2	1.020	0.310	
			3	1.010	0.320	
0.5	7.5	3	1	0.905	0.310	260
			2	0.905	0.310	
			3	1.000	0.305	
0.5	0	7	1	1.100	0.300	200
			2	1.100	0.305	
			3	1.100	0.305	
0.5	3.75	7	1	0.965	0.318	240
			2	0.995	0.313	
			3	1.015	0.305	
0.5	7.5	7	1	1.010	0.320	260
			2	1.020	0.300	
			3	1.020	0.300	
0.6	0	3	1	1.015	0.315	100
			2	1.015	0.310	
			3	1.000	0.320	

TABLE 9 (cont.)

W/C RATIO	S.F %	CURING (DAYS)	REP. #	DIAMETER (INCH)	HEIGHT (INCH)	PRESSURE (PSI)
0.6	3.75	3	1	1.000	0.320	150
			2	0.990	0.310	
			3	1.015	0.300	
0.6	7.5	3	1	0.990	0.317	150
			2	1.150	0.300	
			3	1.000	0.323	
0.6	0	7	1	0.962	0.315	130
			2	1.000	0.318	
			3	0.995	0.315	
0.6	3.75	7	1	1.000	0.310	240
			2	1.010	0.320	
			3	1.000	0.310	
0.6	7.5	7	1	1.000	0.320	242
			2	0.990	0.315	
			3	1.000	0.315	
0.7	0	3	1	1.000	0.315	71
			2	1.000	0.310	
			3	0.998	0.310	
0.7	3.75	3	1	0.950	0.310	110
			2	0.900	0.320	
			3	1.000	0.330	

TABLE 9 (cont.)

W/C RATIO	S.F %	CURING (DAYS)	REP. #	DIAMETER (INCH)	HEIGHT (INCH)	PRESSURE (PSI)
0.7	7.5	3	1	1.010	0.320	150
			2	0.990	0.320	
			3	1.010	0.310	
0.7	0	7	1	1.000	0.315	110
			2	1.000	0.310	
			3	1.005	0.305	
0.7	3.75	7	1	1.000	0.307	253
			2	1.005	0.310	
			3	1.005	0.310	
0.7	7.5	7	1	1.005	0.310	239
			2	1.005	0.310	
			3	1.005	0.307	

TABLE 10

THE COEFFICIENTS OF PERMEABILITY OF TEST SPECIMENS WITH
THE COEFFICIENTS OF VARIATION WITHIN EACH GROUP

W/C RATIO	S.F %	CURING (DAYS)	REP. #	PERMEABILITY COEFFICIENT "K" cm/s x 10 ⁻¹¹	COEFFICIENT OF VARIATION (%)
0.5	0	3	1	11.80	52.7
			2	-	
			3	25.80	
0.5	3.75	3	1	-	-
			2	-	
			3	15.50	
0.5	7.5	3	1	2.88	62.4
			2	7.43	
			3	-	
0.5	0	7	1	15.40	-
			2	-	
			3	-	
0.5	3.75	7	1	-	106.0
			2	20.00	
			3	1.68	
0.5	7.5	7	1	-	15.7
			2	3.16	
			3	3.95	

TABLE 10 (cont.)

W/C RATIO	S.F %	CURING (DAYS)	REP. #	PERMEABILITY COEFFICIENT "K" cm/s x 10 ⁻¹¹	COEFFICIENT OF VARIATION (%)
0.6	0	3	1	248.00	46.0
			2	619.00	
			3	360.00	
0.6	3.75	3	1	35.50	73.0
			2	101.50	
			3	28.00	
0.6	7.5	3	1	-	1.3
			2	47.80	
			3	46.90	
0.6	0	7	1	88.20	7.1
			2	101.70	
			3	96.90	
0.6	3.75	7	1	16.10	26.1
			2	25.60	
			3	17.40	
0.6	7.5	7	1	-	-
			2	4.47	
			3	-	
0.7	0	3	1	1050.00	88.9
			2	172.00	
			3	346.00	

TABLE 10 (cont.)

W/C RATIO	S.F %	CURING (DAYS)	REP. #	PERMEABILITY COEFFICIENT "K" cm x 10 ⁻¹¹	COEFFICIENT OF VARIATION (%)
0.7	3.75	3	1	155.55	43.0
			2	171.00	
			3	65.40	
0.7	7.5	3	1	107.50	19.5
			2	142.00	
			3	-	
0.7	0	7	1	142.00	83.9
			2	921.00	
			3	369.00	
0.7	3.75	7	1	204.00	106.4
			2	-	
			3	28.80	
0.7	7.5	7	1	33.10	55.2
			2	38.20	
			3	10.10	

TABLE 11
 PERCENTAGE VOLUME OF PERMEABLE VOIDS
 OBTAINED FROM ASTM C 642-90

W/C RATIO	S.F %	CURING (DAYS)	REP. #	% VOLUME OF PERMEABLE VOIDS	COEFFICIENT OF VARIATION (%)
0.5	0	3	1	15.70	0.57
			2	15.54	
			3	15.55	
0.5	3.75	3	1	16.03	0.75
			2	16.21	
			3	16.26	
0.5	7.5	3	1	16.08	1.52
			2	16.57	
			3	16.39	
0.5	0	7	1	15.15	0.41
			2	15.06	
			3	15.03	
0.5	3.75	7	1	16.17	1.18
			2	15.89	
			3	15.81	
0.5	7.5	7	1	16.95	0.72
			2	16.87	
			3	17.11	

TABLE 11 (cont.)

W/C RATIO	S.F %	CURING (DAYS)	REP. #	% VOLUME OF PERMEABLE VOIDS	COEFFICIENT OF VARIATION (%)
0.6	0	3	1	18.68	3.99
			2	19.80	
			3	20.18	
0.6	3.75	3	1	19.86	1.99
			2	20.57	
			3	19.89	
0.6	7.5	3	1	20.52	2.02
			2	20.14	
			3	20.97	
0.6	0	7	1	19.33	1.79
			2	19.78	
			3	20.03	
0.6	3.75	7	1	20.43	1.41
			2	20.01	
			3	20.56	
0.6	7.5	7	1	20.81	0.80
			2	20.79	
			3	21.09	
0.7	0	3	1	22.69	2.57
			2	21.77	
			3	21.66	

TABLE 11 (cont.)

W/C RATIO	S.F %	CURING (DAYS)	REP. #	% VOLUME OF PERMEABLE VOIDS	COEFFICIENT OF VARIATION (%)
0.7	3.75	3	1	22.98	2.49
			2	24.15	
			3	23.53	
0.7	7.5	3	1	24.55	1.47
			2	24.81	
			3	24.10	
0.7	0	7	1	21.30	0.82
			2	21.00	
			3	21.00	
0.7	3.75	7	1	22.54	0.41
			2	22.38	
			3	22.38	
0.7	7.5	7	1	22.52	1.21
			2	22.92	
			3	23.05	

APPENDIX B

FIGURES

**SCHEMATICS FOR
PERMEABILITY APPARATI**

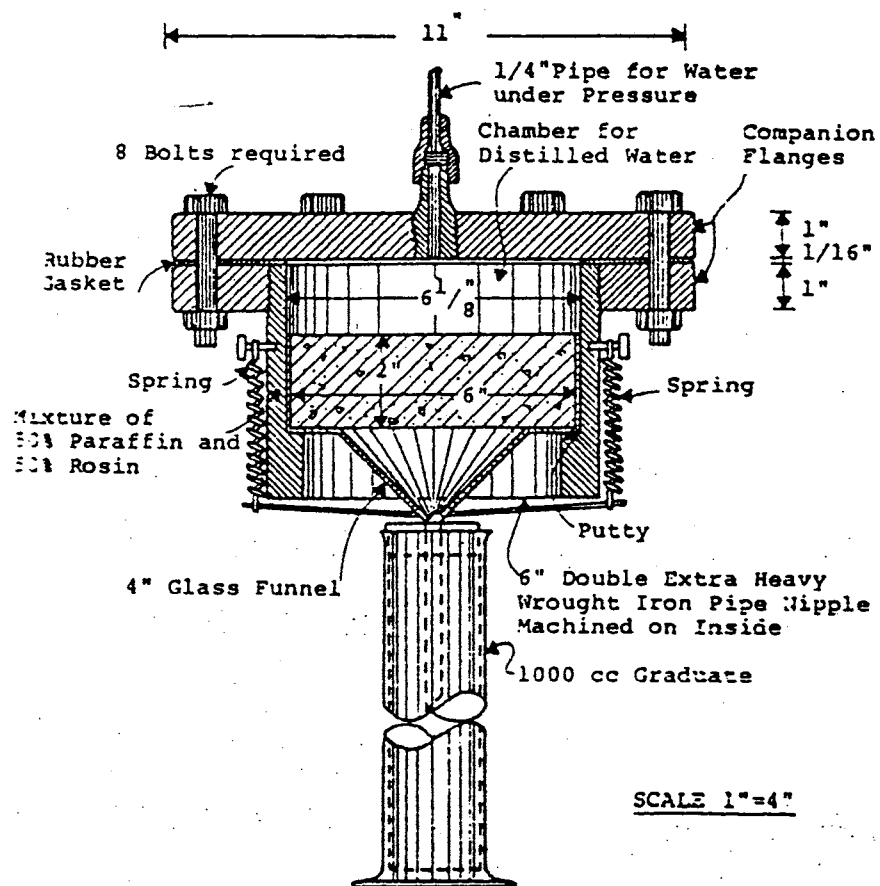


Figure 9. Schematic of the Permeability Apparatus Developed by McMillan and Lyse.

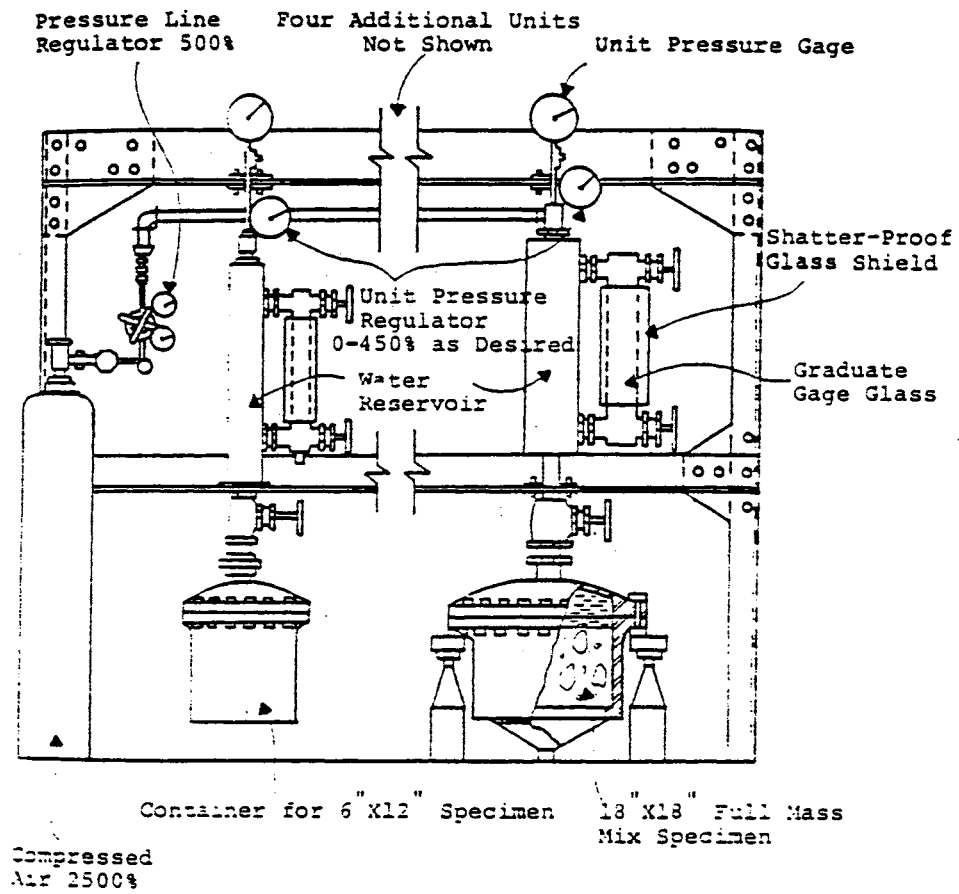


Figure 10. Schematic of the Permeability Apparatus Developed by Ruetters et. al.

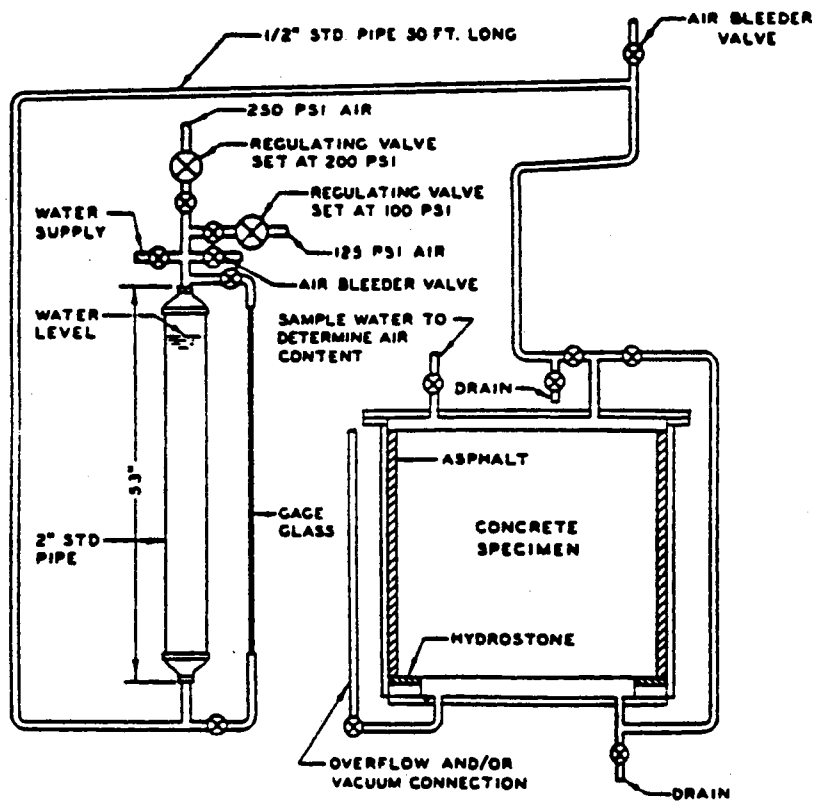


Figure 11. Schematic of the Permeability Apparatus Developed by US Army Corps of Engineers

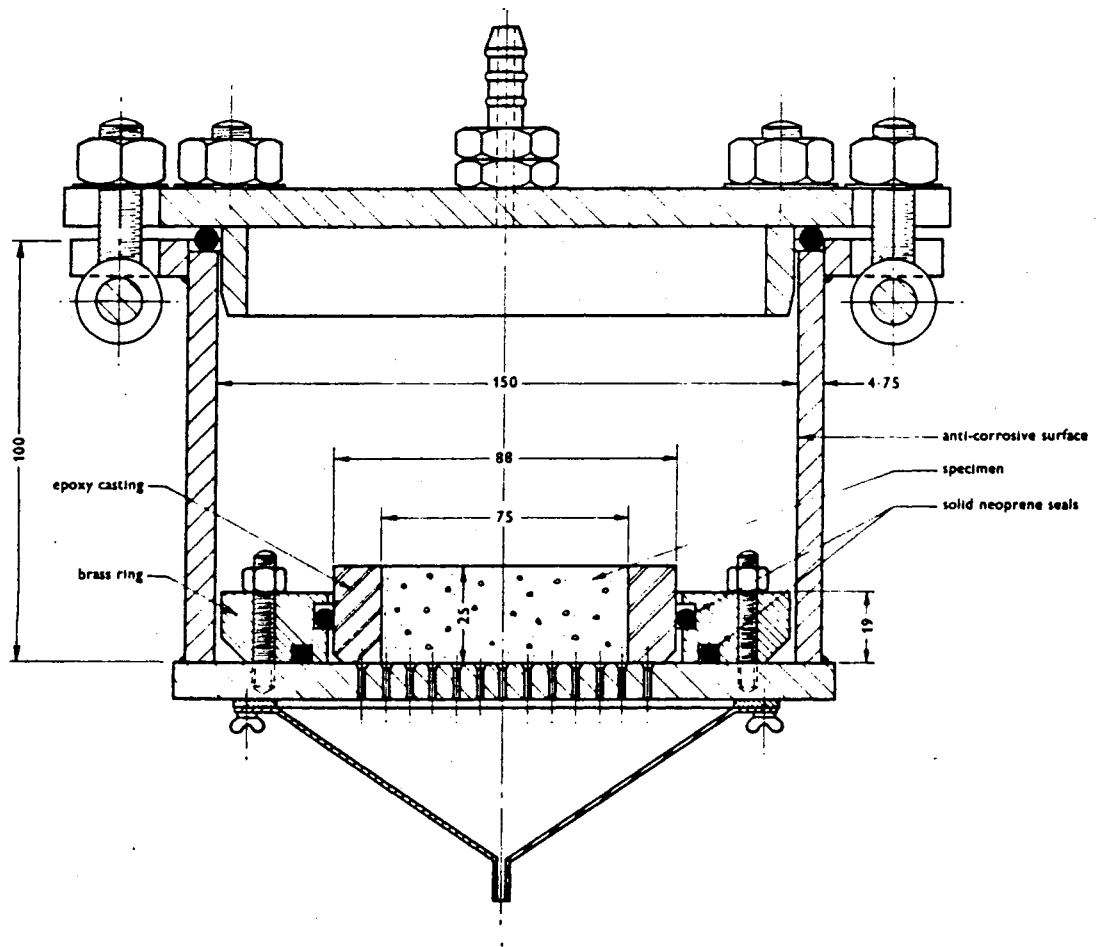


Figure 12. Section View of the Permeability Apparatus Developed by Meulen and Dijk

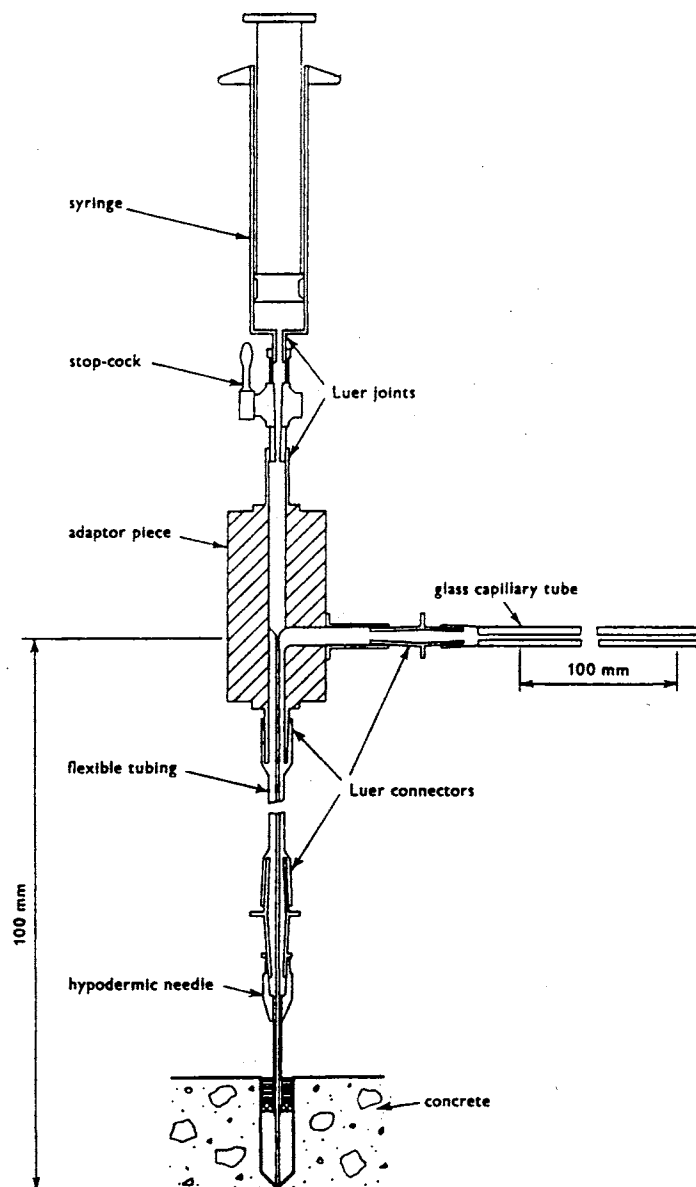


Figure 13. The Water Permeability Apparatus Developed by Figs.

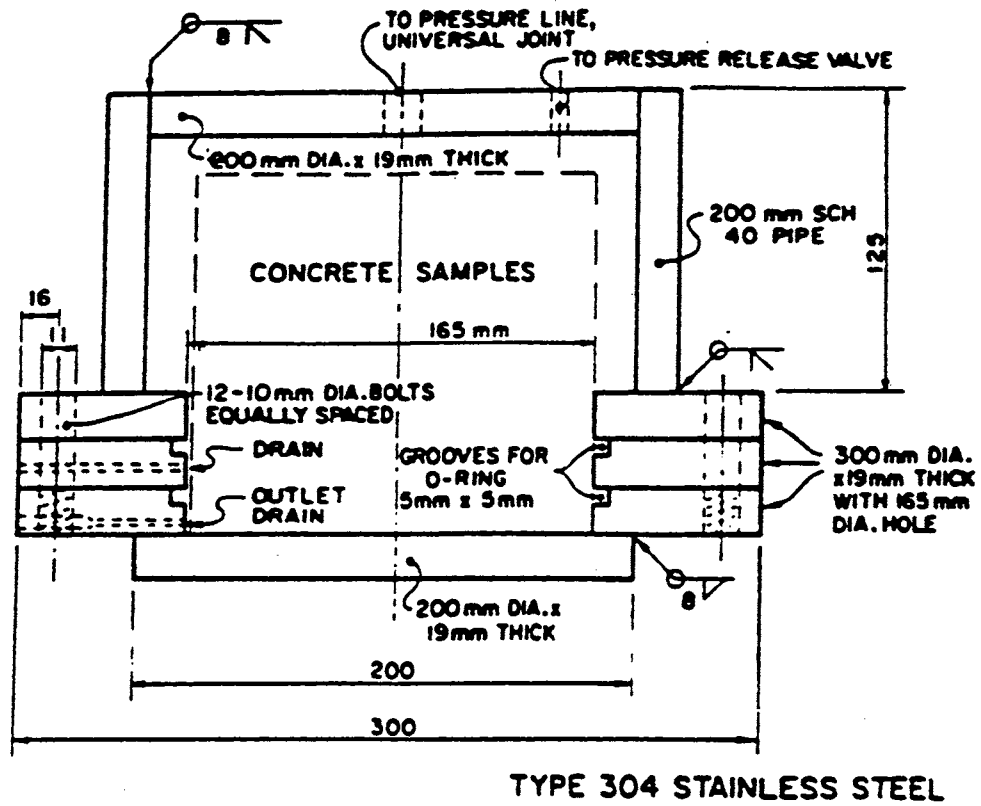


Figure 14. Section View of the Permeability Pressure Cell Developed by Hope and Malhotra

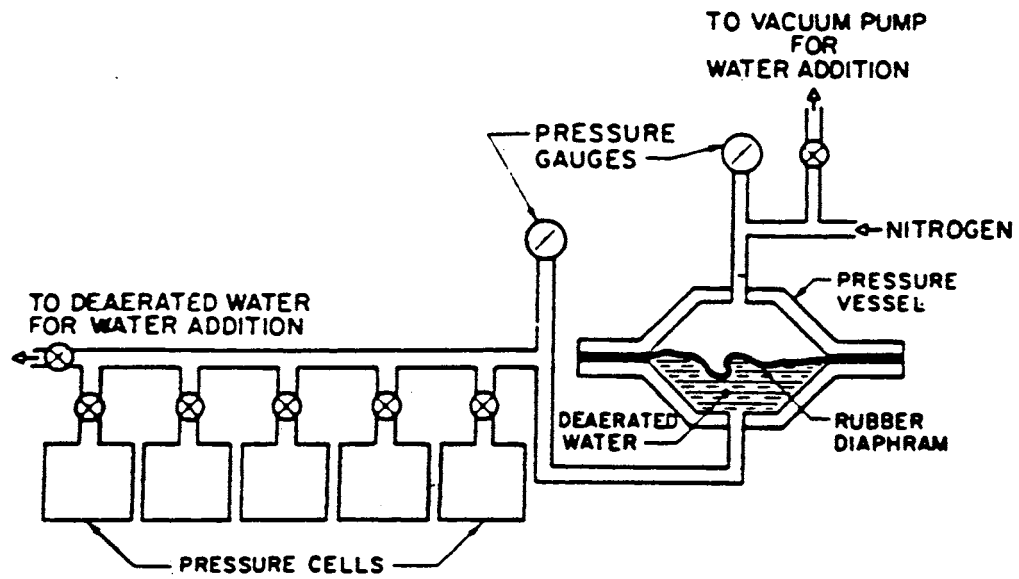


Figure 15. Schematic of the Permeability Apparatus Developed by Hope and Malhotra

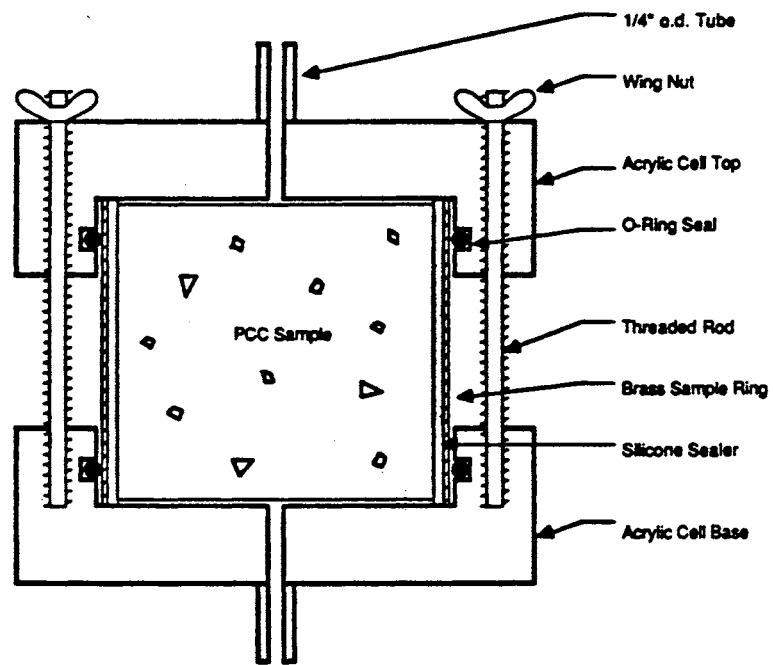


Figure 16. Section View of the Permeability Cell Developed by Janssen

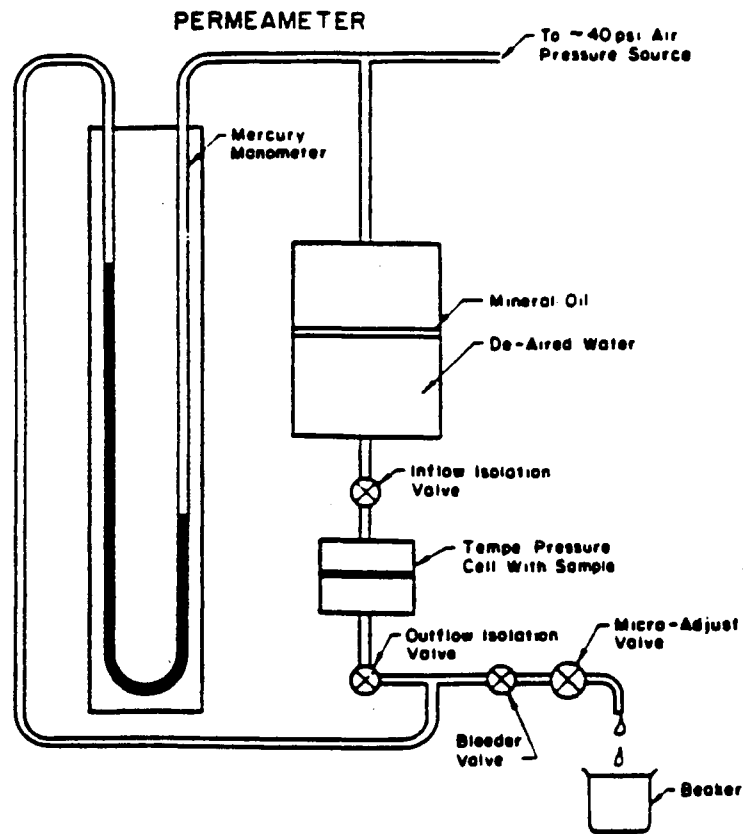


Figure 17. Schematic of the Permeability Apparatus Developed by Janssen

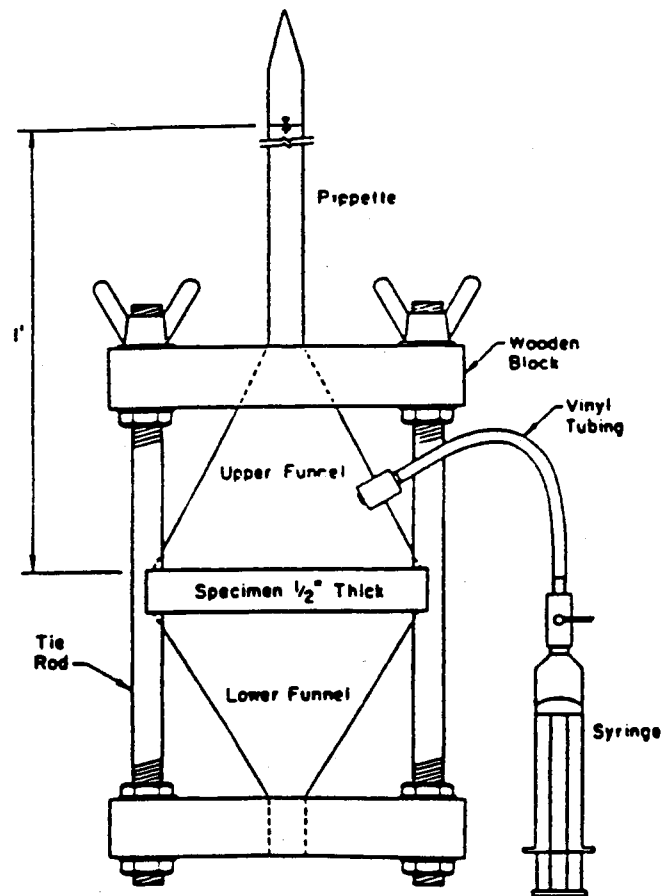


Figure 18. Schematic of the "Old" Permeability Apparatus Developed by Ludirdja, Berger and Young

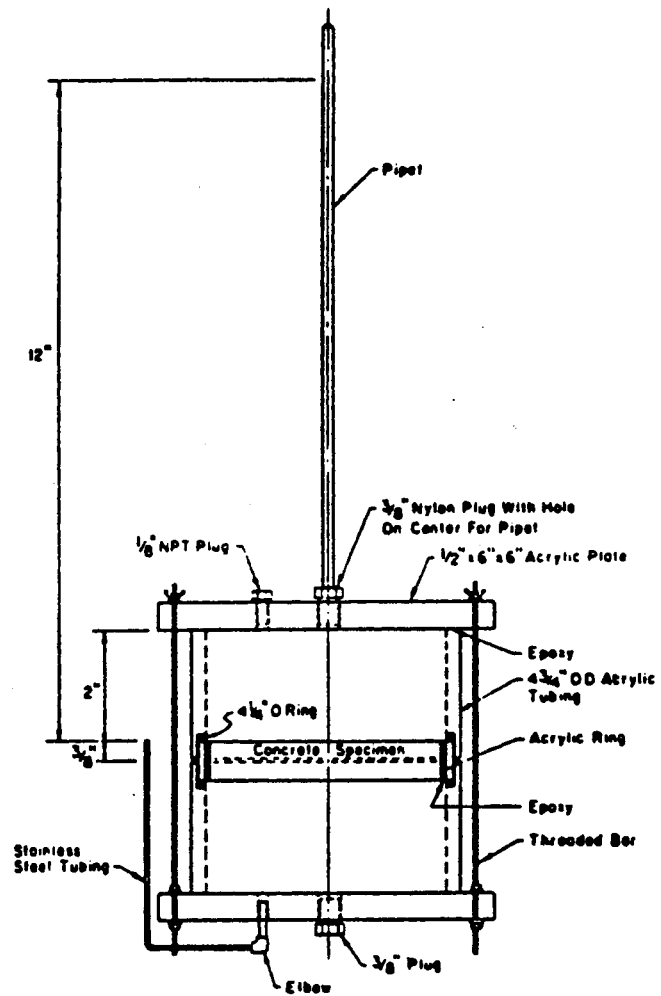


Figure 19. Schematic of the "New" Permeability Apparatus Developed by Ludirdja, Berger and Young

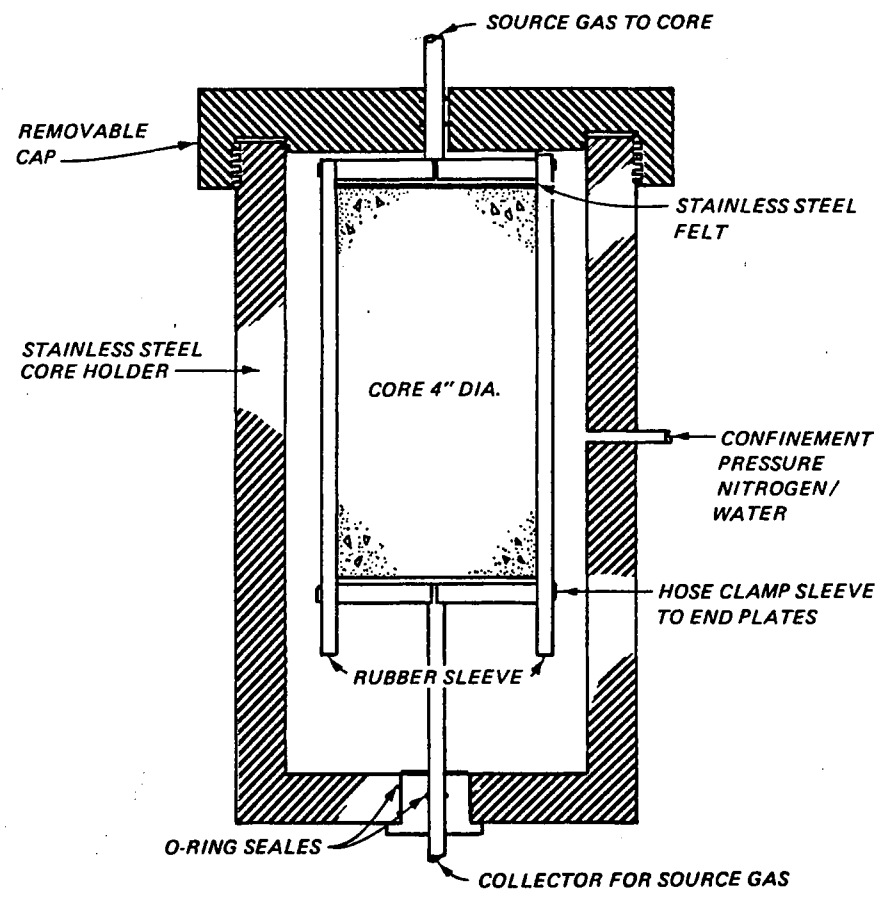


Figure 20. A Cross section View of Hassler Permeability Core Holder Used by Sullivan.

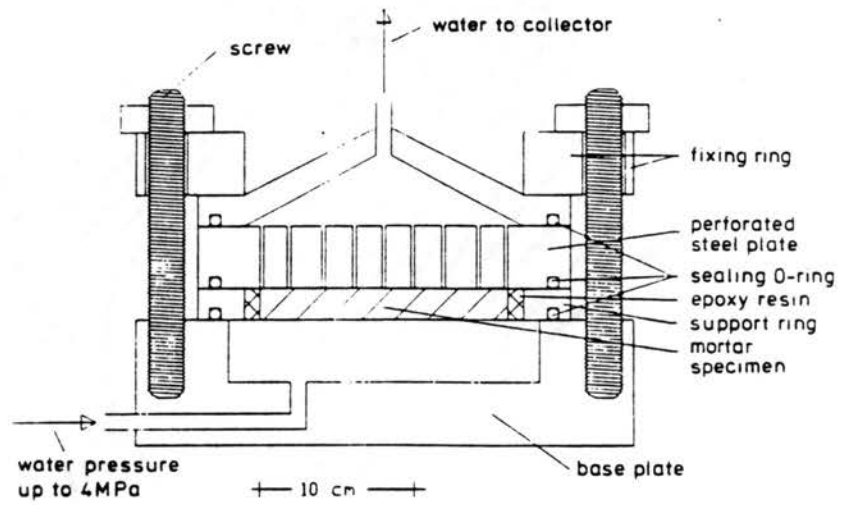


Figure 21. Schematic of the Permeability Apparatus Developed by Reinhardt and Gaber

REGRESSION RELATIONSHIPS

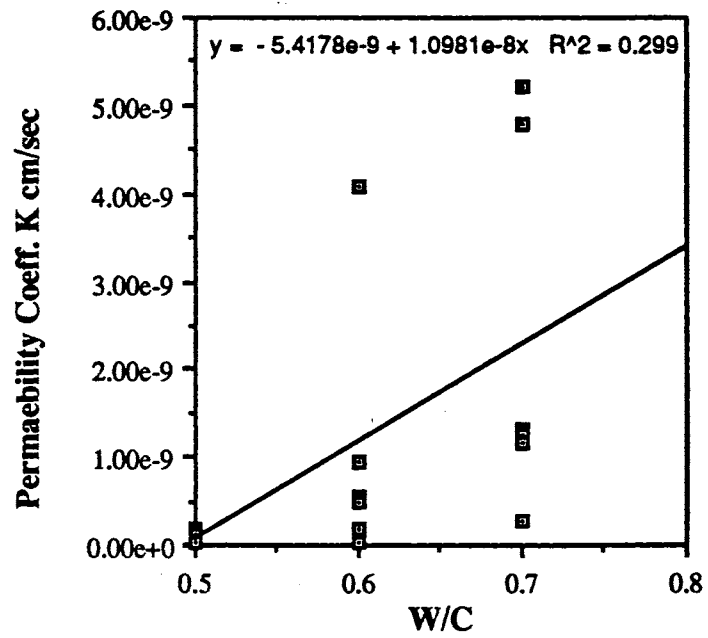


Figure 22. The Correlation of the Permeability Coefficient on the Water/Cement Ratio at all Silica Fume Contents

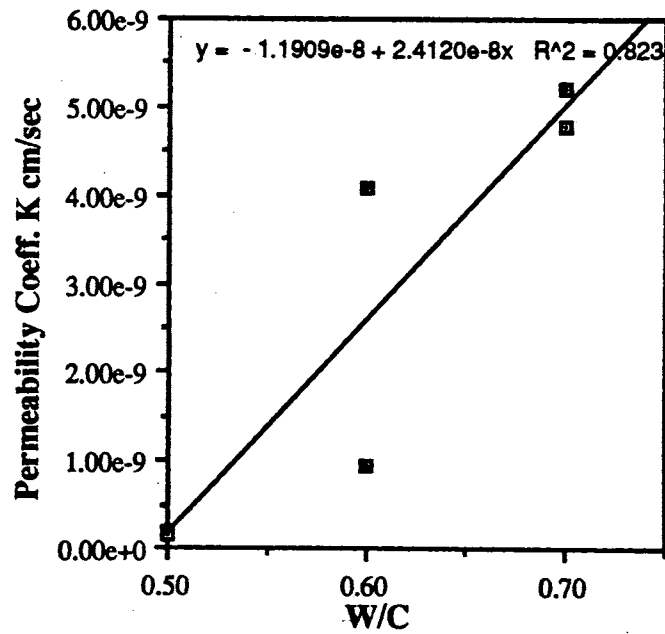


Figure 23. The Correlation of the Permeability Coefficient on the Water/Cement Ratio at 0 Percent Silica Fume Content

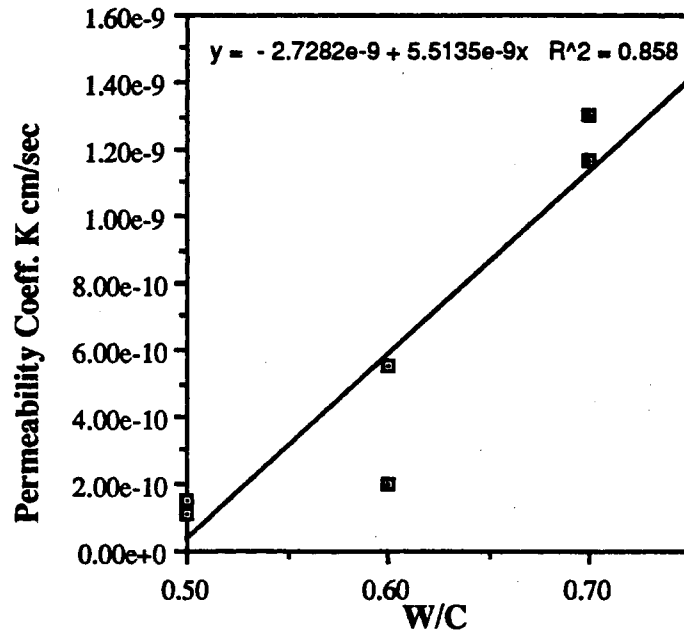


Figure 24. The Correlation of the Permeability Coefficients on the Water/Cement Ratio at 3.75 Percent Silica Fume Content

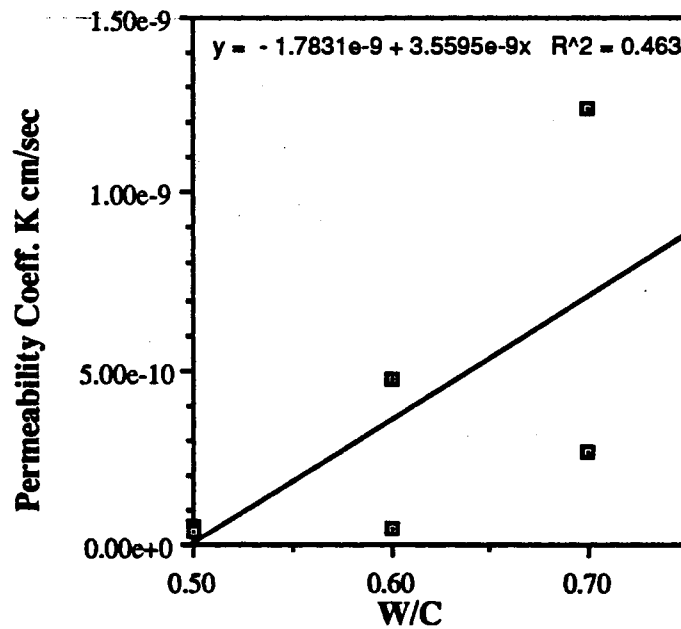


Figure 25. The Correlation of the Permeability Coefficient on the Water/Cement Ratio at 7.5 Percent Silica Fume Content

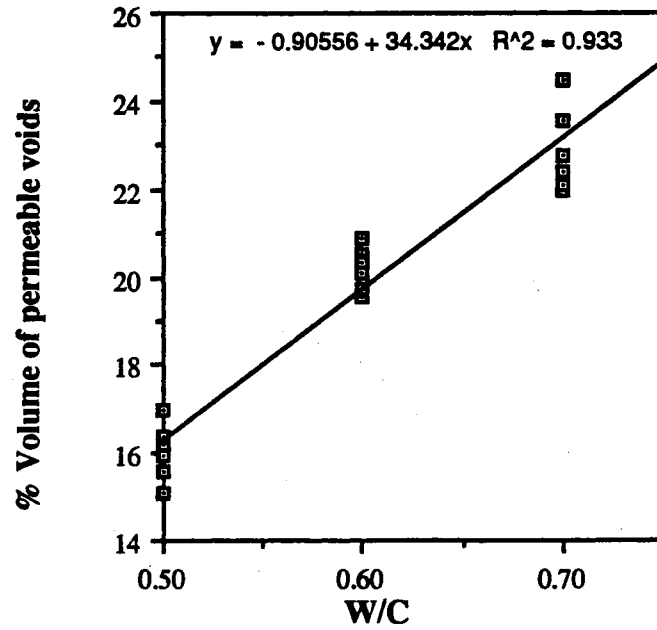


Figure 26. The Correlation of the percent volume of Permeable Voids on the Water/Cement Ratio at all Silica Fume Contents

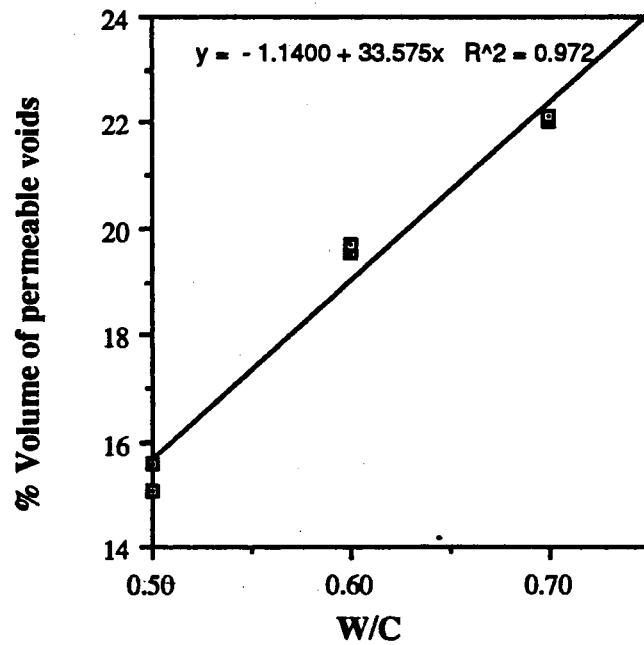


Figure 27. The Correlation of the Percent Volume of Permeable Voids on the Water/Cement Ratio at 0 Percent Silica Fume Content

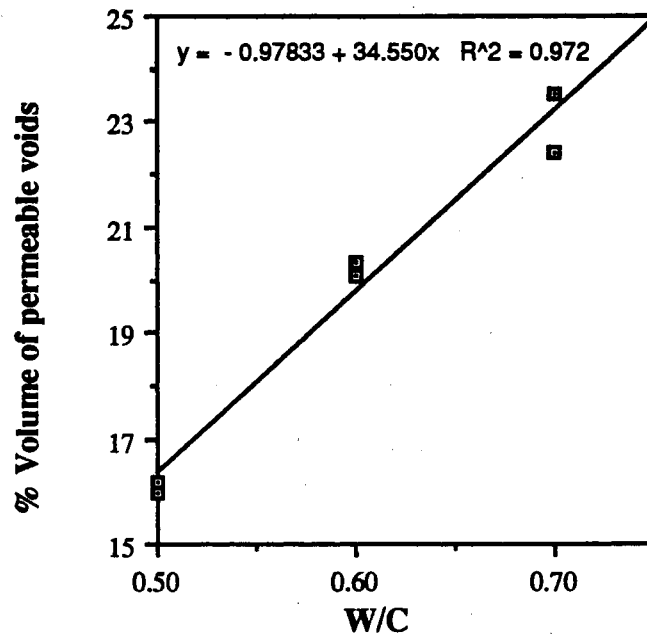


Figure 28. The Correlation of the Percent Volume of Permeable Voids on the Water/Cement Ratio at 3.75 Percent Silica Fume Content

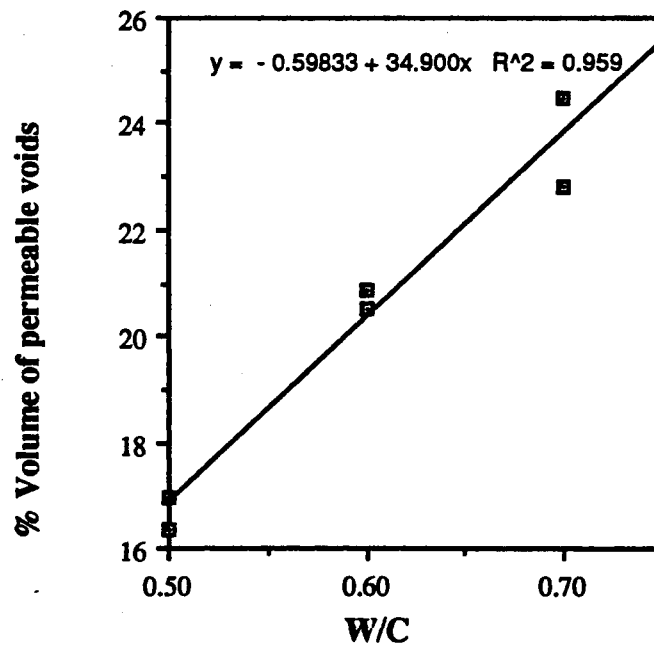


Figure 29. The Correlation of the Percent Volume of Permeable Voids on the Water/Cement Ratio at 7.5 Percent Silica Fume Content

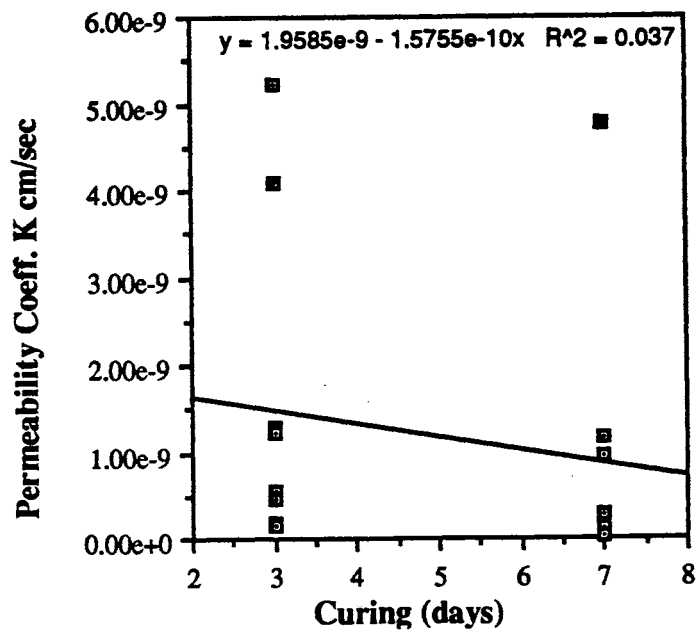


Figure 30. The Correlation of the Permeability Coefficient on the Curing Period at all Silica Fume Contents

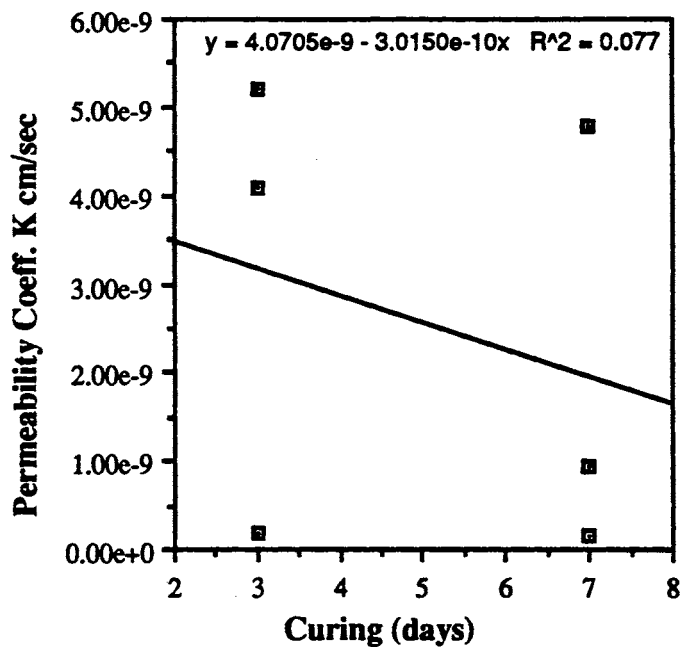


Figure 31. The Correlation of the Permeability Coefficient on the Curing Period at 0 Percent Silica Fume Content

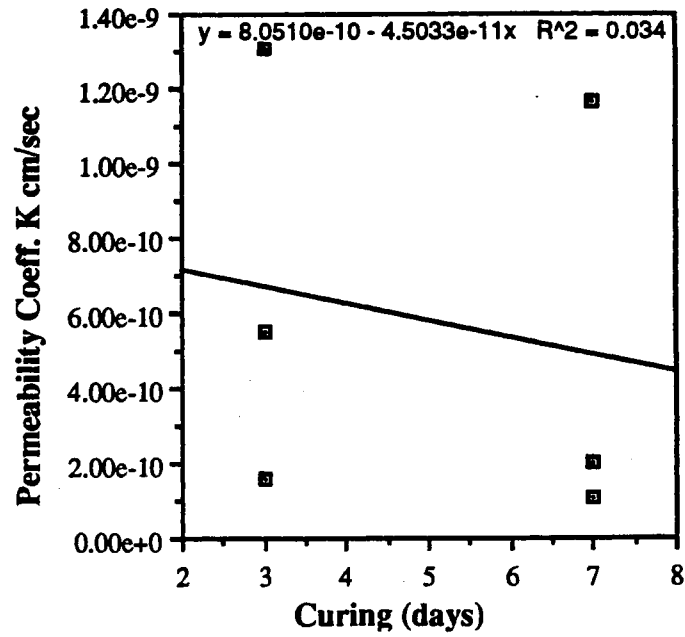


Figure 32. The Correlation of the Permeability Coefficient on the Curing Period
3.75 Percent Silica Fume Content

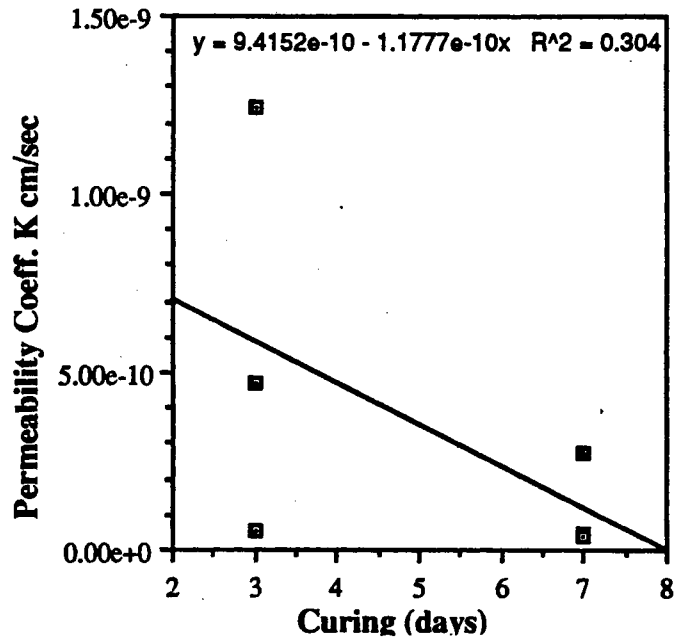


Figure 33. The Correlation of the Permeability Coefficient on the Curing Period
at 7.5 Percent Silica Fume Content

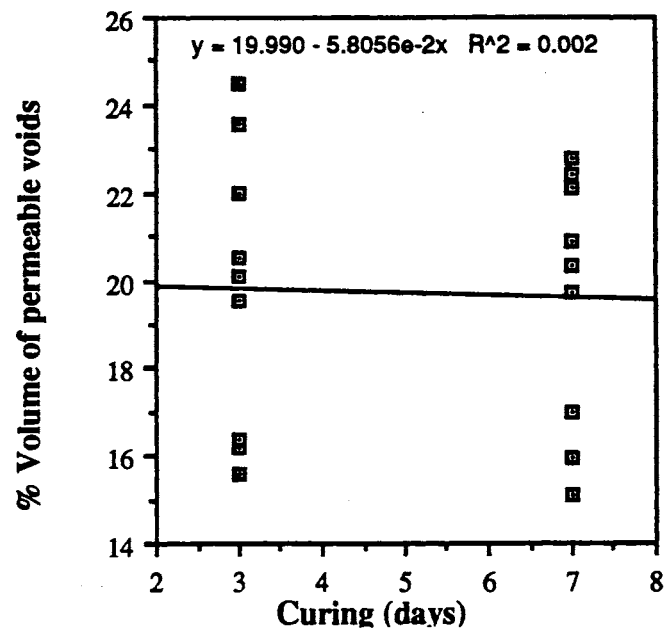


Figure 34. The Correlation of the Percent Volume of Permeable Voids on the Curing Period at all Silica Fume Contents

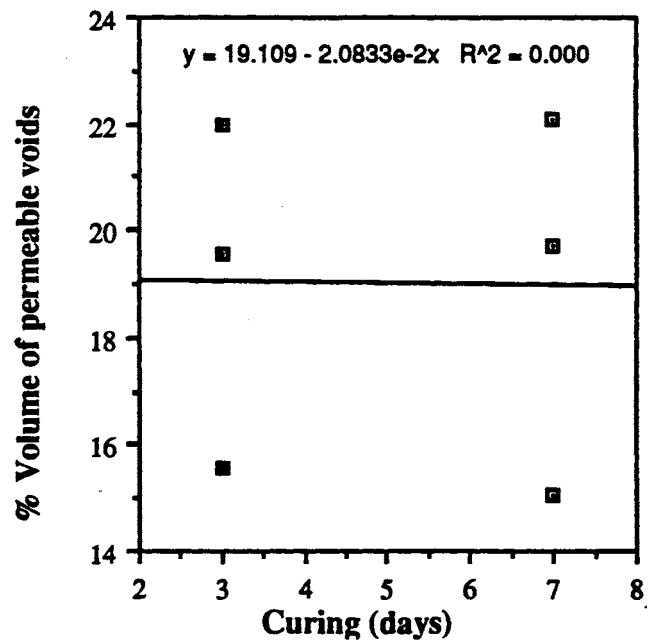


Figure 35. The Correlation of the Percent Volume of Permeable Voids on the Curing Period at 0 Percent Silica Fume Content

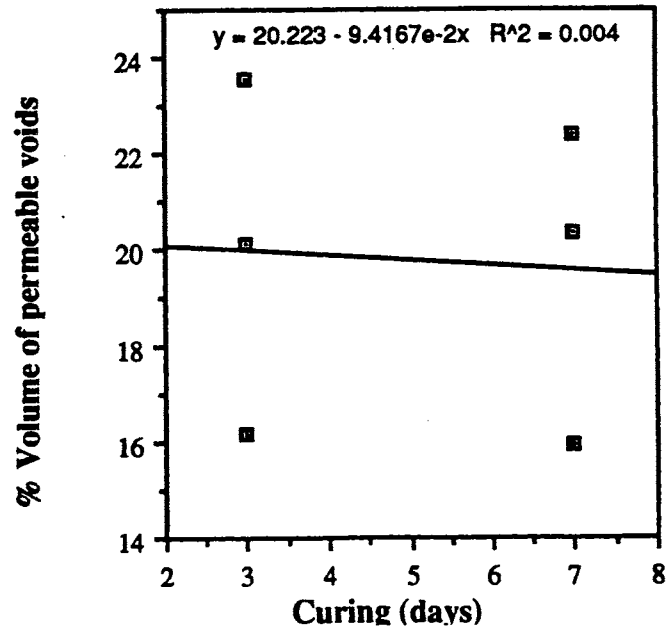


Figure 36. The Correlation of the Percent Volume of Permeable Voids on the Curing Period at 3.75 Percent Silica Fume Content

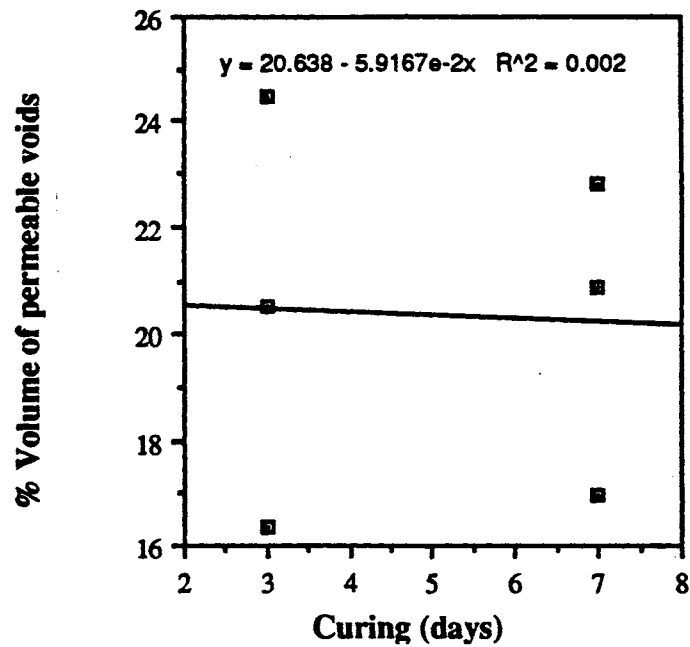


Figure 37. The Correlation of the Percent Volume of Permeable Voids on the Curing Period 7.5 Percent Silica Fume Content

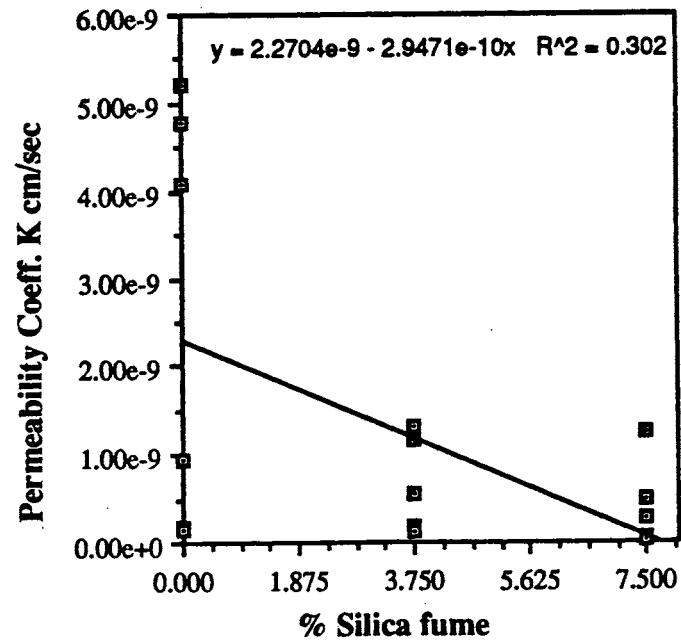


Figure 38. The Correlation of the Permeability Coefficient on the Silica Fume Content at all Water/Cement Ratios

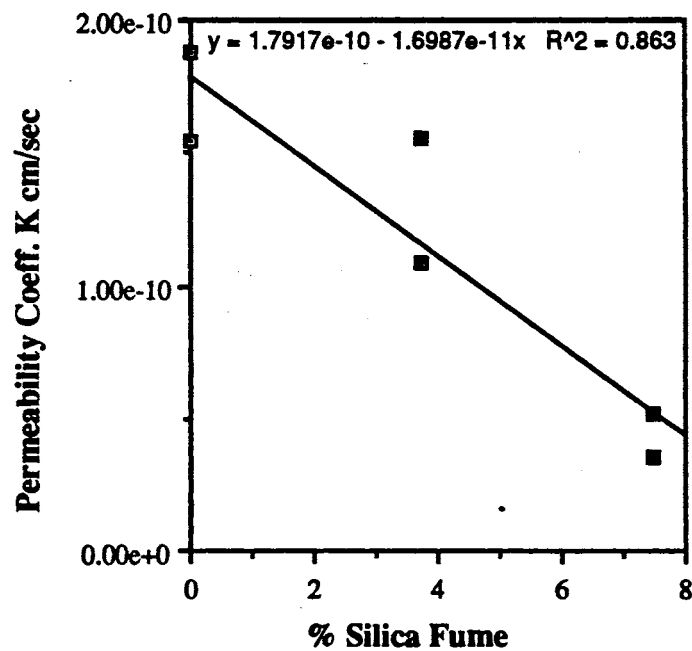


Figure 39. The Correlation of the Permeability Coefficient on the Silica Fume Content at 0.5 Water/Cement Ratio

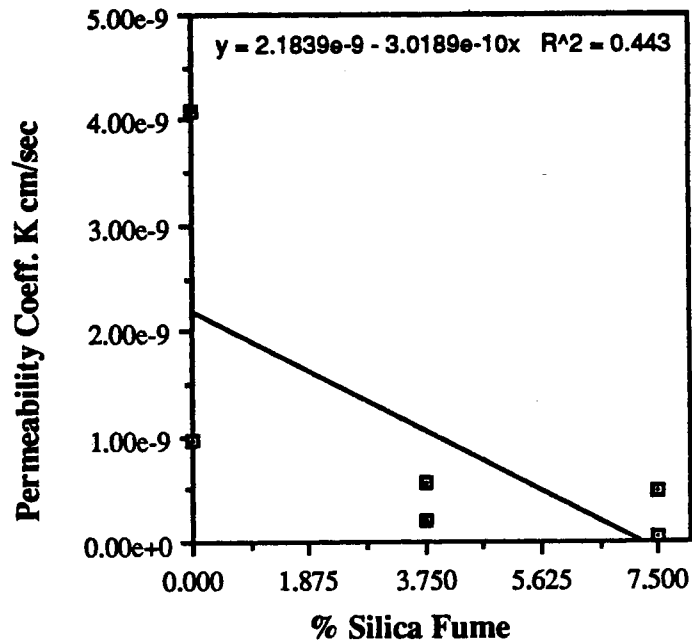


Figure 40. The Correlation of the Permeability Coefficient on the Silica Fume Content at 0.6 Water/Cement Ratio

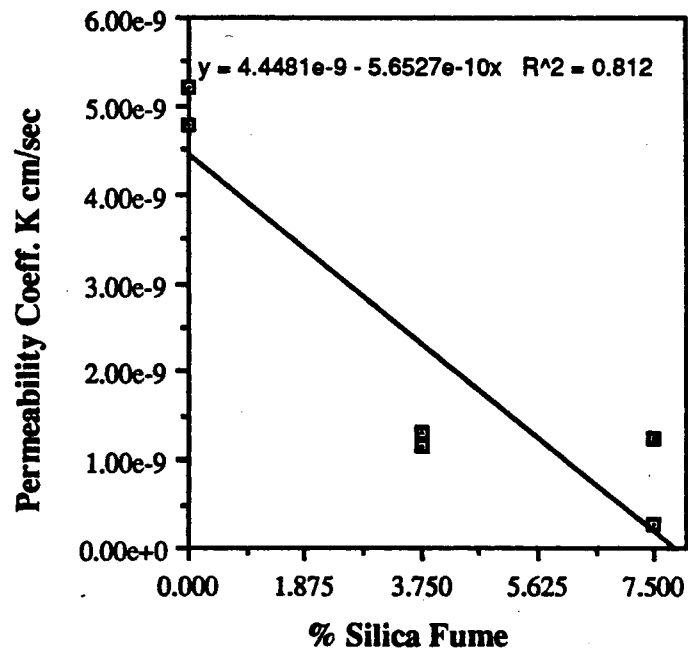


Figure 41. The Correlation of the Permeability Coefficient on the Silica Fume Content at 0.7 Water/Cement Ratio

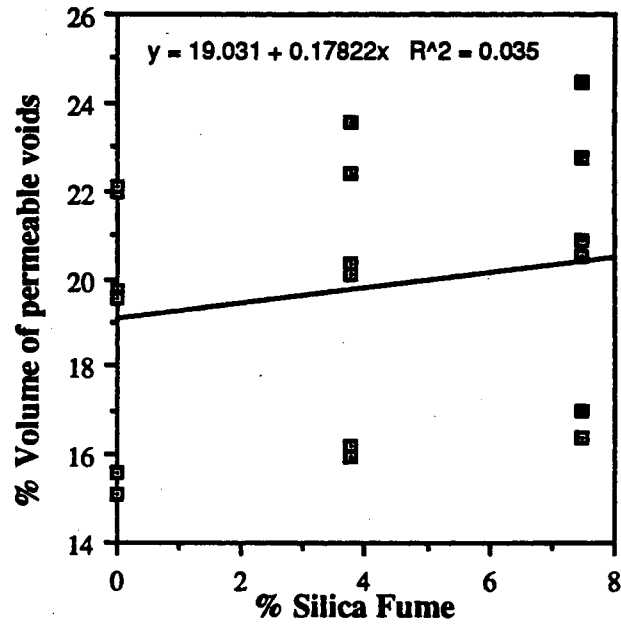


Figure 42. The Correlation of the Percent Volume of Permeable Voids on the Silica Fume Content at all Water/Cement Ratios

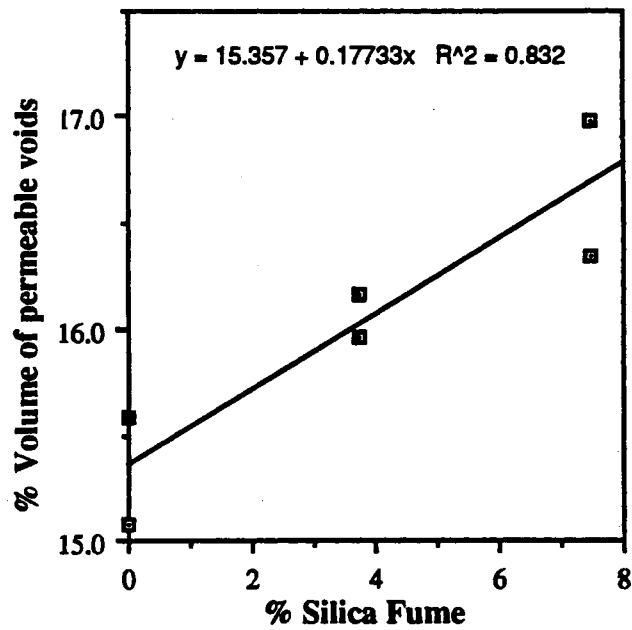


Figure 43. The Correlation of the Percent Volume of Permeable Voids on the Silica Fume Content at 0.5 Water/Cement Ratio

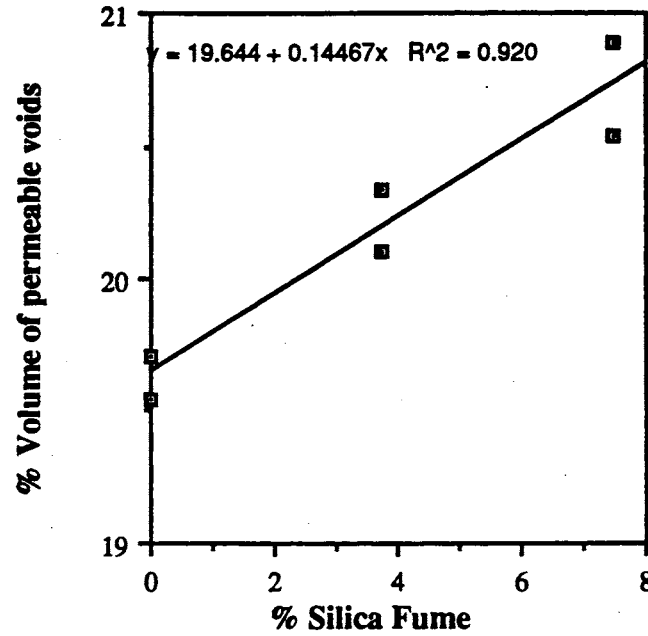


Figure 44. The Correlation of the Percent Volume of Permeable Voids on the Silica Fume Content at 0.6 Water/Cement Ratio

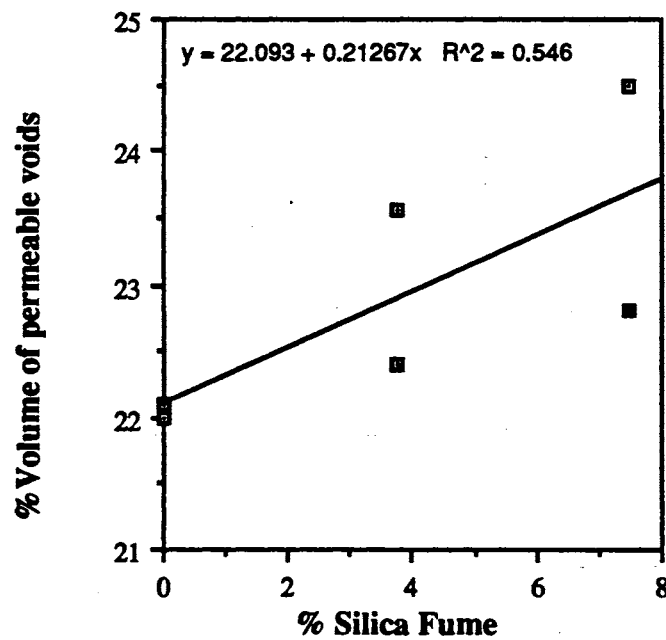


Figure 45. The Correlation of the Percent Volume of Permeable Voids on the Silica Fume Content at 0.7 Water/Cement Ratio

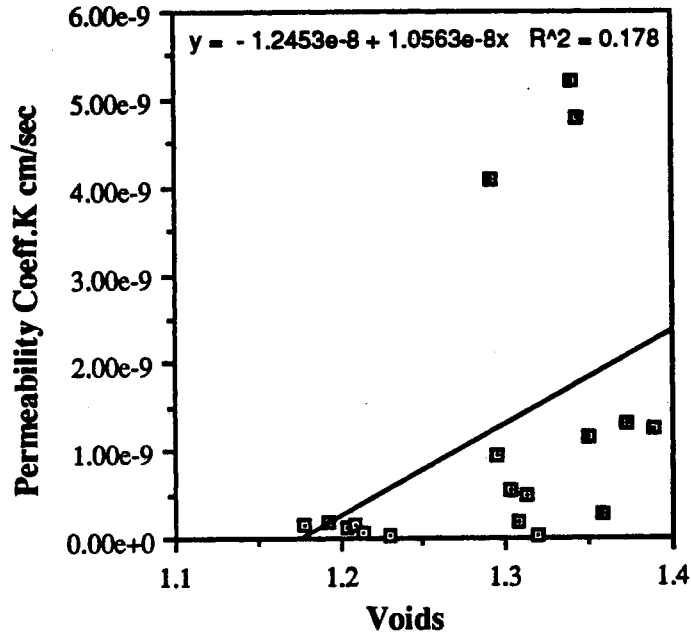


Figure 46. The Correlation of the Permeability Coefficient on the Percent Volume of Permeable Voids at all Silica Fume Contents

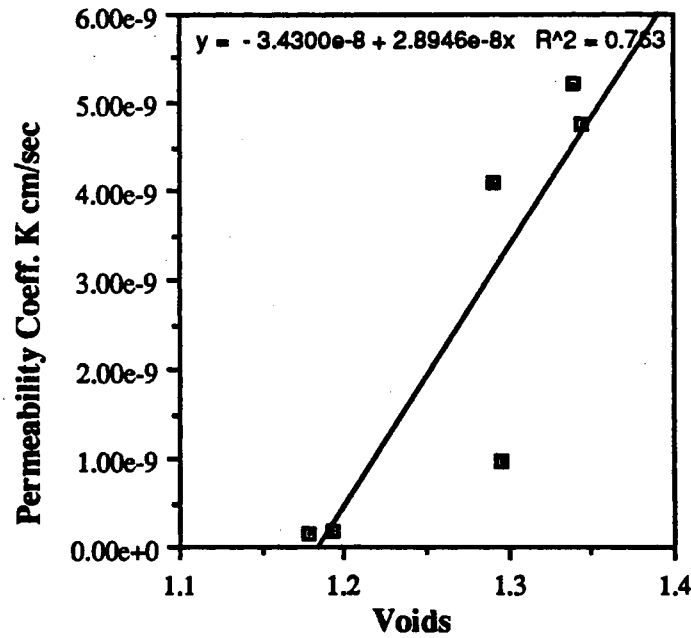


Figure 47. The Correlation of the Permeability Coefficient on the Percent Volume of Permeable Voids at 0 Percent Silica Fume Content

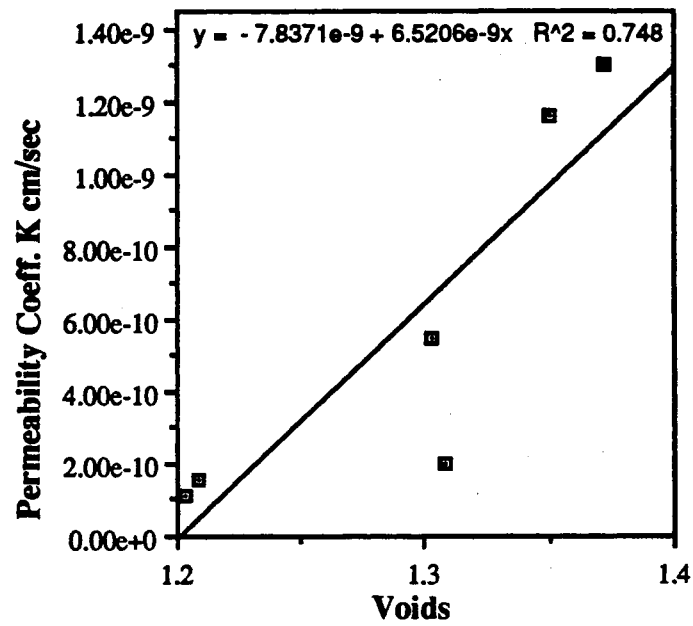


Figure 48. The Correlation of the Permeability Coefficient on the Percent Volume of Permeable Voids at 3.75 Percent Silica Fume Content

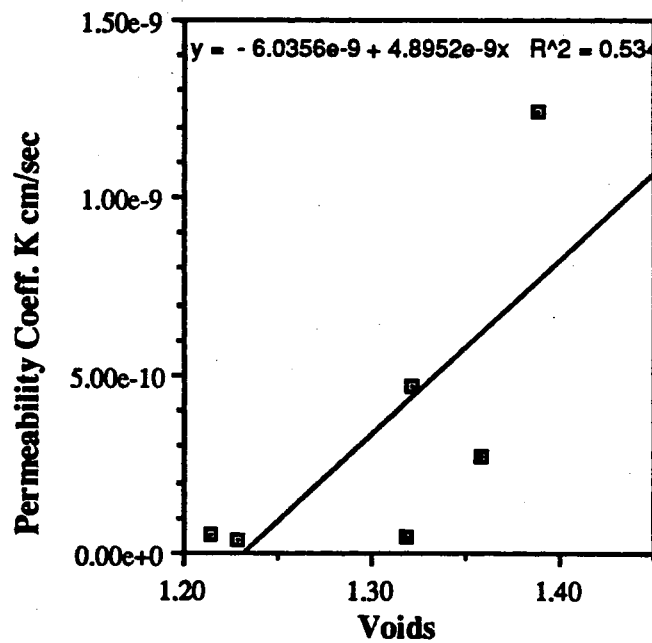


Figure 49. The Correlation of the Permeability Coefficient on the Percent Volume of Permeable Voids at 7.5 Percent Silica Fume Content

APPENDIX C

MEASURED PERMEABILITY DATA

SET # 1

S.F content = 0% ; Curing (days) =3 ; w/c ratio=0.5

Time	Hours	Day	Flow (cm ³ /hr)		
			Specimen #1	Specimen #2	Specimen #3
7:00 PM	0	1	0.3300	0.580	-
9:00 PM	2	1	0.3600	0.540	-
11:00 PM	4	1	0.3500	0.520	-
1:00 AM	6	1	0.3300	0.478	-
3:00 AM	8	1	0.3100	0.470	-
5:00 AM	10	1	0.3100	0.447	-
9:00 AM	14	1	0.2500	0.330	-
9:00 PM	26	2	0.1900	0.250	-
9:00 AM	38	2	0.1400	0.218	-
9:00 PM	50	3	0.0990	0.174	-
9:00 AM	62	3	0.0680	0.155	-
9:00 PM	74	4	0.0460	0.119	-
9:00 AM	86	4	0.0366	0.080	-

SET # 2

S.F content = 3.75% ; Curing (days) = 3 ; w/c ratio =0.5

Time	Hours	Day	Flow (cm ³ /hr)		
			Specimen #1	Specimen #2	Specimen #3
9:30 AM	0	1	-	-	-
12:30 AM	3	1	-	-	0.240
5:30 PM	8	1	-	-	0.219
10:30 PM	13	1	-	-	0.185
8:30 AM	23	1	-	-	-
7:00 AM	45.5	2	-	-	-
4:00 PM	54.5	3	-	-	0.095
8:00 PM	59.5	3	-	-	0.088
9:00 AM	72.5	4	-	-	0.079
8:00 PM	83.5	4	-	-	-
10:00 AM	97.5	5	-	-	0.065

SET # 3

S.F content = 7.5%; Curing (days) = 3; w/c ratio = 0.5

Time	Hours	Day	Flow (cm ³ /hr)		
			Specimen #1	Specimen #2	Specimen #3
12:00 PM	0	1	-	-	-
2:00 PM	2	1	0.0540	-	-
4:00 PM	4	1	0.0518	-	-
6:00 PM	6	1	0.0443	-	-
8:00 PM	8	1	0.0390	-	-
10:00 PM	10	1	0.0353	-	-
8:00 AM	20	1	0.0289	-	-
1:00 PM	25	2	0.0222	-	-
5:00 PM	29	2	0.0258	-	-
9:00 PM	33	2	0.0214	-	-
8:00 AM	44	2	0.0177	-	-
1:00 PM	49	3	0.0162	-	-
7:00 PM	55	3	0.0165	-	-
8:00 AM	68	3	0.0114	-	-
1:00 PM	73	4	0.0099	0.0255	-

SET # 4

S.F content = 0% Curing (days) = 7 w/c ratio = 0.5

Time	Hours	Day	Flow cm ³ /hr		
			Specimen # 1	Specimen #2	Specimen #3
3:00 PM	0	1	1.81	-	-
5:00 PM	2	1	1.54	-	-
7:00 PM	4	1	1.47	-	-
9:00 PM	6	1	1.04	-	-
6:00 AM	15	1	0.50	-	-
12:00	21	1	0.39	-	-
5:00 PM	26	2	0.33	-	-
11:00 PM	31	2	0.27	-	-
2:00 PM	46	2	0.18	-	-
8:00 PM	52	3	0.16	-	-
8:00 AM	64	3	0.09	-	-
9:00 AM	65	3	0.08	-	-

SET # 5

S.F content = 3.75% Curing (days) = 7 w/c ratio = 0.5

Time	Hours	Day	Flow cm ³ /hr		
			Specimen #1	Specimen #2	Specimen #3
12:00	0	1	-	0	-
2:00 PM	2	1	-	0.1965	-
4:00 PM	4	1	-	0.1860	-
6:00 PM	6	1	-	0.1905	-
8:00 PM	8	1	-	0.1703	-
10:00 PM	10	1	-	0.1688	-
8:00 AM	20	1	-	-	-
4:00 PM	28	2	-	0.1449	-
9:00 PM	33	2	-	0.1458	-
7:00 AM	43	2	-	-	-
5:00 PM	53	3	-	0.1217	-
9:00 PM	57	3	-	0.2030	0.0281
8:00 AM	68	3	-	0.1102	0.0237
7:00 PM	79	4	-	0.0988	0.0218
7:00 AM	91	4	-	0.0956	0.0176
7:00 PM	103	5	-	0.0954	0.0203
9:00 AM	117	5	-	-	0.0139
9:00 PM	129	6	-	0.0889	0.0102
9:00 AM	141	6	-	0.0769	0.0169
9:00 PM	153	7	-	0.0814	0.0125
12:00	168	8	-	0.0745	0.0055
10:00 PM	178	8	-	0.0865	0.0128

SET # 6

S.F content = 7.5%; Curing (days) = 7; w/c ratio = 0.5

Time	Hours	Day	Flow (cm ³ /hr)		
			Specimen #1	Specimen #2	Specimen #3
8:00 AM	0	1	-	-	0
11:00 AM	3	1	-	-	0.0585
2:00 PM	6	1	-	-	0.0639
5:00 PM	9	1	-	-	0.0515
8:00 PM	12	1	-	-	0.0465
8:00 AM	24	2	-	-	0.0515
8:00 PM	36	2	-	-	0.0467
7:00 AM	47	2	-	-	0.0423
9:00 PM	61	3	-	-	0.0392
8:00 AM	72	4	-	0.0256	0.0360
8:00 PM	84	4	-	0.0246	0.0357
7:00 AM	95	4	-	0.0214	0.0326
7:30 PM	107.5	5	-	0.0206	0.0311
8:00 AM	120	6	-	0.0194	0.0304
9:00 PM	133	6	-	0.0187	0.0304
9:00 AM	145	7	-	0.0174	0.0215
9:00 PM	157	7	-	0.0144	0.0180

SET # 7

S.F content = 0%; Curing (days) = 3; w/c ratio = 0.6

Time	Hours	Day	Flow cm ³ /hr		
			Specimen #1	Specimen #2	Specimen #3
7:30PM	0	1	3.39	5.14	2.26
9:30PM	2	1	2.63	3.44	2.20
11:30PM	4	1	2.05	2.76	1.98
1:30AM	6	1	1.62	2.32	1.75
3:30AM	8	1	1.47	2.04	2.14
5:30AM	10	1	1.36	1.75	1.53
11:30AM	16	1	1.02	1.34	1.15
5:30PM	22	1	0.94	1.19	1.09
11:30PM	28	2	0.80	2.69	1.00
5:30AM	34	2	0.67	1.33	0.76
11:30AM	40	2	0.64	1.16	0.93
5:30PM	46	2	0.66	1.14	0.77
11:30PM	52	3	0.59	1.15	0.79
5:30AM	58	3	0.51	1.14	0.67
11:30AM	64	3	0.48	1.10	0.62
5:30PM	70	3	0.46	1.09	0.62
11:30PM	76	4	0.41	1.04	0.57

SET # 8

S.F content = 3.75% Curing (days) = 3 w/c ratio = 0.6

Time	Hours	Day	Flow cm ³ /hr		
			Specimen #1	Specimen #2	Specimen #3
11:00AM	0	1	-	9.82	-
1:00PM	2	1	-	4.46	-
3:00PM	4	1	-	2.28	1.27
5:00PM	6	1	-	1.59	1.20
7:00PM	8	1	-	1.34	1.04
9:00PM	10	1	-	1.15	0.927
11:00PM	12	1	-	0.969	0.809
1:00PM	14	1	-	0.812	0.718
9:00AM	22	1	-	0.551	0.423
12:00	25	2	0.244	-	-
2:00PM	27	2	0.240	-	-
4:00PM	29	2	0.224	-	-
6:00PM	31	2	0.220	0.466	0.279
8:00PM	33	2	0.208	-	-
10:00PM	35	2	0.196	0.436	0.231
9:00AM	46	2	0.158	0.342	0.132
3:00PM	52	3	0.128	0.333	0.122
9:00PM	58	3	0.104	0.304	0.094
9:00AM	70	3	0.084	0.243	0.073

SET # 9

S.F content = 7.5% Curing (days) = 3 w/c ratio = 0.6

Time	Hours	Day	Flow cm ³ /hr		
			Specimen #1	Specimen #2	Specimen #3
1:30PM	0	1	-	6.35	-
3:30PM	2	1	-	2.90	1.54
5:30PM	4	1	-	1.87	1.27
7:30PM	6	1	-	1.34	1.11
9:30PM	8	1	-	1.06	0.78
11:30PM	10	1	-	0.78	0.90
1:30AM	12	1	-	0.75	0.79
3:30AM	14	1	-	0.68	0.73
5:30AM	16	1	-	0.62	0.65
11:30AM	22	1	-	0.48	0.51
5:30PM	28	2	-	0.41	0.41
11:30PM	34	2	-	0.35	0.34
5:30AM	40	2	-	0.31	0.27
11:30AM	46	2	-	0.26	0.24
5:30PM	52	3	-	0.28	0.22
11:30PM	58	3	-	0.23	0.18
11:30AM	70	3	-	0.20	0.15
5:30PM	76	4	-	0.20	0.14
11:30PM	82	4	-	0.19	0.12
8:30PM	91	4	-	0.16	0.11

SET # 10

S.F content = 0%; Curing (days) = 7; w/c ratio = 0.6

Time	Hours	Day	Flow (cm ³ /hr)		
			Specimen #1	Specimen #2	Specimen #3
12:30 PM	0	1	-	9.31	-
1:30 PM	1	1	3.33	8.71	-
2:30 PM	2	1	3.23	2.95	2.46
4:30 PM	4	1	2.32	1.66	2.16
6:30 PM	6	1	1.64	1.29	1.92
8:30 PM	8	1	1.26	1.03	1.70
10:30 PM	10	1	1.02	0.87	1.45
12:30 AM	12	1	0.79	0.77	1.16
6:30 AM	18	1	0.52	0.52	0.81
12:30 PM	24	2	0.40	0.42	0.66
6:30 PM	30	2	0.33	0.35	0.53
12:30 AM	36	2	0.29	0.30	0.44
6:30 AM	42	2	0.25	0.26	0.33
12:30 PM	48	3	0.23	0.24	0.32
6:30 PM	54	3	0.23	0.25	0.31
12:30 AM	60	3	0.21	0.21	0.27
12:30 PM	72	4	0.22	0.19	0.23
6:30 PM	78	4	0.20	0.24	0.22
12:30 AM	84	4	0.17	0.21	0.20

SET # 11

S.F content = 3.75% Curing (days) = 7 w/c ratio = 0.6

Time	Hours	Day	Flow cm ³ /hr		
			Specimen #1	Specimen #2	Specimen #3
10:30 PM	0	1	1.35	-	-
12:30 AM	2	1	1.32	1.80	-
2:30 AM	4	1	1.14	1.74	-
4:30 AM	6	1	0.898	1.83	0.892
6:30 AM	8	1	0.527	1.63	0.818
8:30 AM	10	1	0.503	1.24	0.775
10:30 AM	12	1	0.490	1.08	0.736
12:30 PM	14	1	0.467	0.966	0.704
2:30 PM	16	1	0.452	0.875	0.729
9:30 PM	23	1	0.348	0.679	0.443
9:30 AM	35	2	0.260	0.338	0.269
9:30 PM	47	2	0.173	0.261	0.313
9:30 AM	59	3	0.425	0.194	0.143
9:30 PM	71	3	0.098	0.140	0.112
9:30 AM	83	4	0.082	0.120	0.090
9:30 PM	95	4	0.063	0.099	0.068

SET # 12

S.F content = 7.5% Curing (days) = 7 w/c ratio = 0.6

Time	Hours	Day	Flow cm ³ /hr		
			Specimen #1	Specimen #2	Specimen #3
3:00 PM	0	1	-	0.066	-
5:00 PM	2	1	-	0.075	-
7:00 PM	4	1	-	0.062	-
9:00 PM	6	1	-	0.062	-
11:00 PM	8	1	-	-	-
12:00	33	2	-	0.039	-
9:00 AM	42	2	-	0.038	-
12:00	45	2	-	0.037	-
6:00 PM	51	3	-	-	-
12:00	57	3	-	0.034	-
9:00 AM	66	3	-	0.030	-
12:00	69	3	-	0.029	-
6:00 PM	75	4	-	0.033	-
8:00 AM	89	4	-	0.024	-
4:00 PM	97	5	-	0.025	-
12:00	106	5	-	-	-
10:00 AM	116	5	-	0.020	-
6:00 PM	124	6	-	0.023	-
10:00 PM	128	6	-	0.022	-
9:00 AM	139	6	-	0.017	-
1:00 PM	143	6	-	0.019	-
10:00 PM	152	7	-	0.023	-
8:30 AM	162.5	7	-	0.017	-

SET # 13

S.F content = 0% Curing (days) = 3 w/c ratio = 0.7

Time	Hours	Day	Flow cm ³ /hr		
			Specimen #1	Specimen #2	Specimen #3
1:00 PM	0	1	21.61	-	14.60
3:00 PM	2	1	8.18	2.81	6.50
5:00 PM	4	1	6.42	2.88	4.25
7:00 PM	6	1	5.00	2.37	3.37
9:00 PM	8	1	4.28	2.23	2.67
11:00 PM	10	1	3.43	1.62	1.52
9:00 AM	20	1	2.05	0.56	0.91
9:00 PM	32	2	1.65	0.22	0.58
9:00 AM	44	2	1.20	0.20	0.40

SET # 14

S.F content = 3.75%; Curing (days) = 3; w/c ratio = 0.7

Time	Hours	Day	Flow cm ³ /hr		
			Specimen #1	Specimen #2	Specimen #3
1:00 PM	0	1	9.82	8.85	6.20
3:00 PM	2	1	6.13	3.82	3.41
5:00 PM	4	1	4.35	2.76	1.94
7:00 PM	6	1	3.33	2.37	1.85
9:00 PM	8	1	2.64	1.69	1.47
11:00 PM	10	1	2.22	1.83	1.08
9:00 AM	20	1	1.24	1.11	0.39
9:00 PM	32	2	0.88	0.85	0.23
9:00 AM	44	2	0.52	0.34	0.17
9:00 PM	56	3	0.40	0.30	0.13
9:00 AM	68	3	0.25	0.24	0.11

SET # 15

S.F content = 7.5%; Curing (days) = 3; w/c ratio = 0.7

Time	Hours	Day	Flow cm ³ /hr		
			Specimen #1	Specimen #2	Specimen #3
12:00	0	1	3.35	-	-
1:00 PM	1	1	2.59	-	-
2:00 PM	2	1	2.01	-	-
3:00 PM	3	1	1.95	-	-
5:00 PM	5	1	1.74	-	-
7:00 PM	7	1	1.56	0.60	-
9:00 PM	9	1	1.35	0.58	-
11:00 PM	11	1	1.23	0.59	-
1:00 AM	13	1	1.13	0.55	-
3:00 AM	15	1	1.02	0.59	-
5:00 AM	17	1	0.95	0.59	-
9:00 PM	33	2	0.59	0.68	-
9:00 AM	45	2	0.47	0.89	-
9:00 PM	57	3	0.41	0.94	-
9:00 AM	69	3	0.37	1.27	-
9:00 PM	81	4	0.35	0.77	-
9:00 AM	93	4	0.32	0.52	-
3:00 PM	99	5	0.31	0.46	-
9:00 PM	105	5	0.29	0.43	-
9:00 AM	117	5	0.26	0.33	-

SET # 16

S.F content = 0%; curing (days) = 7; w/c ratio = 0.7

Time	Hours	Day	Flow cm ³ /hr		
			Specimen #1	Specimen #2	Specimen #3
11:00 AM	0	1	-	18.00	7.29
1:00 PM	2	1	-	14.59	4.25
3:00 PM	4	1	1.50	10.59	3.01
5:00 PM	6	1	1.49	8.31	2.17
7:00 PM	8	1	1.40	7.29	1.84
9:00 PM	10	1	1.20	4.46	1.47
11:00 PM	12	1	1.00	4.15	1.30
1:00 AM	14	1	0.83	3.43	1.17
9:00 AM	22	1	0.46	2.19	0.81
9:00 PM	34	2	0.25	1.65	0.68

SET # 17

S.F content = 3.75% Curing (days) = 7 w/c ratio = 0.7

Time	Hours	Day	Flow cm ³ /hr		
			Specimen #1	Specimen #2	Specimen #3
3:30 PM	0	1	8.71	10.19	-
5:30 PM	2	1	5.51	7.10	-
7:30 PM	4	1	4.06	7.50	-
9:30 PM	6	1	3.17	14.21	1.25
11:30 PM	8	1	2.87	-	1.48
1:30 AM	10	1	2.48	13.50	1.66
3:30 AM	12	1	2.16	10.59	1.62
5:30 AM	14	1	1.92	8.18	1.67
7:30 AM	16	1	1.82	6.66	1.71
9:30 PM	30	2	1.35	13.18	0.89
9:30 AM	42	2	1.12	9.47	0.49
9:30 PM	54	3	1.05	-	0.31
9:30 AM	66	3	0.89	-	0.20
9:30 PM	78	4	0.97	-	0.17
9:30 AM	90	4	0.85	-	0.12

SET # 18

S.F content = 7.5% Curing (days) = 7 w/c ratio = 0.7

Time	Hours	Day	Flow cm ³ /hr		
			Specimen #1	Specimen #2	Specimen #3
8:30 AM	0	1	0.99	1.94	1.06
10:30 AM	2	1	1.02	1.88	0.88
12:30 PM	4	1	1.01	1.68	0.65
2:30 PM	6	1	1.00	1.42	0.58
4:30 PM	8	1	0.98	1.27	0.53
6:30 PM	10	1	0.89	0.92	0.42
9:00 PM	12.5	1	0.79	0.81	0.37
9:00 AM	24.5	2	0.50	0.51	0.19
9:00 PM	36.5	2	0.37	0.40	0.12
9:00 AM	48.5	3	0.24	0.28	0.09
9:00 PM	60.5	3	0.21	0.24	0.07
9:00 AM	72.5	4	0.17	0.20	0.06
9:00 PM	96.5	5	0.13	0.15	0.04

2
VITA

Ashraf Elazouni

Candidate for the Degree of

Doctor of Philosophy

Thesis: WATER PERMEABILITY OF SILICA FUME/CEMENT MORTARS

Major Field: Civil Engineering

Biographical:

Personal Data: Born in Giza, Egypt, August 26, 1962, the son of Mr. and Mrs. Elazouni.

Education: Received the Bachelor of Engineering degree in Civil Engineering in May, 1984, from Zagazig University, Zagazig, Egypt; received Master of Science in Civil Engineering in April, 1989, from Zagazig University, Zagazig, Egypt; completed the requirements for Ph.D. degree at Oklahoma State University in July, 1993.

Professional Experience: Worked as a teaching assistant in the Civil Engineering Department, Zagazig University from 1984 to 1989 in teaching Construction Management; Worked as a Teaching Assistant in the School of Civil Engineering, Oklahoma State University, in Construction Management and Transportation Engineering during the period from January, 1990 to May, 1993.